ISSN: 1224-7626

ANALELE UNIVERSITĂŢII DIN ORADEA

Fascicula CHIMIE
XXXII (32) 2025

EDITURA UNIVERSITĂŢII DIN ORADEA

2025

Editorial Adress
University of Oradea, Chemistry Departament
Str. Universitatii, nr.1, 410087, Oradea, Bihor, România
General Information
ISSN: 1224-7626
Place of publishing: Oradea, Romania
Year of the first issue: 1995
Releasing frequency: 1 issue / year
Language: English
Abstracting/Indexing:

Chemical Abstracts Service-CAS Source Index (CASSI)

Academic Research Index- ResearchBiB

Google Scholar

TABLE OF CONTENTS

USING VARIO TOC ANALYZER FOR THE WATER, LEACHATE AND SOIL POLLUTION ASSESSMENT OPPORTUNITIES

Tiberiu HARTMANN[1], Alexandrina FODOR[2] , Gabriela Elena BADEA[2], Anda Ioana Graţiela PETREHELE[2], Claudia Mona MORGOVAN[2]

[1] Physico-chemical Analysis Laboratory, Stilo Evora Suplacul de Barcau, Bihor Romania, tibihartmann@gmail.com
[2] Department of Chemistry, Faculty of Informatics and Sciences, University of Oradea, afodor@uoradea.ro

Abstract: *This work aims are to determine the organic carbon content of different environments (water, soil) using the Vario TOC analyser, a high-performance instrument for measuring total organic carbon. During the work, experimental determinations were carried out for several types of samples, including wastewater, leachate and contaminated soil, to highlight the transfer of organic carbon under different conditions. Significant variations in total organic carbon (TOC) and dissolved organic carbon (DOC) concentration were observed, depending on the sample source and the pre-processing process. The analyses revealed a direct correlation between the degree of pollution of the samples and high TOC and DOC values, demonstrating the efficiency of the method in assessing the anthropogenic impact on the aquatic environment.*

Keywords: *total organic carbon (TOC), dissolved organic carbon (DOC), surface water, leachate, soil*

INTRODUCTION

The problem of environmental pollution has become a central topic in the context of sustainable development. Among the main quality indicators of the environment (water, soil, waste) are the content of total organic carbon (TOC) and dissolved organic carbon (DOC), which reflect the degree of pollution with organic substances.

TOC (Total Organic Carbon) – can be defined as the sum of organic carbon compounds present in water or soil, in dissolved form or in the form of suspended matter. Total organic carbon represents the total amount of carbon bound in organic compounds. In the aquatic environment, TOC can come from natural (plant, animal) or anthropogenic sources (wastewater, leachate).

DOC (dissolved organic carbon) - represents the sum of carbon compounds present in water or leachate, resulting from filtration on a 0.45µm membrane.

The determination of these parameters in water, leachate and soil samples allows the assessment of anthropogenic impact and associated ecological risks.

The determination of total organic carbon (TOC) content is essential in many scientific and industrial fields, such as drinking and wastewater analysis, pharmaceutical and food industries, environmental protection and industrial process control.

EXPERIMENTAL

The study aimed to evaluate the degree of pollution of the area in the vicinity of the SC STILO MONITORING SRL laboratory, in the commune of Suplacu de Barcau, place Suplacu de Barcau, Bihor County, an area considered to be polluted with petroleum.

The activities carried out were:

1. Determination of TOC/DOC in samples of wastewater, leachate and soil.
2. Evaluation of the variation of organic carbon content depending on the type of samples (leachate, water and soil).
3. Interpretation of TOC and DOC values with the degree of pollution of the analyzed environment in accordance with the legislation.

The experimental activity was carried out within the laboratory of SC STILO MONITORING SRL, in the commune of Suplacu de Barcau, place Suplacu de Barcau, Bihor County.

Analysed Samples

Water, contaminated soil and industrial soil samples were taken from the vicinity of the unit where the Laboratory operates. The company in question owns a Platform for inerting waste and contaminated soils (the

most common contaminants being hydrocarbons).

Equipment

For the determination of TOC and DOC, the VARIO TOC ELEMENTAL Analyzer produced by the German company Elemental was used, it is a high-performance instrument for determining the organic and inorganic carbon content in liquid and solid samples. By using the principle of catalytic oxidation at high temperatures and infrared detection, the method provides accurate, fast and reproducible results. It is an indispensable instrument in environmental, water, pharmaceutical and chemical industry laboratories, being a standard in modern carbon content determinations.

The VARIO TOC Analyzer offers numerous advantages over other carbon determination methods:

1. High accuracy and reproducibility thanks to automated control and sensitive detection.
2. Wide range of applications, from ultra-pure water to concentrated industrial effluents.
3. Short analysis time, which allows the analysis of a large number of samples in a short time.
4. Modular flexibility – the system allows adaptation to various types of samples (liquids, solids, suspensions).
5. Easy operation – the intuitive software allows the programming and automatic monitoring of analysis cycles.

To obtain accurate results, regular maintenance of the analyser and periodic calibration of the NDIR detector with standard carbon solutions are important. Also, complete removal of TIC is essential before TOC determination to avoid overlapping CO_2 signals.

Parameters such as reactor temperature, catalyst type, carrier gas flow rate, and sample volume can be optimized depending on the matrix being analysed to achieve the best analytical performance.

Operating principle

The Vario TOC analyzer operates on the basis of catalytic thermal oxidation of organic compounds at high temperatures (680–1200°C). Carbon is oxidized to carbon dioxide (CO_2), which is then quantified by an NDIR (non-dispersive infrared) detector.

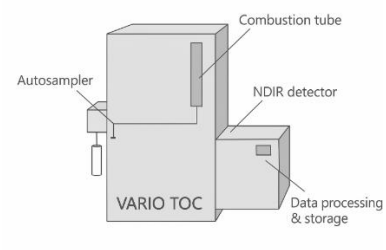

Figura 1. Schema Analizorului TOC şi DOC
https://pdf.directindustry.com/pdf/elementar/vario-toc-cube/117397-452807.html

Device components

• Automatic injection module
• Combustion oven
• NDIR detector
• Data processing software

Advantages of using Vario TOC

• Short analysis time
• High accuracy
• Full automation
• Possibility of analysing different types of samples

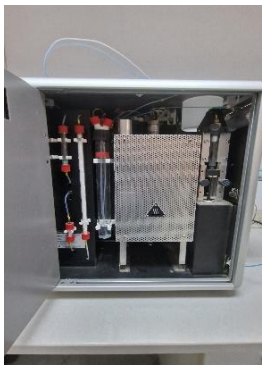

Figure 2. VARIO TOC ELEMENTAL - interior

Sample Preparation

For TOC analysis, liquid samples are typically filtered (for DOC) and may be treated to remove inorganic compounds, such as carbonates and bicarbonates, prior to analysis. In the case of TIC analysis, an acid treatment is applied to release CO_2 from the inorganic compounds.

Injection and oxidation

The sample is automatically introduced into the analyser's oxidation reactor, which is heated to high temperatures (typically between 680 and 950°C) in the presence of a catalyst (e.g., platinum or copper oxide). Under these conditions, the organic compounds in the sample are completely oxidized to CO_2 and H_2O.

Gas separation and detection

The gases resulting from the reaction (mainly CO_2 and water vapor) are transported by a carrier gas (usually synthetic air or oxygen) to a condensation unit, where the water is removed. The CO_2 is then directed to the NDIR detector.

CO_2 Measurement

The NDIR detector works on the basis of the absorption of infrared radiation by CO_2 molecules. The intensity of the absorption signal is proportional to the CO_2 concentration, and through prior calibration, this value is converted into carbon content.

Sampling:

Water samples were taken from the technological wastewater collection channel, from the premises of the Inerting Platform of the company SC STILO EVORA SRL. The sampling was carried out in October 2024 and March 2025. The sampling methods are those described in the standards SR EN ISO 5667-1:2022-"Water quality. Sampling. Part 1: General guide for establishing sampling programs and techniques" and SR ISO 5667-10:2021-"Water quality. Sampling. Part 10: Guide for sampling wastewater".

Contaminated soils:

Sampling was carried out in October 2024 and March 2025, taking samples from the contaminated soil dump that was to be inertised within the Inerting Platform. The sampling methodology was in accordance with STAS 7184/1-84 – "Soils. Collection of samples for pedological and agrochemical studies.

For the determination of TOC/DOC in the leachate, the same industrial soil sample was used, performing the leaching test according to SR EN 12457/4:2003 "Waste characterization. Leaching. Conformity test for leaching of granular waste and sludge. Part 4: Test with a batch stage liquid/solid ratio 10l/kg for materials with particle size below 10mm. (without size reduction)"

Sample preparation:

Technological wastewater:

The sample taken is subsampled, placing 50 mL of the sample in a Berzelius beaker, acidified with 2-3 drops of concentrated phosphoric acid. The acidified sample is checked with pH paper, if the pH is between 2-3 pH units the sample is bubbled with inert gas, then it is ready to be analysed.

Contaminated soil:

The sample taken will be air-dried in the laboratory for about 24 hours, then ground (by mortar or with a laboratory grinder so that it does not contain particles larger than 2mm).

After sieving on a 1mm mesh sieve, weigh 30g of sample on an analytical balance with a precision of 3 decimals into a crucible. Acidify with cc37% hydrochloric acid to eliminate the inorganic component, bicarbonates. (Avoid strong foaming, the amount of acid should not exceed 10 percent of the sample mass). The crucible will be dried in a water bath at 40^0C.

Figure 3. Contaminated soil sample

Leachate:

Leachate test:

Definition: the test in which a material is placed in contact with a leaching agent and certain constituents are extracted from the material.

Leaching agent: the liquid used in the leaching test (e.g. water)

Eluate: solution recovered from the leaching test.

The sample taken is crushed, sieved on a 4mm mesh sieve, then brought into contact with water under the conditions established by SR EN 12454-4/2003. The solid/liquid ratio will be 1:10, . The eluate will be kept under gentle agitation for 24 hours, then left to settle for 30 minutes, filtered on a vacuum pump with a 0.45µm membrane. The pH will be adjusted with nitric acid, until the level is between 2-3 pH units.

Device Calibration:

In order to be able to perform the determinations, the device must be calibrated/standardized by drawing a calibration curve and defining the measurement range. The device has 2 different modules, one for the liquid phase and one for the solid phase, the difference between them being the temperatures at which combustion occurs (solid module at 950^0C, liquid module at 850^0C).

To draw the calibration curve, analytical purity reagents were used, the water used was bidistilled water.

For the liquid module: the working range was defined from 0-100mg/l.
The standard solution of 1000 mgC/L was prepared from potassium acid phthalate, purity 99.9%, thus -2.125g $C_8H_5KO_4$ were dissolved in 1000 mL distilled water, resulting in a standard solution of 1000 mgC/L
From the standard solution, working solutions of cc 20 mg/L, 40 mg/L, 60 mg/L, 80 mg/L, 100 mg/L will be prepared, as follows in table 1.

Table 1.

Point on the curve	20mg/L	40mg/L	60mg/L	80mg/L	100mg/L
Standard solution	2ml	4ml	6ml	8ml	10ml
Distilled water	98	96	94ml	92ml	90ml

The concentrations are read, the device will display the peak area as a function of concentration, the R coefficient of the curve must be above 99.9%.

For the solid samples, the curve is drawn as follows: The oven temperature will be set to 9500C, for drawing the calibration curve, all potassium acid phthalate, $C_8H_5KO_4$, will be used.
According to SR EN 15936-2022 "Soil, waste, treated biowaste and sludge. Determination of total organic carbon content by dry combustion (indirect method). In this case, the concentrations that can be determined are those above 0.1%, or 1000 mg/kg. The calibration curve will be drawn for different masses of potassium acid phthalate (the C concentration for $C_8H_5KO_4$ is 47%).

$C_8H_5KO_4$ (mg)	**Peak area (mm^2)**
1	1203
2.1	2380108
3.7	3805474
8.1	8460673
10.8	11212678

Analytical method:
Working method for technological wastewater:
After acidifying the sample, you can proceed directly to reading TOC/DOC from the wastewater, the device draws a sample amount between 0.2-2 mL, then it will be evaporated in the presence of the Pt catalyst, CO_2 is detected, the result will be displayed depending on the peak area.

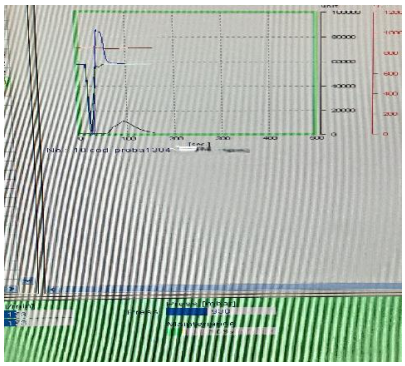

Figure 4. Sample reading example.

Working method for leachates:
In the case of leachates, the working method is identical to that for wastewater, after the eluate has been filtered on the vacuum pump, the sample will be read. If the determined concentrations are higher than the working range (i.e. <100mg/L) we will proceed to dilutions. The calculation of the result in the case of leachates will be done as follows:
Conc. read on the device x 10 (if the L/S ratio is 10:1).
Working method for soils:
From the acidified sample in the crucible, a quantity of 30-50mg will be weighed with an accuracy of 0.001g, which will be rolled into the previously weighed aluminium foil capsule. The capsule is manually inserted into the sample hole located on the upper part of the analyser. The device will make the determination by displaying the result in percentages, displaying TC=TOC (TIC being eliminated by prior acidification of the sample).
Analysed samples
The samples were taken in two sessions, the first in October 2024 and the second in March 2025. The determinations were made respecting the conditions of transport and preservation of the samples, in the SC

STILO MONITORING SRL Laboratory, in the commune of Suplacu de Barcau. Both samples of technological wastewater and samples of contaminated soil prepared for treatment were taken.

Results, experimental determination of TOC and DOC from soil and technological wastewater samples.
The results obtained from TOC and DOC determinations from samples taken on 21.10.2024 are presented in table 2.

Tabel 2. Results of sample analysis taken on 21.10.2024

Sample	TOC/DOC (mg/L / mg/kg)	Maximum allowed value
Wastewater	3.4 mg/L	5*
Contaminated soil leachate (Before inertization treatment)	869 mg/kg	500**
Contaminated soil	7850 mg/kg	30000**

*Decision 352 of 21.04.2005, amending and supplementing GD 188/2002 for the approval of certain norms regarding the conditions for the discharge of NTPA-001 wastewater into the aquatic environment.
**ORDER 95 OF 12.02.2005 regarding the preliminary procedures for accepting waste at landfills and the national list of waste accepted in each class of landfill.
**Order no. 756/3.11.1997 for the approval of the Regulation regarding the assessment of environmental pollution. Chemical pollutants in soil.

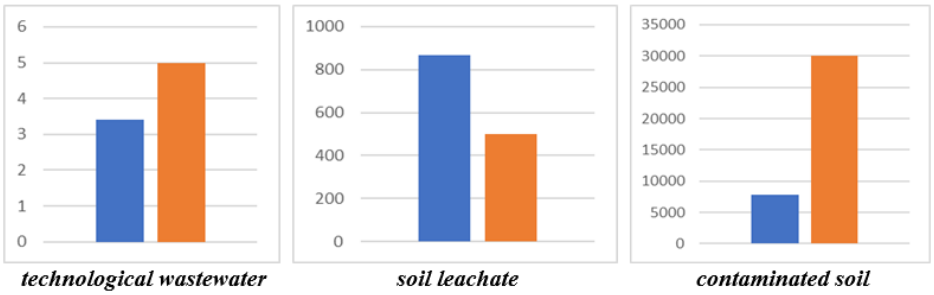

Fig.5.Comparative graphic representation of the results obtained for the samples taken on 21.10.2024

Tabel 2. Results of sample analyses taken on 12.03.2025

Sample	TOC/DOC (mg/L / mg/kg)	Maximum allowed value
Wastewater	2.8 mg/l	5*
Contaminated soil leachate (Before inertization treatment)	324 mg/kg	500**
Contaminated soil	5425 mg/kg	30000**

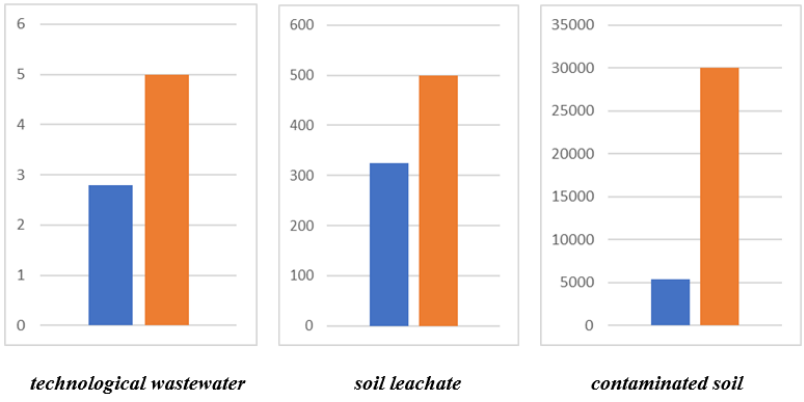

Fig.6. Comparative graphic representation of the results obtained for the samples taken on 12.03.2025

DISCUSSIONS

Regarding the values of technological wastewater, in both sampling sessions the values fall within the limits allowed by the legislation in force, respectively NTPA-001.

Regarding the values obtained for leaching from contaminated soil, a value exceeding the legally allowed limit can be observed in October 2024 before treating the soil with a binder that will block the leaching of chemical elements.

The TOC value for the soil falls within the maximum allowed limit in both sampling situations.

The Vario TOC Elemental instrument provided a reliable platform for the complete oxidation of organic compounds and the measurement of total carbon content, both in the solid and liquid phases. By using catalytic combustion technology and non-dispersive infrared (NDIR) detection, high accuracy of the determinations could be ensured. Also, the possibility of differentiating between TOC, TIC (total inorganic carbon) and DOC brings added value in the analysis of environmental quality and industrial processes.

The examples presented in the paper demonstrated not only the practical applicability of the method, but also the need for constant monitoring of organic parameters of water and soil, especially in the context of increasingly strict environmental regulations. The determinations made can constitute an important analytical support in processes of monitoring pollution sources or in ecological impact studies.

CONCLUSIONS

The use of the Vario TOC Elemental device in the determination of TOC and DOC represents a modern, fast and efficient method for the characterization of organic compounds in liquid media. Considering the results obtained, this technique is recommended for environmental laboratories, water treatment plants and research institutions, contributing to a more responsible management of aquatic resources and to the protection of the environment.

Bibliography

[1] APHA Standard Methods for the Examination of Water and Wastewater, 23rd Edition, 2017, https://www.scirp.org/reference/referencespapers?referenceid=2459667, 23.05.2025

[2]Manual de utilizare Vario TOC, Elementar GmbH, https://pdf.directindustry.com/pdf/elementar/vario-toc-cube/117397-452807.html, 23.05.2025

[3]Rump, H. H., Krist, H., Laboratory Manual for the Examination of Water, Wastewater and Soil, 1992, https://www.amazon.com/Laboratory-Manual-Examination-Water-Waste/dp/3527284400, 23.05.2025

[4] Hotararea 352 din 21.04.2005,privind modificarea si completarea HG 188/2002 pentru aprobarea unor norme privind conditiile de descarcare in mediu acvatic a apelor uzate NTPA-001.

[5]ORDINUL 95 DIN 12.02.2005 privind procedurile preliminare de acceptare a deseurilor la depozitare si lista nationala de deseuri acceptate in fiecare clasa de deposit de deseuri.

[6]Ordin nr 756/3.11.1997 pentru aprobarea Reglementarii privind evaluarea poluarii mediului .Poluanti chimici in sol.

[7]Directivele europene privind apa potabilă și protecția solului.

[8]SR EN 12457/4:2003"Caracterizarea deseurilor.Levigare.Test de verificare a conformitatii pentru levigarea deseurilor granulare si a namolurilor.Partea 4:Test cu o etapa de sarja raport lichid/solid 10l/kg pentru materiale cu dimensiunea particulei sub 10mm.(fara reducerea dimensiunii)"

[9]SR EN ISO 5667-1:2022-" Calitatea apei.Prelevarea.Partea1:Ghid general pentru stabilirea programelor si a tehnicilor de prelevare" si SR ISO 5667-10:2021-"Calitatea apei. Prelevare.Partea 10:Ghid pentru prelevarea apelor uzate".

[10]SR EN 1484:2001 Analiza apei.Linii directoare pentru determinarea carbonului organic total si a carbonului organic dizolvat.

[11]SR EN 15936-2022-Sol,deseuri biodeseuri tratate si namol. Determinarea continutului de carbon organic total prin combustie uscata.

[12]SR CEN/TR 16192/2020-Deseuri. Linii directoare pentru analiza eluatelor.

DETERMINATION OF THE PHYSICO-CHEMICAL PROPERTIES OF NATURAL AGGREGATES FOR ROADS (PART I)

Iuliana-Laura TIMIS (TOMOIOAGA)[1], Gabriela Elena BADEA[2], Sorin HODISAN[2], Alexandru BADEA[1], Petru CREȚ[3], Rares Mihnea HODISAN[4]

[1]University of Oradea, Faculty of Informatics and Sciences, student
[2]University of Oradea, Faculty de Informatics and Sciences, Department of Chemistry
[3]University of Oradea, National Centre of Geothermal Research, Oradea
[4]Iuliu Hateganu University of Medicine and Pharmacy, Cluj-Napoca, Romania

Abstract: *The category of natural aggregates for roads includes materials of mineral origin obtained by extracting and manually or mechanically processing rocks from massive deposits, in shapes and sizes necessary for road works. Minerals are substances, well individualized from a chemical and physical point of view, which, isolated or grouped in different ways, form a wide variety of rocks, which differ from each other in: the mode of formation, their mineralogical composition, their structure and texture. The essential quality conditions are related to the following characteristics: intrinsic characteristics of the source rock that cannot be improved (improved): mineralogical, physical (porosity), mechanical (compressive strength, wear resistance), manufacturing characteristics that can be improved: grain size, grain shape and impurity content, complementary, specific to limited areas of use such as: angularity, adhesiveness, reactions to alkalis, etc. Each rock must meet certain conditions related to physical and mechanical characteristics, depending on the type of product to be obtained, the field of application and the technical class of the road or the category of street on which it is to be used.*

Key words: aggregates,rocks,minerals,sand,huma,granules,density

1.INTRODUCTION

Based on these characteristics, rocks are divided into three main categories:[1]

Igneous rocks, which are formed by the cooling and solidification of molten material (generic name magma) that has emerged from the Earth's interior. The character of the rocks formed depends on how the magma cooled and solidified. If the cooling occurred slowly, at great depth in the Earth's crust, all the minerals in the composition of the magma were able to crystallize completely, forming a uniform, granular structure in which all the elements are well crystallized. These rocks are known as intrusive or deep-seated and are found in the form of massive deposits, called batholiths. If the cooling was somewhat faster, in the layers at the surface of the crust, then only a part of the minerals were able to crystallize completely during the consolidation of the magma, and the rest remained either in the form of a mass of very fine crystals, or in the form of an amorphous mass. The rocks thus formed have a semi-crystalline structure. Deposits of such rocks are very close to the surface of the crust. If the cooling occurred suddenly, by the exit of magma to the surface of the crust, in the form of leaks or gases that gathered in depressions, no mineralogical element could crystallize and the formed rock presents itself with a completely glassy or vitreous structure. The main igneous rocks found in our country are: granites, granodiorites, rhyolites, dacites, trachytes, diorites, andesites, gabbros, basalt, diabases, etc.[1]

Sedimentary rocks originate from the deposition of fragments resulting from the disintegration and crumbling of the rocks that make up the earth's crust under the direct action of atmospheric agents (rain, wind, repeated freezing-thawing, permanent variations in humidity-dryness), rivers and glaciers. The mineralogical nature of sedimentary rocks depends on the nature of the rocks in the basin from which they were dislocated and transported.

According to their origin and mode of formation, sedimentary rocks are divided into three groups: rocks of mechanical or detrital origin are made up of materials resulting from

the disintegration of pre-existing rocks, transported and deposited by waters in depressions of the earth's crust [1-14].

These rocks are divided into the following groups:[2]

a. Mobile or uncemented rocks:
- gravel and boulders
- sands
- dusts

b. Consolidated or cemented rocks:
- conglomerates - formed by the cementation of rounded materials from pebbles
- breccias - formed by the cementation of angular materials from scree
- sandstones - formed by the cementation of sands

Rocks of chemical or precipitation origin are formed by the precipitation of substances dissolved in water. In this way, the following rocks were born: [3]

- gypsum, anhydrite, sodium chloride, etc. deposited in the waters of the seas and oceans;
- freshwater limestone deposited in the waters of lakes and travertine deposited in the waters at the mouths of springs.

Rocks of organic origin, formed by the accumulation of skeletons and remains of plants and animals, deposited and mineralized in waters. This is how limestones were born, in which calcium carbonate predominates.

Sedimentary rocks are characterized by high porosity and pronounced stratification, with an uneven texture, pores or cracks, and a content of unstable minerals, which causes mechanical resistance to be reduced and to differ according to the direction of the stress.[4]

Metamorphic rocks come from igneous or sedimentary rocks that, under certain temperature and pressure conditions, have undergone transformations in terms of texture, structure and mineralogical composition.

Metamorphic rocks are characterized by a pronounced crystalline structure and a pronounced schistosity, with minerals grouped in separate layers (they are also called crystalline schists). The most widespread metamorphic rocks in our country are: gneisses, crystalline limestones, quartzite. [5]

Rocks can also be classified by their silicon dioxide SiO_2 content, as follows:[6]

- acidic rocks, with a content of 65÷75% SiO_2
- neutral rocks, with a content of 50÷65% SiO_2
- basic rocks, with a content of 40÷50% SiO_2

Acidic rocks are not recommended for use in the preparation of asphalt mixtures because the binder (bitumen) does not have good adhesion to the surface of acid rocks. In the case of using these aggregates in the preparation of asphalt mixtures, to improve adhesion, it is necessary for the bitumen to be added with surfactants. The adhesion of bitumen to rock decreases in the following order: limestone, basalt, porphyry, granite and quartz.

Basic rocks provide good adhesion to bitumen, which is why they are mainly used in the preparation of asphalt mixtures.

Differentbtypes of rocks are presented in figure 1 and 2, [6]

Figure 1. General clasification of rocks

Figure 2. Types of rocks

Natural aggregates are granular materials of mineral origin, resulting from the natural or artificial crushing of rocks. Natural aggregates resulting from the natural crushing of rocks are called natural ballast aggregates, and those resulting from the manual or mechanical crushing of boulders or raw quarry stone form the group of natural aggregates and processed stone for roads (figures 3 and 4).

Depending on their nature we have: [7]

- mineral aggregates
- organic aggregates

Depending on the size of the granules:from natural rock crushing (ballast aggregates), Sand 0 - 4 mm; Gravel 4 - 31 mm; Large stone 63 - 350 mm; Ballast (natural mixture) 0 - 63 mm

Figure 3. Ballast aggregates

From artificial crushing of rock: Crushing sand 0-4 mm; Screening 4-25 mm;Slag 0-8 (16) mm;Broken stone (split) 8-40 mm;Large broken stone 40-80 mm;Rough stone >80 mm

Figure 4. Quarry aggregates

Natural aggregates for ballast (sand, gravel, ballast) can be unprocessed or processed by washing, sorting, crushing (to correct the grain size), according to the needs imposed by the works for which they are to be used. They are found in riverbeds, in ballast pits and in some isolated natural deposits. [7]

2. EXPERIMENTAL

DETERMINATION OF SAND EQUIVALENT (EN)

Preparing the washing solution : Dissolve (219 ± 2) g of crystalline calcium chloride in (350 ± 50) ml of distilled or demineralized water, cool to room temperature and, if necessary, filter through a medium or coarse filter paper. Add (480±5) g of glycerin and (12.5±0.5) g of formaldehyde solution and dilute to 1:1 solution with distilled or demineralized water and mix well.

The determination includes the following steps (figure 5):

Using the funnel, pour a 100±20g test sample (sifted on a 4-0.063 mm sieve) into each graduated cylinder, holding the cylinder vertically. Siphon the washing solution into each graduated cylinder up to the lower mark on the cylinder. Gently tap the bottom of each cylinder several times, using the palm of your hand, to dislodge air bubbles and facilitate wetting of the test sample.

Allow each cylinder to soak for (10±1) min. At the end of the 10-minute period, seal a cylinder using one of the rubber stoppers and attach the cylinder to the shaker. Shake the cylinder for (30±1)s then remove the cylinder from the shaker and place it in a vertical position.

Remove the rubber cap from a graduated cylinder and rinse it over the cylinder using the washing solution, ensuring that all material is returned to the cylinder. Insert the wash tube into the cylinder, first rinse the walls of the cylinder using the wash solution

and then push the tube down through the sediment to the bottom of the cylinder.

Allow each graduated cylinder to settle, undisturbed and free from vibration, for (20±0.25) min. At the end of this period, the height h1 of the upper level of the suspension relative to the base of the graduated cylinder is measured.

Carefully lower the piston assembly into the cylinder until the end piece rests on the sediment. Locate the collar over the cylinder and then lock it onto the piston rod.

.

3. RESULTS AND DISCUSSIONS

The sediment height h_2 is determined by measuring the distance between the lower face of the piston head and the upper face of the collar using the graduated ruler inserted into the slot in the collar.

Record the heights h_1 in millimeters. Also record h_2 to the nearest millimeter and calculate the ratio $(h_2 / h_1) \times 100$ for each cylinder.

The experimental results of the sand equivalent of analysed rocks are presented in table 1.

Figure 5. Sand Equivalent Test Steps

Table 1. Sand equivalent test results

Sand equivalent 19.09.2024		U.M.	Test no.	
			1	2
Rest time after pouring sand into the cylinder and tapping with the palm to eliminate bubbles		10 minutes	10:25	10:38
Decanting time, after shaking (30 sec) and washing, without disturbing or vibrating the cylinder		20 minutes	10:49	11:02
The upper level of the clay slurry	h_1	[mm]	97	96
The upper level of sand	h_2	[mm]	78	77
S.E=(h_2/h_1)x100		[%]	80,4	80,2
Mediate		[%]	80,3	

4. CONCLUSIONS

Acidic rocks are not recommended for use in the preparation of asphalt mixtures because the binder (bitumen) does not have good adhesion to the surface of acidic rocks.

Sand (0-4 mm) is the natural aggregate of ballast, mainly used for the construction of insulating road layers and cement-stabilized sand, for the construction of macadam and pavements, for the preparation of asphalt mixtures and cement concretes and for the construction of the distribution layer on railways, it must have continuous grain size, sand equivalent (EN) min.30-85, humus (color of sodium hydroxide solution) to be colorless or yellow.

Crushing sand is artificially crushed natural aggregate with dimensions of 0…4 mm. Its grain size must be continuous, free of foreign bodies and with a content of grains larger than 4 mm of max. 5%.

5.REFERENCES

[1] SR 667:2000 Agregate naturale și piatră prelucrată pentru lucrări de drumuri. Condiții tehnice de calitate

[2] SR EN 932-1:1998 Încercări pentru determinarea caracteristicilor generale ale agregatelor. Partea 1: Metode de eşantionare

[3] SR EN 933-1:2012 Încercări pentru determinarea caracteristicilor geometrice ale agregatelor. Partea 1: Determinarea granulozității. Analiza granulometrică prin cernere

[4] STAS 9110- 87 Pietre naturale prelucrate pentru construcții. Reguli și metode de verificare a calității

[5] SR EN 933-8+A1:2015 Încercări pentru determinarea caracteristicilor geometrice ale agregatelor. Partea 8: Evaluarea părților fine. Determinarea echivalentului de nisip

[6] Badea G.E., Bazele fizico-chimice ale tehnologiei chimice - Note de curs. Universitatea din Oradea, 2024.

[7] SR 662:2002 Lucrări de drumuri. Agregate naturale de balastieră. Condiții tehnice de calitate

[8]Mondem, N., Balunaini, U. (2025). Optimal Blends of Artificial and Natural Aggregates for Enhanced Pavement Performance. In: Saride, S., Chennarapu, H., Padmavathi, V. (eds) GeoPractices Towards Sustainable Infrastructure, Volume 1. GeoPrac 2024. Lecture Notes in Civil Engineering, vol 589. Springer, Singapore. https://doi.org/10.1007/978-981-96-3220-6_4

[9]Cantisani, G., Del Serrone, G., Moretti, L. et al. Performance Evaluation of Recycled Aggregates from Concrete Railway Sleepers for Unbound Subbase and Base Layers. Transp. Infrastruct. Geotech. 12, 184 (2025). https://doi.org/10.1007/s40515-025-00643-3

[10]AbdElMoaty, A.M.N., Ibrahim, H.H.A. & Ismail, M.K. Mechanical and transport properties of concrete incorporating recycled crushed clay bricks as coarse and fine aggregates. Sci Rep 15, 31782 (2025). https://doi.org/10.1038/s41598-025-16833-5

[11] Sahu, P., Dalai, R. & Sahu, R.L. Experimental Study, Using Recycled Aggregates in Mix Design of Granular Sub Base (GSB) Layer “Close Graded: Grading II Gradation”. Indian Geotech J 55, 512–520 (2025). https://doi.org/10.1007/s40098-024-00881-1

[12] Mambou, L.L.N., Kenmoe, O.R.M., Elat, E. et al. Geological and geotechnical characterization of Ntambeng basalt massif used as aggregates in civil engineering (North-West Cameroon). Discov Geosci 2, 91 (2024). https://doi.org/10.1007/s44288-024-00099-x

[13] Cruz, G.K.A., Arruda, S.M., de Medeiros Melo Neto, O. et al. Comparative analysis of lateritic and granitic aggregates in asphalt mixtures: morphological properties and performance implications. Innov. Infrastruct. Solut. 9, 150 (2024). https://doi.org/10.1007/s41062-024-01472-y

[14] Ok, B., Colakoglu, H. Evaluating the usability of recycled aggregates as fill materials depending on the composition and strength of their grains. Front. Struct. Civ. Eng. 18, 1713–1729 (2024). https://doi.org/10.1007/s11709-024-1115-x

PHYSICO-CHEMICAL STUDY OF THE ESSENTIAL OIL SEPARATED FROM BAY LEAVES (LAURUS NOBILIS L.)

Horea-Radu SEBEŞAN[1], Mioara SEBEŞAN[2] Francisc-Ioan HATHAZI[1], Radu SEBESAN[1], Gabriela –Elena BADEA[2]

[1]*University of Oradea, Faculty of Electrical Engineering and Information Technology, Universitatii 1st., RO-410087, Oradea,Romania*

[2]*University of Oradea, Faculty of Informatics and Sciences, Universitatii 1st., RO-410087, Oradea, Romania*

E-Mail: msebesan@uoradea.ro

Abstract: This paper presents physico-chemical analyses of bay essential oil (laurus nobilis L.). Bay essential oil was analyzed using gas chromatography to determine its chemical composition and identify its main chemical constituents. The antioxidant activity of bay leaf essential oil (laurus nobilis L.) was determined using the 2,2-diphenyl-1-picrylhydrazyl (DPPH) method.

Key words: *gas chromatographic analysis, UV-VIS spectrophotometry, antioxidant activity*

INTRODUCTION

Recently, there has been an increase in the interest of the food and pharmaceutical industries in natural compounds. It has been found that the direct addition of natural products (oils or extracts) of some aromatic plants to food products or medicines exerts an antioxidant and/or antimicrobial effect, due to their free radical scavenging properties., [1].

Bay essential oil contains polyphenols, powerful antioxidants, [2]. This information suggests that bay leaves may help regulate and even prevent diabetes and other cardiovascular diseases. Bay oil is a secondary ingredient and is the distinctive fragrant characteristic of Aleppo soap. According to the pharmacological action, essential oils act exactly like any other natural or synthetic chemical substance and there is no difference between essential oils and synthetic drugs. They all activate or deactivate a process that is happening in the body, but do not remove the cause of the imbalance. They only help the body to balance its already existing mechanisms, [3, 4].Essential oils are much gentler in action than allopathic drugs, so the body puts more effort into healing itself. Which is desirable, but the body doesn't always have the resources to recover with minimal help.Bay essential oil has antibacterial, antiseptic and antiviral properties, is also antispasmodic and helps relieve muscle pain. It is an expectorant (easier breathing), fights cold symptoms and is a tonic for the skin and scalp.Plants and other natural sources can provide a wide range of complex and structurally diverse compounds. Plant extracts and essential oils present a number of properties: antifungal, antibacterial and antiviral. They have been analyzed on a global scale as potential sources of new antimicrobial compounds, agents that promote food preservation and alternatives for treating infectious diseases, [5,6].Bay essential oil (Laurus nobilis) is obtained by steam distillation of the leaves. Among the Lauraceae family, bay leaves stand out for their culinary uses and aromatic virtues.

Figure 1. Bay leaves

Natural antioxidants are a series of atoms joined together by chemical molecules, which help protect other molecules by inhibiting the oxidation process, [7,8].

Most of the components of bay leaf volatile oil belong to the category of monoterpene

hydrocarbons, which represent 70-80% of the oil's composition.

Components that have been identified in some bay leaf oils are: α and β-pinene (10-25%), γ and β-phellandrene (5-10%), linalool (10-20%), geraniol, α-terpineol, 1,8-cineole (50-70%), also known as eucalyptol, borneol, terpinene (10%), 1-methyl-4-(1-methyl ethylidene)-cyclohexene, eugenol, methyl-eugenol, etc. Table 1. presents the components of bay leaf volatile oil and some of their particularities, [9-11].

Table 1. Chemical structure of the constituents of the volatile oil from bay leaves.

Name	Structure	Name	Structure
1,8-cineole	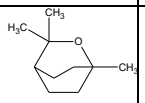	β-phellan-drene	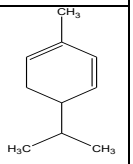
α-pinene	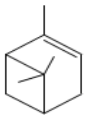	linalool	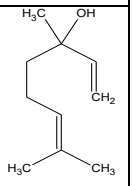
β-pinene	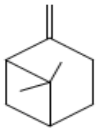	borneol	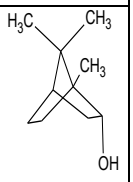
α-terpinene	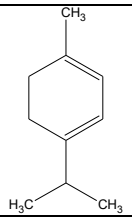	geraniol	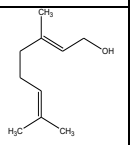
1-terpinene-4-ol sau α-terpinenol	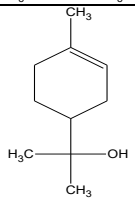	γ-felandre-ne	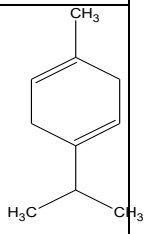

MATERIALS AND METHODS

1. Gas chromatography (GC) analysis of bay essential oil

Gas chromatography represents the analysis of volatile organic compounds found presents in the vapor phase. The analysis it done usually performed with a temperature program in the range of 40 – 300ºC. The samples subjected to analysis, can be separated beforehand by extraction, distillation or steam extraction methods, respectively can be taken from the space above the materials containing such compounds (headspace analysis, SPME or pervaporation) [12, 13, 14].

For gas chromatographic analysis we used the following conditions:

- capillary column TG -5 MS 30 m, I.D. 0.25 mm, film 0.25 µm.
- The sample from the bay oil was processed diluted 1: 50, in dichloromethane. Is obtained a gas chromatogram of the type in the work, from which can be determined the mass concentrations of each odorant - flavoring component present in the essential oil.

2. Spectrophotometric determination of antioxidant activity, [15,16]

The antioxidant activity of bay essential oil was determined using the 2,2-diphenyl-1-picrylhydrazyl (DPPH) method. Known as a powerful radical "scavenger" for neutralizing or suppressing free radicals, DPPH is a solid material (black crystalline powder formed from stable free radical molecules).A spectrophotometric method used to determine the antioxidant capacity of a substance is the hydrogen donation or scavenging free radical method by the DPPH (1,1,-diphenyl-2-picrylhydrazyl) method. This method is used to determine the levels of antioxidants in complex biological systems. The process are basic reaction for determining antioxidant activity by the DPPH method is shown in figure 2.

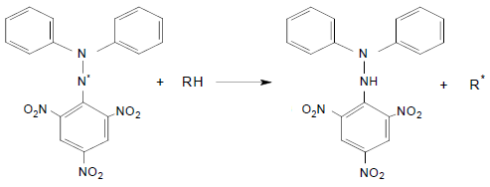

Figure 2. Structure of the 2,2-diphenyl-1-picrylhydrazyl radical (DPPH)·

$I\%(t) = A_{518nm}(t)/ A_{518nm}(t = 0)\cdot 100$

I%(t) depending on the concentration of the solutionsThe 1 mg/ml solutions were diluted to final concentrations of 200, 100, 50 µg/ml in 96% ethyl alcohol. The solutions of different concentrations were mixed: the volume of 1.5 ml with 2.5 ml of ethanolic DPPH solution (0.004%). After 30 minutes of incubation in a place protected from light and at room temperature, the absorbances of the solutions were measured at a wavelength of 518 nm.

The antioxidant activity is determined as follows: 1.5 ml of the solution to be analyzed is mixed with 2.5 ml of 0.004% DPPH solution (4mg = 0.004g in 100 ml of alcohol, ethanol or 0.002 g in 50 ml of alcohol) and then left in the dark for 30 minutes, after which it is introduced into the sample cuvette of the spectrophotometer and the recording is started.

The reaction mixture contains 0.004% DPPH and the test samples; after mixing, the absorbance at 518 nm is recorded; the solution discolors over time as DPPH reacts with the free radicals in the system, and the progress of the reaction is monitored spectrophotometrically. All readings are made against 96% ethanol as a reference.

The antioxidant activities of the samples are evaluated from the curves of the relative absorbance (A%), as the ratio between the absorbance at time t and the initial absorbance (at t= 0) corresponding to the calibration solution.

$$A\%(t) = \frac{A_{518nm}(t)}{A_{518nm}(t=0)} \cdot 100$$

The lower the A%, the higher the antioxidant activity of the studied sample.

The absorbances of the 4 solutions of different concentrations (1mg/1ml, 200 µg/1ml, 100 µg/1 ml, and 50 µg/1 ml) of bay essential oil were measured at 518 nm, in 1 cm cuvettes, against the absolute ethanol solution.

RESULTS AND DISCUSSION

Results of gas chromatographic analysis for bay essential oil

GC-MS is currently the most widely used technique for the analysis of odorants and flavors. GC-IR and GC-FTIR are complementary techniques for these complex analyses.

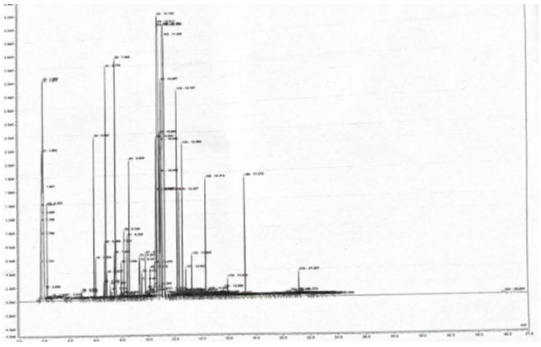

Figure 3. Gas chromatogram of bay essential oil

The technique, GC-MS coupling, usually uses databases of MS spectra with which the data for the separated compounds can be automatically compared and the most probable structures (hits) that can be identified with the real structures can be obtained, [25].

The very large amount of data obtained by gas chromatography following the gas chromatography-mass spectrometry (GC-MS) analysis of the essential oil separated from bay leaves *(Laurus Nobilis L.*) has been evaluated and is presented below.

The chemical compounds, mostly terpenes and terpenoids, which give the aromatizing properties of this oil and which have been identified in bay essential oil by GC-MS chromatography are listed in table 2.

Table 2. Composition of bay essential oil for the sample taken and diluted in CH_2Cl_2.

Registration no.	Product name	Name of the substance	RT(min)	Relative area
4815		m-xilen	3,54	0,01
4816		2-Thujene	5,66	0,79
4817		α-Pinene	5,98	2,41
4819		Camphene	6,33	0,12
4820		β-Pinene	6,57	0,06
4821		1,8-cineole	6,88	3,77
4822		γ-Terpinene	7,04	0,17
4824		p-Cymene	7,49	0,16
4825		3-Carene	7,19	1,09
4826		β-Ocymene	7,38	0,66
4827		Linalool	7,71	0,51
4828		Bornyl-acetate	7,89	0,05
4829		β-Ocymene	8,77	0,03
4830		α-Terpineol	8,83	0,05
4831		3,6-Dimethyl-6-heptan-4-yn-3-ol	8,95	0,07
4832		Cyclopropanecarboxylic acid, 4-nitrophenyl ester	9,10	0,03
4833		Terpenyl acetate	9,25	0,74
4834		Limonene	9,40	0,68
4835		Eugenol	9,54	1,71
4836		5,5-Dimethyl-3-heptyne	9,76	0,01
4837		Metyl- Eugenol	10,86	0,01
4838		Borneol	10,98	0,02
4839	Bay essential oil	3,6-Dimethyl-6-heptan-4-yn-3-ol	11,04	0,01
4840		Geraniol	11,34	3,08
4841		α-Citral	11,58	2,15
4842		Citronellol acetate	12,06	3,42
4843		Neoisopulegol	12,44	0,01
4844		α-Hexyl-Cinnamaldehyde	12,82	0,01
4845		α-Phellandrene	12,96	0,02
4846		Linalyl acetate	13,04	0,01
4847		1-(2,4-Dihydroxyphenyl)-2,4-methoxy-3-nitrophenyl)ethanone	13,54	0,05
4848		(3E,7E,11E)-1-Isopropyl-4,8,12-trimethylcyclotetradeca-3,7,77-trienol	14,08	0,05
4849		Oxiranem,2,2-dimethyl-3-(3,7,12,16,20-pentamethyl-3,7,11,15,19-heneicosapentaenyl)-,(all-E)-	14,41	0,30
4850		24-Norusa-3,12,diene	15,10	0,02
4851		Cyclopentenacetic acid, 3-oxo-2-phentyl-2-methyl ester	15,24	0,05
4852		Bicyclosesquiphellandrene	15,78	0,01

The sample was processed diluted 1:50 in CH_2Cl_2.The capillary column used was TG-5MS 30m, internal diameter 0.25 mm, film 0.25 µm.

2.Results of determining antioxidant activity by the DPPH method

The absorbance values at 518 nm of the analyzed samples, based on which was calculated the antioxidant activity for $A_{518nm}(t = 0) = 0.103$, are presented in table 3.

Table 3. Absorbance values at 518 nm, A%(t) of the 4 bay essential oil solutions

Samples of bay essential oil	Solution 1 (1mg/1 ml)	Solution 2 (200 µg/1 ml)	Solution 3 (100 µg/1 ml)
Absorban-ce value $A_{518}(t)$	0.0598	0,0782	0,0841
Inhibi-tion %	58.058	75.922	81.650

The antioxidant capacity by the DPPH method had high values. Thus, the bay essential oil presented the values in the table of antioxidant activity measured by the DPPH method.Thanks to these tests were confirmed the antioxidant properties of bay essential oil.

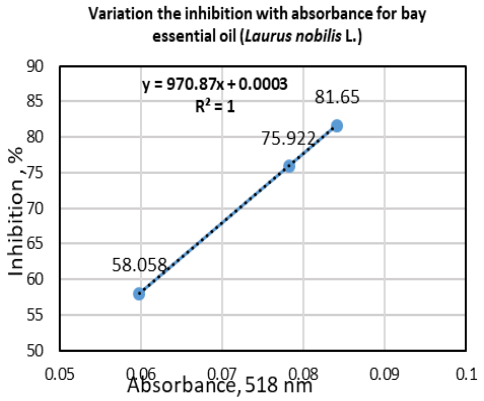

Figure 4. % Inhibition or antioxidant activity for bay essential oil.

For interpret the results obtained with the DPPH method, was introduced a parameter called "effective concentration" or IC_{50} value (or EC_{50}, as some authors call it) defined as the substrate concentration value, that causes a 50% reduction activity for DPPH.

Antioxidant activity is expressed as IC_{50}, defined as the concentration of test material required, to reduce the initial DPPH concentration by 50% (causes a 50% decrease in the initial DPPH concentration).

The DPPH method is used to determine the antioxidant/anti-radical activity of pure

phenolic compounds as well as natural extracts, [12].
Some researchers have reported that most phenolic compounds reactions slowly with DPPH, requiring several hours.
Thes, indicates that using DPPH, antioxidant activity should be evaluated in a timely manner because the interference of the 2,2-diphenyl-1-picrylhydrazyl (DPPH) color with that of the samples will lead to an underestimation of the antioxidant activity.

CONCLUSIONS

The purpose of the paper was to present the results of gas chromatographic analysis and to highlight the antioxidant properties by spectrophotometric analyzes of bay essential oil.The chemical composition of a bay essential oil (Laurus Nobilis L.) was established, determining the bioactive compounds in this oil by mass spectrometry (MS) coupled with gas chromatography (GC-MS) from a bay essential oil used in food and aromatherapy.
Mass spectrometry is a suitable method for the study of substances because it provides a lot of information about the structure and composition of a sample. Mass spectrometry, MS, including GC-MS coupling, is the most widely used technique in chemical analysis for the evaluation of the chemical composition of a sample, [17-20]
The antioxidant activity of a system can be estimated by spectrophotometric monitoring of the color reactions that occur when 2,2-diphenyl-1-picrylhydrazyl radicals, DPPH, are reduced by the tested substrate - in our case, solutions of bay essential oil (the DPPH solution in contact with the sample to be analyzed, discolors and the progress of the reaction is monitored spectrophotometrically at 518 nm).
The results obtained indicated that ethanolic solutions of bay essential oil (Laurus Nobilis L.) have significant antioxidant activity.

BIBLIOGRAPHY

[1]. Safta M. (2002). *Super-Antioxidanţi naturali în alimentaţie şi medicină*, Secretul sănătăţii şi longevităţii, Ed. Sudura, Timişoara.
[2]. D.Hădărugă, N.Hădărugă, (2002).*Compuşi odoranţi şi aromatizanţi*, Editura Politehnica Timişoara, Timişoara.
[3]. Ernest J. Parry, B.Sc. (2022). F.I.C., F.C.S.*, The chemistry of essential oils and artificial parfums*, Fourth Edition, Resived and Enlarged , nr.1, pg.1-58
[4]. Nouri A., Mirabzadeh M., Safari N., Ebadi M.T. (2020) . *J. Med. Plants By-Prod., 9*, pg. 159–166.
[5]. Nurzy´nska-Wierdak R., Bogucka-Kocka A., Szymczak G. (2014). *Nat. Prod. Commun*. *9*, pg. 703– 706.
[6]. Ibarra A., Feuillere N., Roller M., Lesburgere E., Beracochea D.(2010). *Phytomedicine* , *17*, pg. 397–403.
[7] Jitoe, A., Masuda, T., Tengah, I. G. P., Suprapta, D. N., Gara, I. W., & Nakatani, N. (1992). Antioxidant activity of tropical ginger extracts and analysis of the contained curcuminoids. *Journal of Agricultural and Food Chemistry*, 40, pg.1337–1340.
[8] Ka¨hko¨nen, M. P., Hopia, A. I., Vuorela, H. J., Rauha, J. P., Pihlaja, K., Kujala, T. S., et al. (1999). Antioxidant activity of plant extracts containing phenolic compounds. *Journal of Agricultural and Food Chemistry,* 47, pg.3954–3962.
[9] A.V. Tkachev. (2008). *Cercetarea uleiurilor volatile din plante*, Editura si topografia“Afset”, Novosebirsk , pg. 969.
[10] Baser, C. H. K. and Buchbauer, G. (2010). *Hand book of essential oils: Science, technology and applications*. Raton Florida: CRC Press, Boca Raton, New York.
[11] C. Cristea, I. Hopartean, I.A. Silberg, (2002), *Chimia organică a produşilor naturali*, Ed. Risoprint, Cluj – Napoca.
[12]. Anshory, H., & Nugraha, A. T. (2017). Gas chromatography – Mass spectrometry analysis and antibacterial activity, *International Conference on Chemistry, Chemical Process and Engineering ,* 020073.
[13].Adams, R. P. (1995). *Identification of essential oils components by gas chromatography/mass spectroscopy*. Allured Publ. Corp., Illinois.
[14]. Naşcu H., Jäntschi L. Hodişan T., Cimpoiu C., Câmpan G.(1999). Some Applications of Statistics in Analytical Chemistry, *Review Anal. Chem.*

[15] Tanruean K, Kaewnarin K, Rakariyatham N. (2014). Antibacterial and antioxidant activities of *Anethum graveolens* L. dried fruit extracts. Chiang Mai Journal of Science, 41(3):649-660.
[16] Frankel, S., & Berenbaum, M. (1999). Effects of light regime on antioxidant content of foliage in a tropical forest community. *Biotropica,* 31, 422–429.
[17]. Culea M. (2008). *Spectrometrie de masă.Principii și aplicații,* Risoprint, Cluj – Napoca.
[18]. McMaster M., McMaster C. (1998). GC/MS *A practical User's Guide, Wiley VCH U.S.A.*
[19]. Culea M. E. Culea, (2004).*Metode fizice de analiză,* Risoprint, Cluj – Napoca.
[20]. Al-hashemi, F. H. Y. (2014). Chromatographic Separation and Identification of some Volatile Oils, Organic Acids and Phenols from the Seeds of *Cuminum Cyminum* Growing in Iraq. *International Journal of Recent Research and Applied Studies.* 19 (1),pag. 80–90.

RECOVERY OF ALUMINUM FROM WASTE AND ITS USE IN THE SYNTHESIS OF ALUMINUM AND POTASSIUM ALUM USED IN THE PREPARATION OF ANTIPERSPIRANTS

Anda Ioana Grațiela PETREHELE, Claudia Mona MORGOVAN, Camelia Daniela IONAȘ, Monica Oana ONCU

University of Oradea, Faculty of Informatics and Sciences, 1 University St., 410048, Oradea, Romania, e-mail: andapetrehele@yahoo.com

Abstract

In this work, with minimal costs and a good yield, aluminum from waste was recovered and transformed into the form of aluminum and potassium alum, a product with very good antiperspirant and antihemorrhagic properties and less aggressive than aluminum chloride, which is widely used in antiperspirant cosmetic products. The chemical method of synthesis used in our research is a simple one based on low energy consumption and the use of cheap resources. The synthesis of aluminum and potassium alum is proven by structural analysis, and the product obtained has been purified to ensure its possibility of use in the cosmetic industry. In the second part of the paper, an attempt to use the alum obtained in the preparation of an antiperspirant with simple and cheap components, as natural as possible, recognized for their beneficial properties on the body, is presented: collagen, as an anti-aging agent, and sodium bicarbonate, respectively borax, known as substances with antibacterial and antifungal action.

Keywords: aluminum, recovery, collagen, cosmetic

INTRODUCTION

Waste is generated from a variety of activities associated with industrial activities in the production of aluminium and other anthropogenic activities due to its widespread use. For example, the use of aluminum as packaging in the food industry, in different sectors, from cans to containers used for beer cans and juices [1]. The widespread use of aluminum foil and aluminum cans for various products has significantly increased the presence of aluminum waste especially in urban areas, but also in natural environments: rivers, seas and oceans, forests, others [2]. The most effective way to reduce/eliminate the impact of waste on the environment is to develop and implement effective waste management and recovery technique. Aluminum recycling is the process by which scrap aluminum can be reused to make products from metallic aluminum or aluminum compounds. The process simply involves remelting the metal or through the chemical recovery method, which is much less expensive and energy-consuming than creating new aluminum by electrolysis of aluminum oxide (Al_2O_3), which must be extracted from bauxite ore and then refined using the Bayer process. The ecological benefits of recycling aluminum are enormous [3]. Carbon dioxide production is reduced by 95% when recycling aluminium, compared to the amount of CO_2 emitted during the production of raw aluminum, and by an even lower percentage when considering the complete aluminum extraction and transport cycle. Also, the open mining technique, most often used to obtain aluminium ore, destroys large sections of the world's natural earth. That is why it is recommended that much of the used aluminum be recovered and converted back into aluminum or aluminum compounds through various recycling methods [4].

In this work, we set out to recover aluminum from containers and aluminum foil in the form of a product with antiperspirant and antihemorrhagic properties, used in cosmetics, aluminum and potassium alum [5-11]. Alum has long been used in paper sizing to improve ink durability and responsiveness, and in water treatment to clear water. Other

uses of alum include wastewater treatment, as a waterproofing agent and accelerator in concrete, as a brightener for greases and oils, and as a foaming agent in fire foams [12].

In the second part of the paper, we set out to try to propose a method of using the alum obtained in the preparation of an antiperspirant with simple and cheap components, as natural as possible, recognized for their beneficial properties on the body: collagen, as an anti-aging agent, and sodium bicarbonate, respectively borax, known as substances with antibacterial and antifungal action [13].

Principle of the synthesis method

The aluminium in the waste is converted into potassium and aluminium alum which is then used in the preparation of an antiperspirant product. Aluminum potassium alum is recognized for its astringent, antihemorrhagic and antiperspirant properties [14-20].

In the first stage, pieces of recycled aluminum are treated with an aqueous solution of KOH with the formation of a soluble complex, potassium tetrahydroaluminate [21-23]:

$$2Al_{recycle_{(s)}} + 2KOH_{(aq)} + 6H_2O \rightarrow 2K[Al(OH)_4]_{(aq)} + 3H_{2_{(g)}} \uparrow \quad (1)$$

Clear solution of aluminum complex, $K[Al(OH)_4]$, is precipitated in white aluminum hydroxide, according to the reaction (2):

$$2K[Al(OH)_4]_{(aq)} + H_2SO_{4_{(aq)}} \rightarrow 2Al(OH)_{3_{(s)}} \downarrow + K_2SO_{4_{(aq)}} + 2H_2O \quad (2)$$

The further addition of sulphuric acid leads to the disappearance of the precipitate and the formation of aluminium sulphate along with the potassium sulphate already present in the solution:

$$2Al(OH)_{3_{(s)}} \downarrow + 3H_2SO_{4_{(aq)}} \rightarrow Al_2(SO_4)_{3_{(aq)}} + 3H_2O \quad (3)$$

The overall reaction that takes place in the treatment of aluminum tetrahydrate with concentrated sulfuric acid can be written according to the reaction (4), in order to highlight more clearly the formation in solution of the double aluminum potassium halo:

$$2K[Al(OH)_4]_{(aq)} + 4H_2SO_{4_{(aq)}} \rightarrow 2KAl(SO_4)_{2_{(aq)}} + 8H_2O \quad (4)$$

Application of aluminium potassium alum in hydrogel synthesis

Hydrogels also possess a degree of flexibility very similar to natural tissues due to their great capacity of the water retention. The ability of hydrogels to absorb water results from the presence of hydrophilic functional groups attached to the polymer chain of the gel, while their resistance to dissolution comes from the bonds between the chains. Over the past two decades, natural hydrogels have been gradually replaced by synthetic hydrogels that have a long lifespan, high water absorption capacity and high strength. Synthetic polymers have the advantage of a well-defined structure that can be modified with more rigorous control and are more stable to temperature fluctuations. Recently, hydrogels have been defined as two-component or multi-component. systems made up of a three-dimensional network of polymer chains and water, which fills the space between macromolecules [24].

Depending on the properties of the polymer, it can reach structures in a balance with different water content; Usually in a swollen state, the mass fraction of the water in a hydrogel is much higher than the mass fraction of the polymer. In practice, in order to achieve high degrees of swelling, it is common to use polymers that are soluble in water when it is in non-cross-linked form [25].

The functional characteristics of an ideal hydrogel are high absorption capacity, low price, high stability in the swelling medium and during storage, biodegradable properties, a neutral pH after swelling with water, to be colorless, odorless and non-toxic. Also, a hydrogel used for the manufacture of cosmetics should have low rewetting capacity, the hydrogel must be able to return the absorbed solution or maintain it, depending on the requirements of the application (e.g. in hygienic applications) and a very good absorption capacity [26].

The hydrogel we use is based on collagen, a product that is used in food gelatins. Collagen, like most gels of animal origin, is sensitive to changes in temperature and pH. Different studies have shown that the stability of hydrogels increases with the concentration of the gel used in the solution. This increase is due to the formation of a stronger hydrogel network as a result of the expansion of the hydrogen bonds formed between the gel and the water molecules. This demonstrates that the viscosity of the environment, which is closely related to the concentration of the hydrogel, can affect the stability of the hydrogel network. Stability can reach a maximum value at a certain concentration of hydrogel, but also at the other components of the solution studied, alum and pH regulation solutions. In fact, the

pH and cooking temperature also intervene on the stability of hydrogel. Hydrogels exhibit viscoelastic properties. Viscosity and density increase with increasing hydrogel concentration [27, 28].

MATERIALS AND METHODS

Quantitative analysis of aluminum and potassium ions was performed with an AAS Spectrophotometer Analitik Jena atomic absorption spectrophotometer. The concentration of sulphate ions was determined with an ion chromatograph, Dionex ICS-6000 Ion Chromatography System, with a mobile phase of Na_2CO_3 with flow rates by 2.0 mL min^{-1}, on an anionite column, Dionex ATC 500, 4 mm, with a conductivity detector. Thermal stability analyses for the determination of crystallization water molecules and the study of the stability of the compound were performed in air on a Paulik-Erdely OD-103 Derivatograph (20-800°C) at 5 °C min^{-1}. FT-IR spectra were recorded in the 400-4000 cm^{-1} on a Shimadzu spectrophotometer using KBr pellets. All reagents were purchased from commercial sources and used as received. Distilled water was used in all procedures.

Synthesis of aluminium potassium alum

Weigh 4 g of recycled aluminium, cut into small pieces, pre-washed in water with hot detergent to remove residues and rinsed with distilled water and left to air dry until the next day. The weighed aluminium was placed in a 250 mL Berzelius beaker. Over it, 100 mL of 10% KOH was added solution slowly, under continuous stirring, by trickling it onto a wand. The mixture was heated slightly to speed up the chemical reaction. Under stirring, aluminum granules reacted with the basic KOH solution for a half of an hour. The reaction was considered to be over when no more hydrogen release is observed and the aluminum particles are completely decomposed. The solution obtained must be clear and no unreacted pieces of aluminum should be observed. If the release of hydrogen has ceased, but aluminum is still present, 10% KOH solution will be added hot by pipetting. Traces impurities from solution were removed by filtration. The filtered sample was reheated and concentrated at two-thirds of the volume. Over the filtrate, concentrated sulfuric acid droplets are added until the reformed aluminum hydroxide precipitate is completely dissolved. The sample is concentrated at half the volume by light heating. The potassium and aluminum alum crystals cold resulting on the ice bath are separated by a vacuum filtration system. The resulting product is dried in the oven at 110 °C, weighed and recrystallized in hot water. Thus, for recrystallization in 40 mL boiling water, 65 g of alum synthesized were dissolved. A pinch of animal charcoal spatula was added, and the sample was brought to a boil. It was quickly filtered hot on a curly filter to remove insoluble impurities remaining on the filter paper and better retained with the help of animal charcoal. The clear, colorless filtrate was cold passed on the ice bath, and it was observed how aluminum and potassium alum began to form quantitatively in the mass of the solution. The crystals were quantitatively passed on vacuum filter paper and then dried in the oven at 110 °C. The yield of $KAl(SO_4)_2 \cdot 12H_2O$ synthesis was 90.8% (59,02 g). Analytical studies releaved the next percentual composition for the produce of this synthesis, $KAl(SO_4)_2 \cdot 12H_2O$ practical (theoretical): K 8,2% (8,22%); Al 5,5% (5,69%); SO_4^{-2} 40,3% (40,46%); H_2O 45,17% (45,52%)

Application of aluminium potassium alum in hydrogel synthesis

The materials used in the preparation of the hydrogel with an antiperspirant role were aluminium and potassium alone prepared by us, $KAl(SO_4)_2 \cdot 12H_2O$ and edible gelatin, which is a collagen obtained from pig cartilage and bones by boiling and subsequently dried, a product with a very low marketing price, non-toxic.

During the study, several attempts were carried out in which products with a different appearance and different consistency were obtained, which aimed to obtain a product as homogeneous as possible, preferably transparent, with a pH of at least 5.5 close to that of the skin, but not higher than pH 8, which would be as well tolerated as possible and would not cause irritation or intense dehydration of the skin. All these aspects are complicated by the fact that aluminum ions tend to precipitate as $Al(OH)_3$ at pH values higher than 3.42 and return to the solution in the form of complex tetrahydroxyaluminate ions $[Al(OH)_4]^-$. So for pH regulation we tried to use solutions of sodium bicarbonate and borax. Unfortunately, in both situations, precipitation was observed when the pH value increased, and the chemical reaction

that occurred in the case of the use of bicarbonate is as follows:

$$KAl(SO_4)_2 + 4NaHCO_3 \rightarrow Al(OH)_3 \downarrow + KHCO_3 + 2Na_2SO_4 + 3CO_2 \uparrow \quad (5)$$

RESULTS AND DISCUSSION

The thermogravimetric analysis for 0.186 g $KAl(SO_4)_2{\cdot}12H_2O$ are recorded in Table 1. In the diagrams, the presence of an endothermic dehydration process that takes place in several steps was observed. At this stage, the crystallization water of the alum was lost. The mass loss in a percentage by 45.17% corresponds to 12 water molecules [29]. This process took place in the temperature range of 50-350 °C and would be described by the chemical equation:

$$KAl(SO_4)_2 \cdot 12H_2O \rightarrow KAl(SO_4)_2 + 12H_2O \quad (6)$$

The loss of crystallization water, also called land water, because it is responsible for the creation of the crystal lattice, leads to the decomposition of the double sulfate structure, of the alum type, into simple sulfates of the component ions, aluminum and potassium, according to the reaction:

$$2KAl(SO_4)_2 \rightarrow K_2SO_4 + Al_2(SO_4)_3 \quad (7)$$

It can be seen in reaction (7) that the decomposition into simple sulfates is only a result of the destruction of the crystal lattice, which is not accompanied by real chemical reactions of modification of the chemical compounds and implicitly by mass losses. This process may take place in a temperature range, somewhere above 400°C, when the last water molecules are lost, up to 600°C, when aluminum sulfate is decomposed. It is usually characterized by an exothermic signal [30]. In the third stage, from 750°C to 950°C, aluminum sulfate was decomposed to aluminum oxide, Al_2O_3 and sulfur trioxide, SO_3. This stage is characterized by a mass loss of 24,08 % due to the formation of SO_3 gaseous and according to the DTA curve it turns out that this decomposition reaction is an endothermic process. The remaining residual mass is represented by Al_2O_3 and K_2SO_4 much more stable. The chemical reaction that characterizes this process is:

$$Al_2(SO_4)_3 \rightarrow Al_2O_3 + 3SO_3 \uparrow \quad (8)$$

Table 1. Data from thermogravimetric analysis of alum $KAl(SO_4)_2{\cdot}12H_2O$

Temperature (°C)	DTA	TG	Mass loss		Associated process
			(%)	(g)	
118	Endothermic process	Dehydration	45,17	0.084	$KAl(SO_4)_2 \cdot 12H_2O \rightarrow KAl(SO_4)_2 + 12H_2O$
228	Endothermic process	Dehydration			H_2O lost
400-600	Exothermic process	Network Destruction	-	-	$2KAl(SO_4)_2 \rightarrow K_2SO_4 + Al_2(SO_4)_3$
750	Endothermic process	Decomposition	24,08	0,048	$Al_2(SO_4)_3 \rightarrow Al_2O_3 + 3SO_3 \uparrow$ SO_3 lost
750-1100			Residue left 30,75%	0,057	K_2SO_4 and Al_2O_3 remained
1100	Endothermic process	Decomposition			$K_2SO_4 \rightarrow K_2O + SO_3 \uparrow$ SO_3 lost
Sample table			100%	0,186	

The IR spectral method allows the determination of the types of groupings and bonds in different molecular groups with a dominant covalent character based on the signals obtained in the range 660-4000 cm^{-1} due to the vibrations of symmetrical and asymmetric stretching of the bonds also called valence vibrations (ν), as well as due to the deformation vibrations (δ) – of bending in plane or out of plane, symmetrical or asymmetrical, of covalent bonds, i.e. angular deformations.

Comparing FT-IR spectrum obtained for the $KAl(SO_4)_2 \cdot 12H_2O$ alum with one for simple aluminium sulfate and potassium sulphate from literature, it can be observed that in all there are very intense vibrations, characteristic of the presence of the sulfate group, SO_4^{2-}, in the range 1080-1200 cm^{-1} asymmetric tension vibrations (ν_{as}) are found at frequencies higher than 110 cm^{-1}, respectively the vibrations of symmetrical tension (ν_s) at slightly lower frequencies.

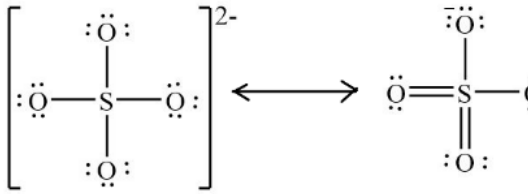

(1) (2)

The frequencies in the 580-680 cm^{-1} range also belong to the SO_4^{2-} group, due to the asymmetric deformation vibrations (δ_{as}), and in the 300-400 cm^{-1} range symmetrical deformation vibrations (δ s) can be observed. The signals encountered around 1600 cm^{-1} are asymmetrical deformation vibrations δ ace within the H-O-H bonds in crystallizing water molecules. The asymmetric tensile vibrations ν_{as} of the O-H bond in the water molecule are observed in the range of 3000-3400 cm^{-1}. In the case of the K_2SO_4 spectrum, an intense signal can be observed with shoulders just above 900 cm^{-1}, which shows that the symmetrical stretching vibration is very intense and attenuates the asymmetrical stretching vibration. The same can be observed in the case of deformation vibrations that the signal corresponding to the symmetrical deformation is more intense than the asymmetrical one, which appears split in this case. This is due to the strong ionic character of the bond between potassium and sulfate ions. The sulfate ion in this case will look closer to the form (1), in which the S atom is hybridized sp^3 with the four S-O bonds of equal lengths, symmetrically oriented in space. In the $Al(SO_4)_2 \cdot 12H_2O$ spectrum, it can be seen that the molecule is less symmetrical, the asymmetric stretch signal of the sulfate group appears split, which shows that already in this case the bond made with aluminum acquires a covalent character, and in a unit there are three sulfate ions whose behavior is not exactly identical due to the different position occupied within the crystal lattice. Moreover, the presence of a stretching vibration of the Al-O link can be observed. In this case, the sulfate ion will have an appearance closer to the boundary structure (2), with two bonds with a double character and two with character by single covalent bonds, with a lower degree of symmetry. Here one can also observe the asymmetrical stretching and deformation vibrations, specific to the H-O bonds in crystallization water molecules [31-32].

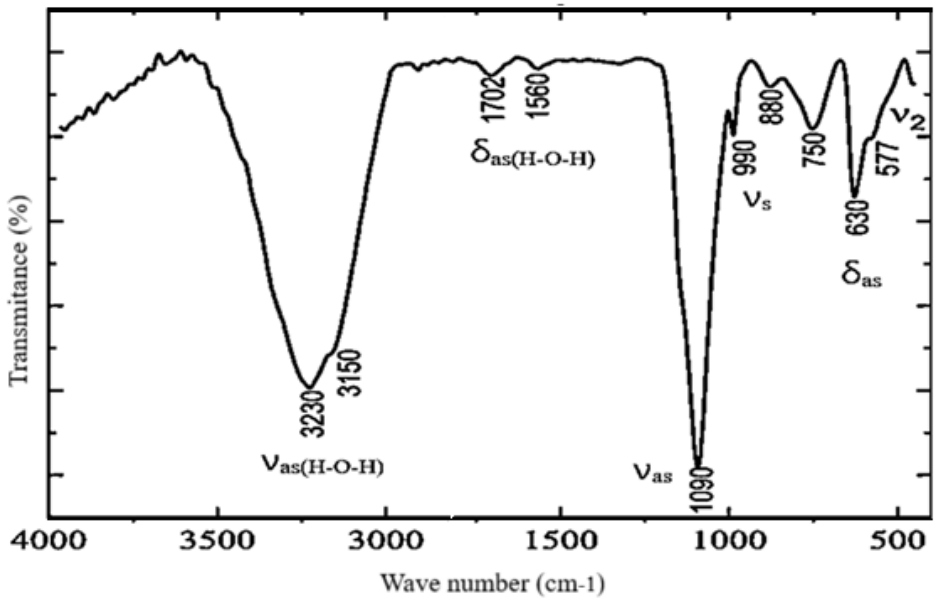

Fig.1. IR spectrum of $KAl(SO_4)_2 \cdot 12H_2O$

In the case of the IR spectrum of alum $KAl(SO_4)_2{\cdot}12H_2O$, the presence of water molecules can be clearly observed by the existence of vibrations of the O-H bond of asymmetric stretch (ν_{as}) from 3230 and 3150 cm^{-1}, respectively of the vibrations of asymmetric deformation (δ_{as}) from 1702 and 1560 cm^{-1}. The existence of two vertices shows us that the water molecules occupy different positions within the crystal lattice of the alum which leads to changes in both the length of the O-H bonds and distortions within the angle between the H-O-H bonds. It can also be seen that the two sulfate ions SO_4^{2-} are not exactly identical in the presence of the two cations K^+ and Al^{3+} with different binding tendencies. This explains the splitting of the signals for all three vibrations of the group, the asymmetrical stretch vibration, (ν_{as}) at 1090 and 990 cm^{-1}, the symmetrical stretch vibration (ν_s) at 880 and 750 cm^{-1}, respectively the asymmetric strain vibration (δ_{as}) from 630 and 557 cm^{-1} recorded in Fig. 1 [23, 30-32].

Application of aluminium potassium alum in hydrogel synthesis

Experiment 1

3 g of $KAl(SO_4)_2{\cdot}12H_2O$ alum was dissolved in a minimum amount of distilled water and 5% $NaHCO_3$ solution was added in cold droplets up to pH 5.5 under strict pH monitoring with a pH meter. The release of CO_2 and the subsequent precipitation of $Al(OH)_3$ were observed. The heterogeneous mixture was, however, gelled with 1.5 g of gelatin per 50 mL 3% gel solution, hot on a water bath at 60 °C, under stirring, for 10 minutes. A product with a heterogeneous appearance was obtained, which had antiperspirant properties, without causing dryness or irritation, as can be seen in Fig. 2.a. The disadvantages consisted in the heterogeneous structure, with influences on the desired properties for the hydrogel (Fig. 2.b).

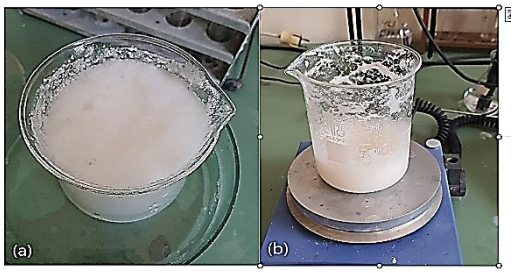

Fig. 2. Samples of antiperspirant hydrogel 3% obtained from alum at pH 5.5 with baking soda

Experiment 2.

In the second experiment, the disadvantages created by reaching a pH of 5.5 were taken into account and we set out to drive the pH regulation to the limit of obtaining a clear, transparent and homogeneous product. This time to the sample of 3 g of alum dissolved in a minimum amount of water, $NaHCO_3$ 5% solution was added until no more CO_2 release was observed, and the maximum pH point reached in this case was pH 4.6. The sample was brought to 50 mL with distilled water. Gelling was done with 1.5 g of dietary collagen, at 60 °C, on the water bath, for 10 minutes, under continuous homogenization. The product obtained this time was a compact, transparent gelatin (Fig. 3), not quite fluid, with good antiperspirant properties, non-irritating, but which causes a slight sensation of dryness of the skin, probably due to the slightly low pH.

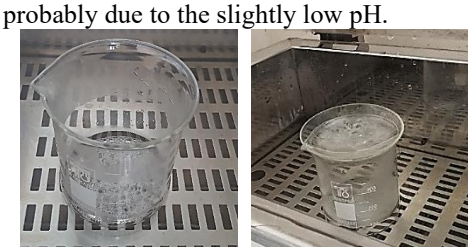

Fig. 3. Antiperspirant hydrogel 3% obtained from alum with baking soda at pH 4.6

Experiment 3

In this experiment we tried to see how the concentration of collagen used in gelling influences the properties of the product obtained. In this experiment, 3 g of alum was dissolved in a minimum amount of water and 5% $NaHCO_3$ solution was added under stirring until no more CO_2 release was observed (pH 4.6). Collagen was added to the sample so as to obtain a solution of 0.5 and 1% concentration, depending on the mass of the sample found before the addition of gelatin. The samples were homogenized at 60 °C in a water bath and left to cool until the next day. All these samples showed an inhomogeneous appearance, gelling being quite bad, with a start of precipitation of $Al(OH)_3$ and foaming. In other words, these gels were not shown to be stable, as can be seen in Fig. 4 for the 0.5 and 1% concentration samples. It was observed that the stability of the compounds increased with the increase in the concentration of collagen in the hydrogel and the structural stability of the hydrogel. In this situation, it can be seen that higher concentrations of collagen are

needed to obtain a homogeneous and stable product.

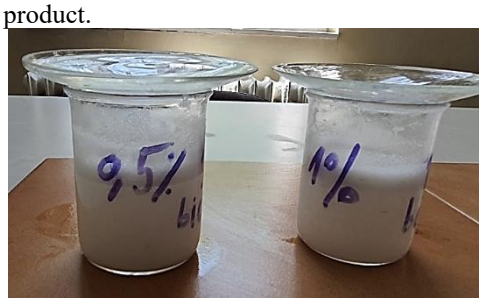

Fig. 4. Hydrogels of concentrations 0.5% and 1% for alum with sodium bicarbonate at pH 4.8

Experiment 4.

In this experiment, the 5% baking soda solution was replaced with the 5% borax solution. 5% borax solution was added to 3 g of saturated alum until the formation of the $Al(OH)_3$ precipitate began. In this case, at pH 3.5, the beginning of precipitation was observed. Here too, they worked below the precipitation point and obtained hydrogels of concentrations of 0.5, 1.0% by dissolving an appropriate amount of collagen in the sample. The gelling was done hot, under continuous agitation and homogenization. As can be seen compared to the sodium bicarbonate hydrogels in fig. 5, the borax samples are even less homogeneous, the lower pH value of these solutions significantly reduced the amount of $Al(OH)_3$ separated. In contrast, the increase in the concentration of gelatin in the solution accentuated the increase in the precipitate $Al(OH)_3$ and shifted the basic hydrolysis reaction of alum to the right.

Fig 4. Hydrogel samples 0.5 % and 1 % of alum with both bicarbonate and borax

CONCLUSIONS

In this paper, the possibility of recovering aluminum from containers and aluminum foil for food use, considered disposable products, was highlighted. The recycling of aluminum was done with a good yield (90.80%) of obtaining a product with cosmetic, antiperspirant and antihemorrhagic applications, aluminum potassium alone, $KAl(SO_4)_2 \cdot 12H_2O$. The chosen method is easy to achieve, with low costs, with low energy consumption. The thermogravimetric analysis method showed the presence of two exothermic transformations accompanied by mass losses, the first was associated with the loss of 12 crystallization water molecules, followed by the destruction of the crystal lattice, characteristic for $KAl(SO_4)_2 \cdot 12H_2O$ studied before. When comparing the IR spectra of K_2SO_4, $Al_2(SO_4)_3$ and alum $KAl(SO_4)_2 \cdot 12H_2O$ synthesized in this work, the spectra differed from each other by the number of signals, the degree of symmetry, which was higher the lower the number of sulfate units in the molecule, and the bond with the cations is more ionic (K^+ towards Al^{3+}). According to the IR spectrum, in the case of alum there is an increase in symmetry and implicit stability with respect to $Al_2(SO_4)_3$. All signals underwent slight displacements associated with an increase in symmetry and stability in the alum.

The prepared antiperspirant was characterized by low costs, the use of natural, non-toxic, even beneficial products for the body, antibacterial, antifungal, antiviral and anti-aging. In addition to aluminum alum, we set out to obtain a product in which we add baking soda and borax as pH regulators. The experiments carried out showed that the hydrogel solution is all the more stable the higher the collagen concentration, at a 3% collagen solution a transparent and homogeneous product was obtained, while at lower concentrations, of 0.5 and 1.0% the products were heterogeneous and the precipitation of $Al(OH)_3$ over time was favored$_3$ from the solution of alum. Precipitation reaction of $Al(OH)_3$ limited the pH range at which the hydrogel can be

obtained, until to pH 4.6 when using $NaHCO_3$, respectively until to pH 3.5 in the case of using borax, which makes the product a good antiperspirant, which does not cause allergies, but dries the skin easily. The attempt to bring the hydrogel to pH 5.5 leads to an unstable, heterogeneous product, in which some of the aluminum ions in the alum precipitate. This product maintains its good antiperspirant properties, does not cause irritation and allergies and leaves the skin velvety without drying it out, but does not exhibit commercial qualities, such as transparency and homogeneity.

REFERENCES

1. Chen, X., Saada, M.B., Lavisse, B. *et al.* Recent advances in the remelting process for recycling aluminium alloy chips: a critical review. *Int J Mater Form*, 2025, 18, pp. 42 https://doi.org/10.1007/s12289-025-01904-9
2. Wang, T., Li, X., Li, Z. *et al.* Upcycled high-strength aluminum alloys from scrap through solid-phase alloying. *Nat Commun*, 2024, 15, pp. 10664, https://doi.org/10.1038/s41467-024-53062-2
3. Laurent-Brocq M., Lilensten L., Récupération et recyclage de l'aluminium-Stratégie. *Tech niques de l'Ingénieur,* 2023, 10.51257/a-v2-m2345, hal-04270047
4. Rabah M., Farghaly F.I., Recovery of Aluminium 319.1 Alloy(S) From Metal Turning Scrap. *Adn Envi Was Mana Rec*, 2021, 4 (3), pp. 213-222
5. Gavhane J., Madankar V., Panchal A., Potassium Alum in Modern Aftershave: Multidimensional Mechanisms, Formulation Advances, and Dermatological Safety for Sustainable Skincare, *Int. J. Sci. R. Tech*., 2025. 2(11), pp. 664-670. https://doi.org/10.5281/zenodo.17682909
6. Irshad M, Younas M, Shabir H, Alam MS, Rehman ZU, Aleem S. In vitro antifungal activity of potash alum against Candida albicans on acrylic resin. *Pak Armed Forces Med J*.. 2020;70(5), pp.1460-1464
7. Gajbhiye S. , Jeurkar M., Chachda N., Belekar M., Raut S., Warhate V., Kakde V., Ingole S., Pharmacological & Physiochemical Properties of Potash Alum: A Comprehensive Review, *Int. J. of Pharm. Sci.*, 2025, 3(3), pp. 2667-2673, https://doi.org/10.5281/zenodo.15092606
8. Oliveira ECV, Salvador DS, Holsback V, Shultz JD, Michniak-Kohn BB, Leonardi GR. Deodorants and antiperspirants: identification of new strategies and perspectives to prevent and control malodor and sweat of the body. *Int J Dermatol.*, 2021, 60(5), pp. 613-619. doi: 10.1111/ijd.15418
9. Alzomor, A. K., Moharram, A. S., & Al Absi, N. M., Formulation and evaluation of potash alum as deodorant lotion and after shaving astringent as cream and gel. *International Current Pharmaceutical Journal*, 2014, 3(2), pp. 228–233. https://doi.org/10.3329/icpj.v3i2.17512
10. Ermenlieva N, Georgieva E, Milev M., Antibacterial and antifungal activity of antiperspirant cosmetic products, *J. of IMAB.,* 2020, 26(4), pp. 3374-3377. DOI: 10.5272/jimab.2020264.3374
11. Teerasumran P., Velliou E., Bai S., Cai Q., Deodorants and antiperspirants: New trends in their active agents and testing methods, *Int J Cosmet Sci.,* 2023, 00, pp. 1–18
12. Kumari S. P., Synthesis, Characterization, and Applications of Potash Alum ($KAl(SO_4)_2 \cdot 12H_2O$) in Water Treatment and Beyond, *International Journal of*

Innovative Science and Research Technology, 2024, 9(11), pp 2362-2364
13. Garg S., Garg A., Hydrogel: Classification, Properties, Preparation and Technical Features, *Asian Journal of Biomaterial Research*, 2016, 2(6), pp. 163-170
14. Zomor, Abdulkarim, Formulation and evaluation of potash alum as deodorant lotion and after shaving astringent as cream and gel, *Int. Curr. Pharm. J*, 2014, 3(2), pp. 228-233
15. Patil, R., & Kale, S., Evaluation of Alum Based Lotion for Post-Shave Applications, *Jour. App. Pharm. Sci.,* 2020, 10(6), pp. 111–119
16. Yoganandam, G. P., Ramesh, B., Review on Formulation and Evaluation of Alum Preparations. *Int. Res. J. Mod. Eng. & Tech. Sci.*, 2023, 12(6), pp.128–139
17. Lanzet, K., Haque, M., Sustainability in Cosmetic Formulation. *Cosmetics*, 2018, 5(2), pp. 37–46
18. Amadi L.O., A Review of Antimicrobial Properties of Alum and Sundry Applications, Acta Scientific Microbiology, 2020, 3(4), pp. 109-117
19. Anand N., Singh S., An overview of Sphatika (Alum), *Int. J. of Research and Analytical Reviews,* 2019, 6(1), pp. 288-294
20. Mohamed R., El-Desoukey A., Comparative Antimicrobial Studies between Commercial Deodorants, Alum, Sodium Bicarbonate and Lemon Against Sweat Odor Bacteria, *Cohesive Journal of Microbiology & Infectious Disease*, 2021, 4(5), pp. 1-5, DOI:10.31031/CJMI.2021.04.000597
21. Meshram, A., Gautam, D. & Singh, K.K., Recycling of White Aluminium Dross: Production of Potash Alum. *Trans Indian Inst Met*, 2020, 73, pp. 1239–1248 https://doi.org/10.1007/s12666-020-01973-1
22. China, C.R., Hilonga, A., Maguta, M.M. & al., Preparation of aluminium sulphate from kaolin and its performance in combination tanning, *SN Appl. Sci.*, 2019, 1, pp. 920, https://doi.org/10.1007/s42452-019-0979-1
23. Nemdilia L., Koutchoukalia O., &Ulrichb J., Crystallization study of potassium sulfate-water system, metastable zone width and induction time measurements using ultrasonic, turbidity and 3D ORM techniques, *Journal of Crystal Growth,* 2018, 500, pp 44-51
24. Pires Figueiredo, M., Rodríguez-Fernández, S., Copes, F. et al., Review of collagen type I-based hydrogels: focus on composition-structure-properties relationships. *npj Biomed. Innov.*, 2025, 2, pp. 16 https://doi.org/10.1038/s44385-025-00018-w
25. Xu Q, Torres JE, Hakim M, Babiak PM, Pal P, Battistoni CM, Nguyen M, Panitch A, Solorio L, Liu JC., Collagen- and hyaluronic acid-based hydrogels and their biomedical applications, *Mater Sci Eng R Rep.*, 2021 146, pp. 100641, doi: 10.1016/j.mser.2021.100641
26. She J., Liu J., Mu Y., & Wei D., Recent advances in collagen-based hydrogels: Materials, Preparation and applications, *Reactive and Functional Polymers*, 2025, 207, pp. 106136, https://doi.org/10.1016/j.reactfunctpolym.2024.106136.
27. Priya A.S., Premanand R., Ragupathi I., Bhaviripudi V.R., Aepuru R., Kannan K., Shanmugaraj K.. Comprehensive Review of Hydrogel Synthesis, Characterization and Emerging Applications. *J. Compos. Sci.* 2024, 8, pp. 457. https://doi.org/10.3390/jcs8110457

28. Steele C., Collagen: A Review of Clinical Useand Efficacy, *Nutr Med J*., 2022 Jul; 1 (2), pp. 1-24
29. Rego A.S.C., Marprates C.V.B., Silva T.S.X., Neto J.G., Navarro R.C.S., Souza R.F.M., Brocchi E.A., $KAl(SO_4)_2$ thermal decomposition kinetics modeling through graphical and PSO methods, *Journal of Materials Research and Technology,* 2021, 14, pp. 1975-1984, https://doi.org/10.1016/j.jmrt.2021.07.086
30. Souemti, A., Mouhammed, M.B., Lozano-Gorrin, A.D. et al., Investigations on $KAl(SO_4)_2{\cdot}12H_2O$: A Candidate α-Alum Material for Energy Storage Applications. *Chemistry Africa*, 2022, 5, pp. 575–587, https://doi.org/10.1007/s42250-022-00336-1
31. Souza R., Navarro R., Grillo A.V., Brocchi E., Potassium alum thermal decomposition study under non-reductive and reductive conditions, *Journal of Materials Research and Technology*, 2019, 8(1), pp. 745-751, https://doi.org/10.1016/j.jmrt.2018.05.017
32. Abdulwahab A.M., Al-magdashi Y. A. A., Meftah A., Al-Eryani D. A., Qaid A.A., Growth, structure, thermal, electrical and optical properties of potassium aluminum sulfate dodecahydrate (potash alum) single crystal, *Chinese Journal of Physics,* 2019, 60, pp. 510-52, https://doi.org/10.1016/j.cjph.2019.05.034

THE INFLUENCE OF THE SARS-COV-2 VIRUS ON THE EVOLUTION OF TRANSAMINASES

Angela Florina DEJEU, Mioara SEBEȘAN, Alexandrina FODOR, Anda Ioana Grațiela PETREHELE

University of Oradea, Faculty of Informatics and Sciences, 1 University St., 410048, Oradea, Romania, e-mail: andapetrehele@yahoo.com

Abstract

This paper is both a retrospective statistical study and a suggestive case presentation on the evolution of transaminases before and after SARS-COV-2 infection. In this paper, the transaminase results for a group of over 200 patients who had Covid 19 disease were determined and recorded. The results obtained were compared with normal values. For statistical processing of the data, patients with Covid 19 were divided into cohorts selected according to age, sex and environment, rural or urban, and the results obtained were compared with normal range values and analyzed. The study includes a critical look at the evolution of transaminase concentration from infection with the SARS-COV-2 virus to recovery. The determination of transaminases was performed on an automatic device of the BioSystems BA 400 type from serum samples collected from patients positive for SARS-CoV-2 virus infection, using a kinetic method of analysis without pyridoxal phosphate, standardized by the International Federation for Clinical Chemistry (IFCC).

Keywords: Covid 19, transaminase, monitoring

INTRODUCTION

The virus responsible for COVID-19 disease was SARS-CoV-2. SARS-CoV-2 uses ACE2 receptors to interact with its host and spreads through the respiratory tract, just like other SARS-CoVs. The primary symptoms experienced by COVID-19 patients were mild-to-severe fever, cough, and fatigue, with only a small percentage reporting gastrointestinal infections. Among the many illnesses that have shook the world in recent history, COVID-19 has emerged as one of the most difficult pandemics to control and cure. The virus consists of five proteins: spike protein (S), envelope protein (E), membrane protein (M), hemagglutinin-esterase dimer protein (HE), and nucleocapsid protein (N). While the S, E, M, and HE proteins are visible on the surface, the genetic material responsible for replication is hidden inside the virion. Host cell receptors known as ACE2, which are present in human cells in the lungs, heart, kidneys, and intestines, are bound by spike proteins on the virion surface [1-7]. When the virus enters the cytoplasm, it disintegrates its own protein shells and releases the viral RNA payload inside the cell, where starts to replicate itself and the virus is transported to other cells. Cell death or apoptosis can occur if the host cell loses its ability to maintain homeostasis, and the immune system is put in difficult situation. The virus's life cycle is mainly dependent on non-structural protein enzymes, and structural glycoproteins are crucial for the virus's entry into the cell [8-12]. A problem in treating COVID-19 disease was that the catalytic enzyme site was protected by antiviral drugs. The SARS-CoV-2 virus's glutamine493, asparagine501, leucine455, phenylalanine486 and serine494 were found to be compatible with two hotspot receptors, ACE2, found in human cells, hot spot 31 and 353 [13-22].

AST (glutamic oxaloacetic transaminase) and ALT (Alanine aminotransferase) are enzymes involved in transamination reactions in protein metabolism. AST ensures the transfer of an amino group between an amino acid and an oxaloacetate and is implicitly involved in the Krebs cycle, in obtaining the oxaloacetate substrate from aspartate. AST is found in cells of the liver, heart, skeletal muscles, kidneys, brain, red blood cells. ALT by transamination converts alanine to pyruvate and is involved in the Krebs cycle and gluconeogenesis. ALT is found mainly in the liver, and its concentration in the rest of the tissues is low, which is why it is considered a specific marker for liver health [23, 24].

Several study groups have shown that during a severe COVID-19 infection, AST increases earlier, more frequently, and progresses to values higher than ALT. Furthermore, increased AST is associated with mortality, especially if the AST to ALT ratio is greater than 1.5. The study groups did not find clear results linking patients' initial liver health and increases in transaminases in

COVID-19 infection [25, 26]. However, the pre-existence of severe diseases such as alcoholic or non-alcoholic hepatitis can lead to more severe forms of COVID-19 [27-30]. This was not very eloquent in the case of obesity. Recent studies following the isolation of RNA from liver cells infected with the SARS-CoV-2 virus have shown that it infected liver tissue. It is assumed that SARS-CoV-2 can cause viral hepatitis and that this infection increases the severity of the disease [31-34].

AST and ALT catalyze reactions inside cells, meaning that their presence in the systemic circulation could indicate liver dysfunction or damage, especially those involved in liver cell membrane disruption. ACE-2 helps convert angiotensin II (Ang II) to angiotensin 1-7 and therefore helps regulate vascular pressure. The virus competes with Ang II, and blood pressure control remains in deficit. It is important to note that people with some comorbidities, such as hypertension, express more ACE-2 receptors, due to upward regulation, which can amplify the effect of the virus on organs. This can also happen in the liver and bile duct: due to the high expression of ACE-2 in bile duct cells, it can lead to damage to these cells, which can lead to liver damage. It's important to note that it's still unclear whether the liver damage is caused by the cytokine storm or direct cellular damage caused by the virus, or both. However, there is no denying the damage that the disease can cause to the liver. It has been shown that SARS-CoV-2 can produce liver damage, especially in people with other comorbidities, thus increasing ALT and AST, which can highlight liver damage [35-38].

According to studies carried out by different groups, it was observed that liver abnormalities, proven by increased ALT and AST, were found in up to 54% of patients. Furthermore, when liver enzymes ALT and AST were analyzed in non-survivors, they were elevated compared to survivors. These studies are important to support the treatment of COVID-19. In conclusion, patients with some chronic liver diseases (liver cirrhosis, nonalcoholic fatty liver) are more vulnerable to SARS-CoV-2 infection, both in terms of risk of infection and severe prognosis. COVID-19 is an important risk factor for liver cirrhosis decompensation and ACLF. Patients undergoing immunosuppressive therapy (autoimmune hepatitis, liver transplants) have an increased risk of infection, without manifesting severe forms of the disease [39-43].

The purpose of this retrospective study is the statistical analysis of transaminases performed within the Medical Analysis Laboratory of the Aleșd City Hospital, the analyzed patients being admitted to the Pulmonology department of the hospital. The statistical period is 2 years, respectively the period March 2020-March 2022.

The patients included in this study arrived to the hospital with various forms of pneumonia, interstitial lung disease, pleurisy, heart failure, Covid. The subsequent test proved in all cases that it was an infection with the SARS CoV 2 virus [64]. The results taken in the study belonged to a number of over 200 Covid patients monitored between March 2020 and March 2022 from different age categories, of both sexes, both in rural and urban areas. With the help of the EXCEL 2021 program, the arithmetic means of the values for the patients' transaminases were determined, the maximum and minimum values recorded and the standard deviation from the mean value were established.

MATERIALS AND METHODS

Samples of serum obtained from patients were collected from venous blood collected without food in tubes without anticoagulant with separator gel, in which the serum was separated by centrifugation. The samples were centrifuged with the laboratory's cooling centrifuge, the Nuve NF 400R, at 3500 revolutions/minute for 10 minutes at a constant temperature of 20 °C. Sample volumes of at least 0.5 mL were required from each patient to perform the determinations. The samples could not be analysed if they were intensely haemolysed, lipemic or were bacterially contaminated. The determinations were carried out immediately after collection, given that the samples are stable for up to 24 hours at room temperature and even for a week kept in the refrigerator at 2-8 °C. Aspartate aminotransferase (AST) in serum and plasma is stable for 7 days at 2-8°C. For the determination of transaminases, a kinetic method without pyridoxal phosphate, standardized by the International Federation for Clinical Chemistry (IFCC) with an automatic spectrophotometer of the BioSystems BA 400 type, was used.

In the case of AST determination, the method is based on the determination of oxaloacetic acid, either directly or indirectly. The kinetic method is the one generally considered as a reference method due to its high precision and specificity. The

oxaloacetic acid produced in the transamination reaction is determined by an enzymatic reaction coupled with malic dehydrogenase (MDH) by measuring the oxidation of NADH (Nicotinamid Adenine Dinucleotide in reduced form) at 340 nm. Basically, this method determines by successive measurements over time the decrease in the concentration of oxaloacetate in the solution. The modifications made to this method introduced for the first time by Karmen allowed the optimization of the reaction according to the concentration of the substrate and the determination temperatures [44, 45]. The chemical reactions that take place are:

$$Aspartate + 2 - Oxaloglutarate \xrightarrow{AST} Oxaloacetate + Glutamate$$

$$Oxaloacetate + NADH + H^+ \xrightarrow{MDH} Malate + NAD^+$$

The following metrological characteristics were obtained with a BA400 analyzer according to the Clinical & Laboratory Standards Institute (CLSI) guideline.

Detection limit: 7.15 U/L = 0.119 µkat/L.
Linearity limit: 500 U/L = 8.33 µkat/L.

The results obtained with these reagents do not show significant systematic differences when compared with reference processes. Details on comparative studies are available upon request. This method of determining the concentration of AST can be limited by the presence of interferants such as a concentration of more than 2 g/L of triglycerides in the case of lipemia, by the presence of substances or drugs. The presence of coloring substances in higher concentrations in the serum, such as bilirubin (intense yellow color) or hemoglobin in a concentration of up to 10 g/L (red color) does not interfere with or alter the determination of transaminase concentration.

Reagents

To make the determinations, we used kits recommended for use with the BA Biosystems type device used under the conditions recommended by the manufacturer, stored in a refrigerator cold, at 2-8 ºC for a maximum of two months after opening. In addition to the reagent kit, additional materials are required, such as pyridoxal phosphate C reagent, AST standard in the form of pyridoxal phosphate with a concentration of 10 mmol/L or the universal standard of clinical biochemistry for several parameters (human biochemistry calibrator) [60]. It is recommended to perform daily zero point adjustment with the help of a blank made up of the mixture of reagents without serum sample. At a maximum of 2 months, 6 days for Reagent A working with pyridoxal phosphate with the role of enzymatic activator or after changing the batch of reagents or as required by the quality control procedures, it is recommended to recalibrate the determination curve by using a standard, either the AST or the human biochemistry calibrator [44, 45].

For the determination of ALT, the chemical reactions specific to the kinetic method used are:

$$Alanine + 2 - Oxaloglutarate \xrightarrow{ALT} Piruvate + Glutamate$$

$$Piruvate + NADH + H^+ \xrightarrow{LDH} Lactate + NAD^+$$

The method is very similar to the one at AST. The difference is that in this case decrease of pyruvate concentration obtained from the alanine transamination reaction with 2-oxaloglutarate in the presence of ALT is kinetically determined. The pyruvate concentration decreased due to its transformation into lactate following the interaction with NADH under the action of lactate dehydrogenase (LDH) enzymes.

The metrological characteristics are [62]:

Detection limit: 8.5 U/L = 0.14 µkat/L
Linearity limit: 500 U/L = 8.33 µkat/L.

According to the studies carried out by the manufacturer, the method is truthful and accredited according to the norms. Within this method, only some substances and drugs can interfere, but triglycerides up to 200 mg/L, bilirubin in concentrations below 20 mg/L and hemoglobin up to 1000 mg/L do not interfere.

RESULTS AND DISCUSSIONS

During the period of patient montorization March 2020-March 2022, AST analyzes were performed for 499 patients, of which 212 came out Covid positive (42%) while the remaining 287 patients (58%) were Covid 19 negative at testing. ALT transaminase determinations were performed for 509 patients, of which 225 (44%) were found Covid positive, and the remaining 284 patients were Covid negative (Fig. 1). The following discussions refer only to patients found Covid 19 positive.

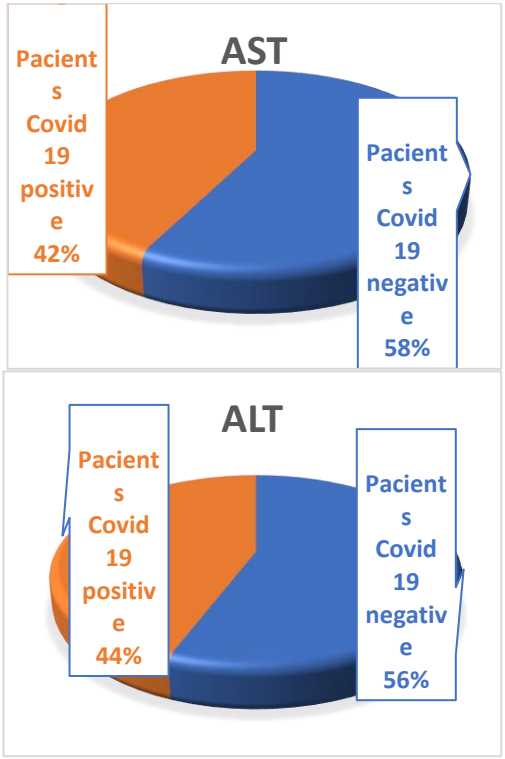

Fig. 1. Percentages of Covid-positive patients for whom transaminases were performed

Table 1 shows the minimum, maximum and mean values obtained and it can be seen that the mean obtained for both transaminases is significantly higher than the normal values. In addition, the minimum values are at the upper accepted limit for transaminase concentrations, which indicates that both AST and ALT are affected by SARS-CoV-2 virus infection. The high values of standard deviations show us the lack of homogeneity of the study group, caused by differences in age, sex, living conditions and health status of the monitored Covid patients.

The ALT values (Table 2) do not differ much for the group under 40 years old with an average value of 57.39±11.62 U/L. The ALT values are slightly increased above the normal value up to a maximum of 72.18 U/L. The standard deviation remains within acceptable limits, which shows a homogeneity of the ALT values in this age group, most likely associated with a very good immune response and good health.

The situation is totally different in the other age groups and there is an increase in the maximum value of ALT with age, with a peak in the 60-69 age group. As for the highest average ALT value, it was obtained in the 50-59 age group, which shows a beginning of the alteration of health status after the age of 50, accompanied by a change in transaminase values, but also the more frequent exposure of this group to the virus due to the fact that it is an active category.

Table 1. ALT and AST of Covid patients monitored

Name of analysis	**ALT (U/L)**	**AST (U/L)**
Minimum value	41.28 U/L	40.58
Maximum value	462.27	281.55
Average value	89.15±39.69	73.48±27.49
Normal values	7-56 (men) 4-19 (women)	8-48

Also, within this group, the standard deviation has a high value (96.84±63.17 U/L), which shows that this group is very inhomogeneous, and the number of conditions associated with transaminase values, such as impairment of liver, myocardial and lung function, begin to be present, but in a smaller number of individuals. Also interesting is the behavior of the 70-95 age group, in which a decrease in the mean (81.89±27.41 U/L) and maximum values of ALT is observed, but this group, according to the value of the standard deviation, is much more homogeneous and are associated with the natural aging process, which also comes with a slower enzymatic and immune response. In the case of AST values, the mean concentration values are quite close for all four age groups studied and do not exceed 2x the maximum permissible normal value of AST (see Table 3). According to the standard deviation, the AST values are quite homogeneous within the groups, with a decrease this time in the homogeneity in the group over 70 years old.

Another criterion chosen for comparing the results obtained is the sex of Covid 19 positive patients (see figure 2). The mean AST and ALT did not vary much in the male compared to the female group, with higher ALT than AST still being recorded. The results were much more homogeneous for AST than for ALT. Within the ALT values for both sexes, heterogeneous values were obtained, due to the multitude of factors that can intervene in their registration: age, health status, degree of Covid infection, etc

Interesting results were also obtained in the grouping of patients according to the environment they come from, urban or rural, a criterion associated especially with living

conditions, food, density of human interactions and addressability to medical units. As can be seen in Figure 3, the average ALT values for all individuals are very similar between urban and rural areas, with a very slight increase in rural areas. The average in both cases is just over 2x higher than the maximum allowed ALT value. On the other hand, when the groups are separated by gender, it can be seen that in urban men a higher average ALT value was obtained than in urban women and rural men, respectively. The situation changes in the case of women in rural areas, who have a higher ALT value than women in urban areas and men in rural areas, respectively. This last group, of rural women, is also the least homogeneous, having a higher standard deviation, from the average of 76.53±31.73 U/L for urban women to the average of 93.76±48.97 U/L for rural women..

Table 2. The influence of age on ALT values in Covid patients

ALT (U/L)					
Age	**18-39**	**40-49**	**50-59**	**60-69**	**70-95**
Minimum value	46.79	42.56	41.33	41.28	42.79
Maximum value	72.18	181.25	367.62	462.27	201.46
Average value	57.39±11.62	76.40±32.40	103.13±48.67	96.84±63.17	81.89±27.41

Table 3. Influence of age on AST values in Covid patients

AST (U/L)					
Age	**18-39**	**40-49**	**50-59**	**60-69**	**70-95**
Minimum value	45	41.72	40.78	40.75	40.58
Maximum value	93.17	141.8	137.23	259.32	281.55
Average value	66.25±13.76	68.78±22.90	69.16±20.44	73.16±25.25	75.72±31.33

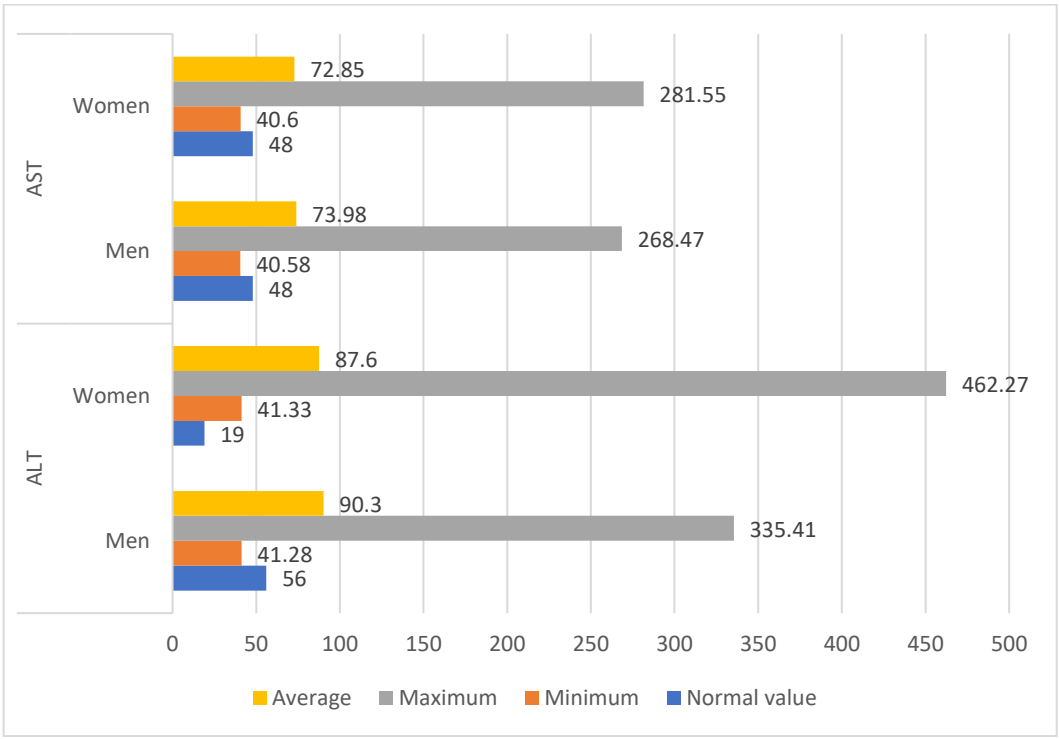

Figure 2. ALT and AST values of Covid patients by sex

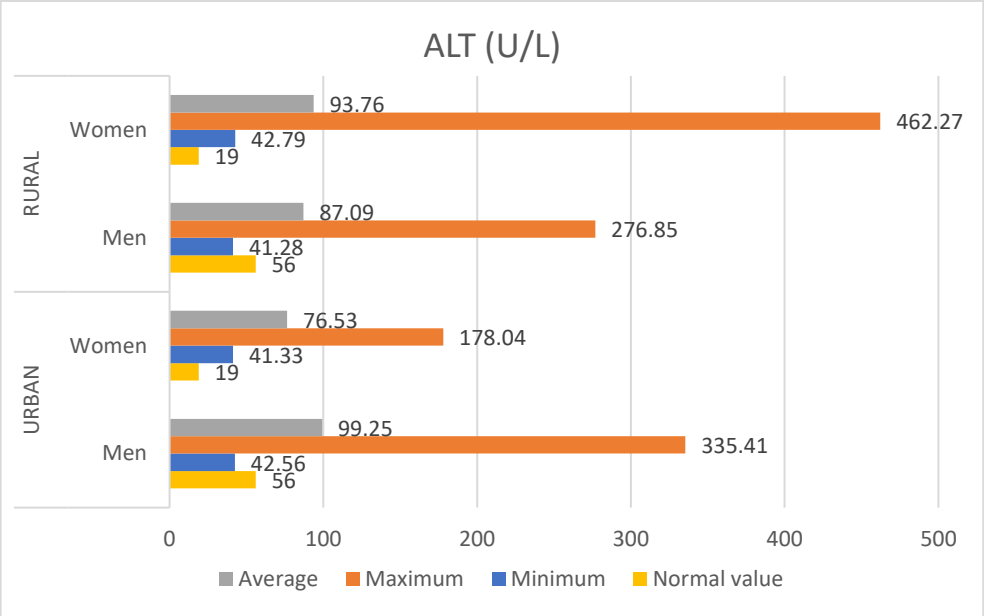

Figure 3.. *ALT values of urban and rural population with Covid 19*

When analyzing the AST values according to the environment, it can be observed that the average value is higher in rural areas compared to urban areas, both for men and women. On the other hand, the average value of AST in urban areas was higher in men than in women, while in rural areas the situation was the opposite (Figure 4). The groups discussed for the AST values proved to be homogeneous in terms of standard deviation in this case. Figure 4 shows that significantly higher maximums were achieved for both men and women in rural areas compared to urban areas, which would indicate the presence of pre-existing conditions, probably with or without poor treatment, due to reduced addressability to the doctor.

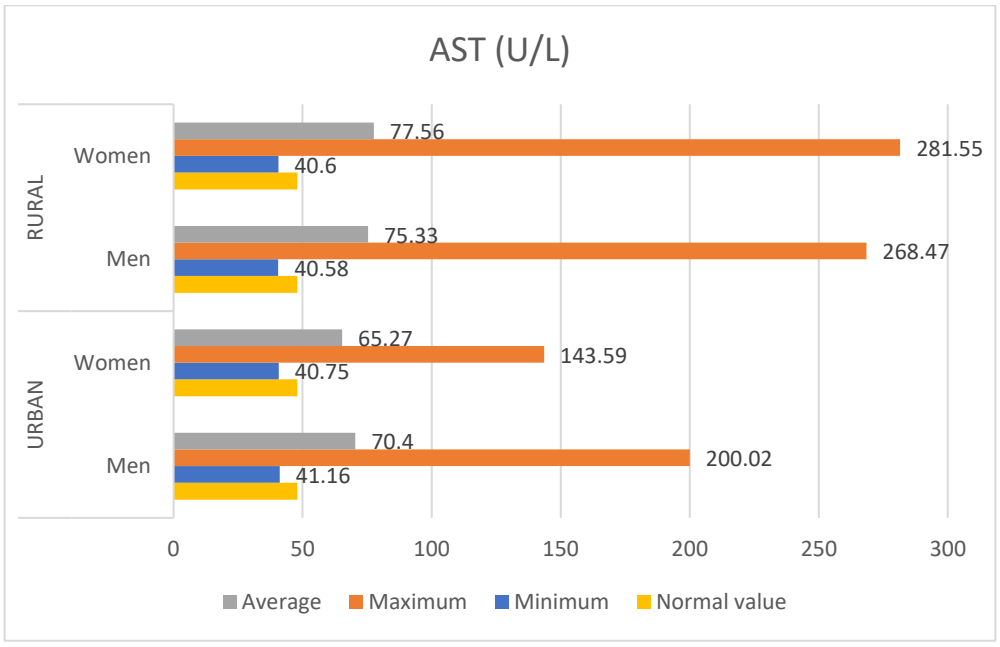

Figure 4. *AST values of the urban and rural population with Covid 19*

Case study

The patient taken in the case study is a 37-year-old male, without chronic diseases, from an urban environment, infected with the SARS-CoV-2 virus. 10 days after the first analysis, she presented altered general condition, fatigue, insufficiency, profuse sweating, fever of 39°C, myalgia, slight dyspnea (O2 saturation being 86%), accentuated tachycardia (pulse 44 beats/min), anosmia (loss of smell) and aguesia (loss of taste). At the doctor's request, medical tests were performed and a marked increase in transaminases of 10x higher for ALT and about 3x higher for AST was observed. The following paraclinical analyzes were collected at the patient's request, two weeks after the second determination and it was observed that transaminases showed significant decreases, and after 3 months from the onset of the Covid 19 disease, transaminases had values close to normal. 7 months after infection, the patient was titrated .

Ig G SARS CoV-2 antibodies, and the value was 757.80 U/mL, 75x higher (n.v. 0-10 U/mL), highlighting the maintenance of normality of the values for transaminases. The SARS CoV-2 Ig G antibodies were titrated again 11 months after the diagnosis of the disease were >1000 U/mL, which confirms that the patient was infected with the SARS-CoV-2 virus, and following treatment and cure the body developed Ig G antibodies, which are in the chronic phase. SARS-CoV-2 Ig G antibodies were performed on the Mindray CL-900 automated analyzer. We mention that the patient has not been vaccinated against the SARS-CoV-2 virus, so the formation of antibodies in this case is strictly associated with the patient's passage through the disease. The decrease in transaminase values to normal values was maintained even when they were determined 11 months after infection, which can be said that their functions returned to normal (Fig. 5)

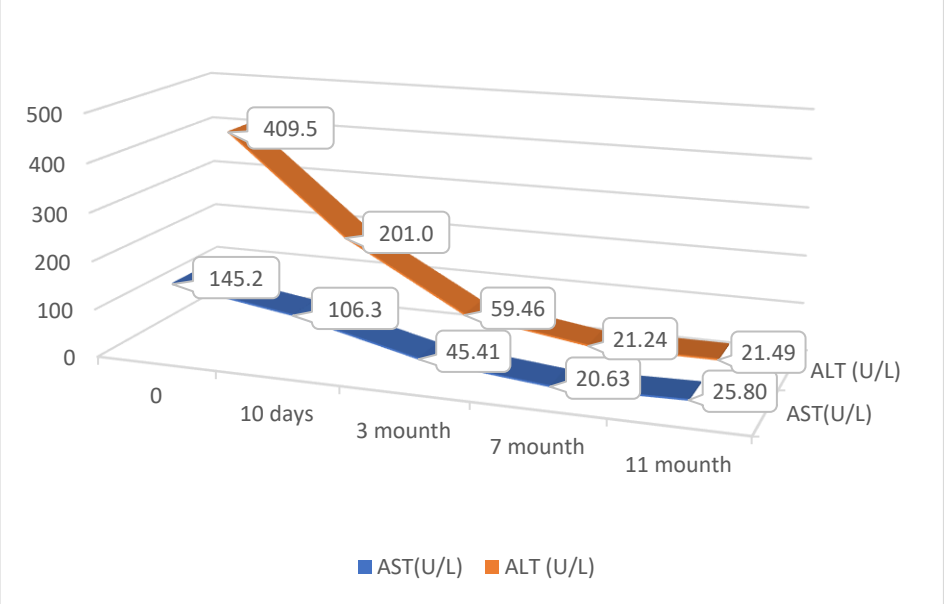

Figure 5. The evolution over time of the transaminase values of a patient, a 34-year-old man, from an urban environment, without chronic diseases

CONCLUSION

The results obtained from the study are consistent with other data in the literature as a result of observations made by other study groups. An increase in transaminases has been frequently observed in COVID-19 patients and although it does not require therapy, its presence indicates a potential for severe progression of respiratory disease. The results obtained demonstrate that it is necessary to monitor liver function samples during infection with the new coronavirus in both patients with normal liver and those with chronic liver disease [46-48]. The maximum value of transaminases was observed in patients aged 60-69 years for ALT (462.27 U/L) and for patients in the age range 70-95 years for AST (281.55 U/L). As already mentioned, ALT transaminase is a good marker of the destruction that occurs under

the action of the SARS-CoV-2 virus in the liver, while the activity of AST is also manifested in other tissues, such as the heart, skeletal muscles, brain and kidneys. The lowest transaminase levels were recorded in young patients. Large increases in ALT were recorded especially in active patients over 50 years of age, and in AST in elderly patients. No significant differences were noticed between the group of Covid-positive male patients and the female group in terms of transaminase values

Higher mean ALT values were found in urban men and rural women, respectively. Both Covid-positive men and women in rural areas had higher AST values. Comparatively, the mean values of ALT were generally higher than those of AST, which shows that in terms of transaminases the conditions for morbidity were relatively low. The exception can be seen at the maximum value of AST compared to ALT in the age category 70-95 years, where the risk of morbidity due to infection with the SARS-CoV-2 virus was higher.

The case study conducted in a 34-year-old, clinically healthy, unvaccinated, Covid-infected patient in the age range of young patients shows that in the acute period transaminases were significantly increased, 10 times ALT and 3.5 times AST. The decrease in transaminase values was progressively achieved over time, reaching normal values in the time interval 3-7 months, given that the patient produced antibodies to the SARS-CoV-2 virus.

REFERENCES

1. Haque S.M., Ashwaq O., Sarief A., Azad John Mohamed AK. A comprehensive review about SARS-CoV-2, *Future Virol.*, 2020, 15(9), pp. 625-648
2. Lotfi M., Rezaei N., SARS-CoV-2: A comprehensive review from pathogenicity of the virus to clinical consequences, *J Med Virol.*, 2020, 92(10), pp.1864-1874
3. Santamaria-Castro I., Leiva-Rebollo R., Marín-Wong S., Jimenez-Guardeño J.M., Ortega-Prieto A.M., Molecular mechanisms of SARS-CoV-2 entry: implications for biomedical strategies, *Microbiol Mol Biol Rev*, 2025, 89:e00260-24. https://doi.org/10.1128/mmbr.00260-24
4. Rabaan A.A. et al., An updated review on pathogenic coronaviruses (CoVs) amid the emergence of SARS-CoV-2 variants: A look into the repercussions and possible solutions, *Journal of Infection and Public Health*, 2023, 16(11), pp. 1870-1883
5. Cui J. et al., Origin and evolution of pathogenic coronaviruses. *Nat Rev Microbiol*. 2019;17(3):181–192. doi:10.1038/s41579-018-0118-9
6. Zhu N. et al., China Novel Coronavirus Investigating and Research Team. A Novel Coronavirus from Patients with Pneumonia in China 2019, *N Engl J Med.,* 2020, doi:10.1056/NEJMoa2001017. [Epub ahead of print] PubMed PMID: 31978945.
7. Zhou, P. et al., A pneumonia outbreak associated with a new coronavirus of probable bat origin. *Nature*, 2020, https:// doi.org/10.1038/s41586-020-2012-7
8. Chan J.F. et al., Genomic characterization of the 2019 novel human-pathogenic coronavirus isolated from a patient with atypical pneumonia after visiting Wuhan, *Emerg Microbes Infect*., 2020, 9(1), pp. 221-236. doi: 10.1080/22221751.2020.1719902
9. Andersen K.G. et al., The proximal origin of SARS-CoV-2, *Nat Med*., 2020, 26(4), pp. 450-452, doi:10.1038/s41591-020-0820-9
10. Lam, T.T. et al., Identifying SARS-CoV-2 related coronaviruses in Malayan pangolins, *Nature,* 2020, 583, pp. 282–285 https://doi.org/10.1038/s41586-020-2169-0
11. Coutard, B. et al., The spike glycoprotein of the new coronavirus 2019-nCoV contains a furin-like cleavage site absent in CoV of the same clade, *Antiviral Res*,, 2020, 104742, doi: 10.1016/j.antiviral.2020.104742. Epub 2020 Feb 10. PMID: 32057769; PMCID: PMC7114094
12. Rothe C, et al., Transmission of 2019-nCoV Infection from an Asymptomatic Contact in Germany. *The New England Journal of Medicine*, 2020, 382(10), pp. 970-971.
13. Zou L, et al., SARS-CoV-2 Viral Load in Upper Respiratory Specimens of Infected Patients. *The New England Journal of Medicine*, 2020, 382(12), pp. 1177-1179
14. Pan X., Chen D., Xia Y., Wu X., Li T., Ou X., Zhou L., Liu J., Asymptomatic cases in a family cluster with SARS-CoV-2 infection, *Lancet Infect Dis.,* 2020, 20(4), pp. 410-411
15. Li R, Pei S, Chen B, Song Y, Zhang T, Yang W, Shaman J., Substantial undocumented infection facilitates the rapid dissemination of novel coronavirus (SARS-CoV-2), *Science*, 2020, 368(6490), pp. 489-493
16. Jin J.M,. Bai P., He W., Wu F., Liu X.F., Han D.M., Liu S., Yang J.K., Gender Differences in Patients With COVID-19: Focus on Severity and Mortality, *Front Public Health*, 2020, 8:152, pp. 1-6

17. Mehta P, McAuley D.F., Brown M., Sanchez E., Tattersall R.S., Manson J.J., COVID-19: consider cytokine storm syndromes and immunosuppression, *Lance,* 2020, 395(10229), pp. 1033–1034
18. Thevarajan, et al., Breadth of concomitant immune responses prior to patient recovery: a case report of non-severe COVID-19. *Nature medicine*, 2020, *26*(4), pp. 453-455.
19. Grifoni, A., et al., Targets of T cell responses to SARS-CoV-2 coronavirus in humans with COVID-19 disease and unexposed individuals. *Cell*., 2020, 181(7), pp. 1489 - 1501
20. Zhao, J., et al., Antibody responses to SARS-CoV-2 in patients of novel coronavirus disease 2019. *Clinical Infectious Diseases*, 2020, 71(16):2027-2034.
21. Wu, C., et al., Risk factors associated with acute respiratory distress syndrome and death in patients with coronavirus disease 2019 pneumonia in Wuhan, China. *JAMA internal medicine*.
22. Guan, et al., Clinical characteristics of coronavirus disease 2019 in China, *New England Journal of Medicine*, 2020, *382*(18), pp. 1708-1720.
23. Huang X.-J., Choi Y.-K., Im H.-S., Yarimaga O., Yoon E., Kim H.-S., Aspartate Aminotransferase (AST/GOT) and Alanine Aminotransferase (ALT/GPT) Detection Techniques. *Sensors,* 2006, *6*, pp. 756-782 AST
24. Liu Z., Que S., Xu J., Peng T., Alanine aminotransferase-old biomarker and new concept: a review. *Int J Med Sci.*, 2014, 11(9), pp. 925-35. ALT
25. Ovale A.F., Charles C., Rosenbaum J., Villalba-Davila P., Sharma S., Khandakar S., Wallach T., Severe acute respiratory syndrome coronavirus 2 transaminase elevation likely of non-hepatic origin, with protection from older age and vaccination, *JPGN Rep*, 2025 6(3), pp. 255-261
26. Sumner M. W., Florin T. A., N. Kuppermann, Xie J., Tancredi D.J., Freedman S.B., Liver transaminase concentrations in children with acute SARS-CoV-2 infection, Clinical Biochemistry, 2023, 118, pp. 110588, https://doi.org/10.1016/j.clinbiochem.2023.110588
27. Bzeizi K., Abdulla M., Mohammed N. et al., Effect of COVID-19 on liver abnormalities: a systematic review and meta-analysis, *Sci Rep*, 2021, 11, pp. 10599, https://doi.org/10.1038/s41598-021-89513-9
28. Wagner J., Garcia-Rodriguez V., Yu A., Dutra B., Larson S., Cash B., DuPont A., Farooq A. Elevated transaminases and hypoalbuminemia in Covid-19 are prognostic factors for disease severity, *Sci Rep*, 2021, 11(1), pp. 10308
29. Menezes Estevam Alves M. H. et al., The enzymes in COVID-19: A review, *Biochimie*, 2022, 197, pp. 38-48
30. Cabibbo G, Rizzo G, Stornello C, Craxi A. SARS-CoV-2 infection in patients with a normal or abnormal liver, *J Viral Hepatol*, 2021, 28, pp. 4-11
31. Metawea M, Yousif W, Moheb I., COVID-19 and liver: an A-Z literature review, *Dig Liv Dis*, 2021, 53, pp. 146-152
32. Nardo A., et al., Pathophysiological mechanisms of liver injury in COVID-19, *Liv Intern*, 2020, 00, pp. 1-13
33. Pan L, et al., Metabolic associated fatty liver disease increases the severity of COVID-19: a meta-analysis, *Dig Liv Dis*, 2021, 53, pp. 153-157
34. Portincasa P, et al., Hepatic consequences of COVID-19 infection. Lapping or biting?, *Eur J Int Med*, 2020, 77, pp 18-24
35. Lei H, et al., Potential effects of SARS-CoV-2 on the gastrointestinal tract and liver, *Biomedicine & Pharmacotherapy,* 2021, 133, 111064, pp 1-6
36. Singh B, Kaur P, Maroules M., Splanchnic vein thrombosis in COVID-19: A review of literature, *Dig Liv Dis,* 2020; 52, pp 1407-1409
37. Anirvan P., et al., Liver injury in COVID-19: The hepatic aspect of the respiratory syndrome-what we know so far, *World J Hepatol,* 2020, 12, pp. 1182-1197
38. Moon A., et al., High mortality rates for SARS-CoV2 infection in patients with pre-existing chronic liver disease and cirrhosis: Preliminary results from an international registry, *J Hepatol*, 2020, 73, pp. 705-708
39. Brito C., Barros F., Lopes E., Mechanisms and consequences of COVID-19 associated liver injury: What can we affirm?, *World J Hepatol*, 2020, 12, pp 413-422
40. Mantovani A., Beatrice G., Dalbeni A. Coronavirus disease 2019 and prevalence of chronic liver disease: a meta-analysis, *Liver Int*, 2020, 40, pp. 1316-1320
41. Reddy R., SARS-CoV-2 and the liver: Considerations in hepatitis B and hepatitis C infections, *Clinical Liver Disease*, 2020, 5, pp 191-194

42. Kushner T., Cafardi J., Chronic liver disease and COVID-19: alcohol use disorder/alcohol-associated liver disease, nonalcoholic fatty liver disease/nonalcoholic steatohepatitis, autoimmune liver disease, and compensated cirrhosis, *Clinical Liver Disease*, 2020, 5, pp 195-199
43. Pawlotsky J., COVID-19 and the liver-related deaths to come, *Nature Reviews Gastroenterol & Hepatol,* 2020, 17, pp 523-525
44. Huang X.-J., Choi Y.-K., Im H.-S., Yarimaga O., Yoon E., Kim H.-S., Aspartate Aminotransferase (AST/GOT) and Alanine Aminotransferase (ALT/GPT) Detection Techniques, *Sensors,* 2006, 6, pp. 756-782
45. Skala, J.H., Waring, P.P., Lyons, M.F., Rusnak, M.G., Alletto, J.S., Methodology for Determination of Blood Aminotransferases, In: Leklem, J.E., Reynolds, R.D. (eds) Methods in Vitamin B-6 Nutrition. Springer, Boston, MA., 1981, https://doi.org/10.1007/978-1-4684-9901-8_10
46. Fix O., Reddy R., Coronavirus disease 2019 (COVID-19): Issues related to liver disease in adults. www.uptodate.com, last updated nov 2025, COVID-19: Issues related to liver disease in adults - UpToDate
47. Boettler T., et al., Impact of COVID-19 on the care of patients with liver disease: EASL-ESCMID position paper after 6 months of the pandemic, *JHEP Reports*, 2020, 2:100169, pp. 1-10
48. Bakkaloglu O.K., Onal U., Eskazan T., Kurt E.A., Candan S., Karaali R., Borekci S., Urkmez S, Dikmen Y., Tabak F., Tuncer M., Hatemi I., Increase in transaminase levels during COVID-19 infection and its association with poor prognosis, *Singapore Med J.,* 2023, 64(10), pp. 640-644

MONITORING OF IRON CONTENT INTO A WATER SOURCE

Caius Marian STĂNĂŞEL[1], Gabriela Elena BADEA[2]

[1]University of Oradea, Faculty of Informatics and Sciences, Department of Chemistry,
CSA Master student caius.stanasel@gmail.com
[2]University of Oradea, Faculty of Informatics and Sciences, Department of Chemistry

Abstract: *The composition of water includes a large number of mineral substances, some of which are present in the tissues of the human body. Normally, the required mineral intake for the body is supplemented through diet and only to a lesser extent through water, but at the same time, the variation in the concentration of minerals in the water compartment has consequences for the human body. Iron is essential for the production of red blood cells, which transport oxygen throughout the body. Any substance present in water above certain concentrations can be toxic to the human body. For the purpose of determining their level in water, the primary contribution is given by the spectral analysis method. In this paper, a water source from a drilled well of a dwelling in Oradea was taken for study. Monitoring was conducted during the summer period, tracking the chemical composition. In the present paper are shown the iron analysis of the samples by atomic absorption spectrometry, and a statistical processing of the data was performed based on the obtained results. The combined analysis of the iron distributions using Ridgeline Charts and Normal Probability Plots over the three months highlights an evolution from a bimodal structure towards a unimodal form with positive skewness.*

Keywords: ***water pollution, distribution, iron***

INTRODUCTION

There is a close correlation between the minerals contained in water and their necessity in the human body[1]. Physiopathologists have described the importance of mineral substances in the body and the disorders that can occur in the case of mineral excesses, thus giving rise to the concepts of mineral excess and mineral deficiency, which lead to imbalances in the body.

The factors that influence the toxic action[2] of chemical substances in water are: concentration, solubility, the substance's stability in water, the simultaneous presence of multiple toxic substances in the water, and the presence of the same substances in the air.

Iron is the most important mineral for the production of red blood cells. Iron deficiency can cause a series of symptoms, such as fatigue, shortness of breath, dizziness, headaches, and decreased immunity.

One of the aims of this paper was to perform the quantitative analysis of iron in water samples collected from a drilled well, to verify whether this water can be used as a potable water source[3]. The well was monitored during three months of the summer time. The intake of this cation is necessary to ensure the body's mineral balance and prevent many diseases.

MATERIALS AND METHODS

The analysis of the mentioned cation in the water samples was carried out by the Atomic Absorption Spectroscopy (AAS) method, through the direct aspiration of the samples into an air-acetylene flame[4-7]. Using this method, iron concentrations of up to 3 mg/l can be optimally measured at a wavelength of 248.33 nm.

The analysis comprises several stages, with the following sequence:

- Selection of the hollow cathode lamp.
- Editing the working method.
- Editing the file with samples information.
- Preparation of the standard solutions.

- Preparation and stabilization of the samples to be analyzed.
- Analysis of the standard solutions.
- Plotting the calibration curve and checking its correctness.
- Analysis of the samples.

Starting from the standard solution with a concentration of 1000 mg Fe^{3+}/l, by successive dilutions made in 100, 50, or 25 ml volumetric flasks were obtained the standard solutions with the following concentrations: 0.02; 0.05; 0.1; 0.5; 1.0; 2.0 mg/l.

The analysis of any set of experimental data was then performed using the statistical method[8]. Having a sufficiently large data sample, the measurements visualized and evaluated in the present paper on graphs for multiple distributions and for testing the normality of a single distribution[9].

The Ridgeline Chart allows for the comparison of multiple distributions and the identification/visualization of differences in central tendency (mean, median), dispersion (variability), skewness, the evolution of measurements, or the distribution trend over time.

Variability or dispersion measures the mean squared deviation of the data from the mean. The sample standard deviation (s) is the square root of the variance and is easier to interpret because it has the same units of measurement as the original data. A larger standard deviation means greater dispersion and a wider peak, while a smaller standard deviation means lower dispersion and a narrower peak.

$$s = \sqrt{\frac{\sum_{1}^{n}(x_i - \bar{x})^2}{n-1}} \qquad (1)$$

where:

$\bar{x}$ - average of the sample values;

x_i - value i in the sample;

n - total number of data in the sample.

Skewness measures the degree of lack of symmetry in a distribution. For a data sample, the sample skewness (g) is calculated as follows:

$$g = \frac{n}{(n-1)(n-2)} \sum_{1}^{n} \left(\frac{x_i - \bar{x}}{s}\right)^3 \qquad (2)$$

The Normal Probability Plot is usually used after exploratory analysis when the verification of a specific distribution is desired. The main purpose of this graph is to visually assess how well the observed data points align with a theoretical normal distribution.

A percentile is a statistical measure that indicates the value below which a given percentage of observations in a data set falls.

RESULTS AND DISCUSSIONS

1. Results of AAS analysis

2.

The calibration curve obtained is presented in Figure 1. The linear regression coefficient was good, 0.998371 being possible to obtain the iron content in the water samples, based on calibration curve. In Figure 2 you may see the values of iron concentration during the three months of evaluation.

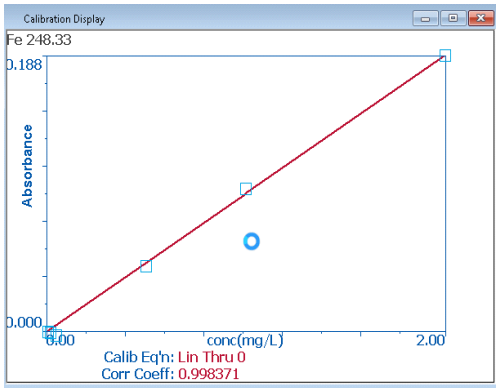

Figure 1. Calibration curve for iron.

Regarding the results of iron analysis in water samples (Figure 2), it is found that there are deviations from the drinking water limit, slightly exceeding the value of 0.1 mg/l on some days.

In June, a single higher value was recorded, 0.15 mg/l, and in July and August there were several days when the iron concentration exceeded the value of 0.1, reaching a maximum in July of 0.159 mg/l, and in August 0.192 mg/l.

The minimum values determined in each of these months are equal, being 0.023 mg/l.

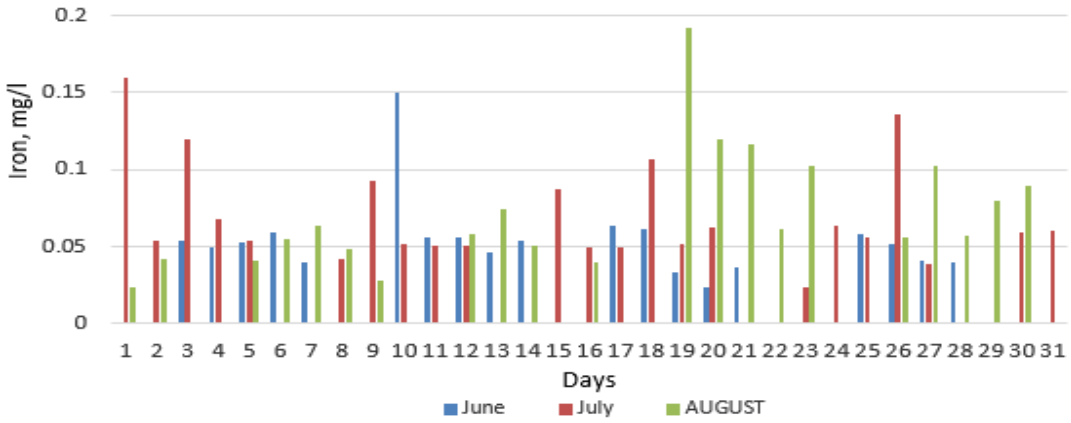

Figure 2. Variation of iron content of water in time

3. Statistic analysis

The graph (Figure 3) presents the measured value of Iron (Fe) over three months: June (black), July (red), and August (blue).

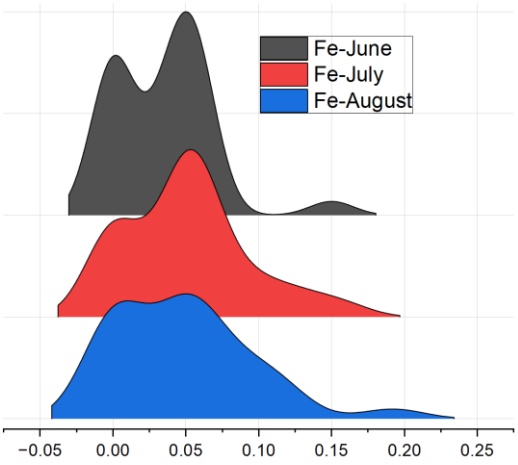

Figure 3. Ridgeline Chart distribution for iron

The Ridgeline Chart indicated in June a bimodal distribution, featuring two important, distinct peaks. The first, smaller peak is centered around the value of 0.00, and the second, more prominent and broader peak, is centered around 0.06-0.07.

The two peaks suggest that there might be two different conditions influencing the Fe levels in June. In July the distribution is also bimodal, but it has a more pronounced peak centered around 0.05-0.06, which is very close to the second peak of the June distribution.

Distribution in August is also bimodal, with the main peak situated around 0.04-0.05, being slightly lower than the main peak in July and the second peak in June.

The results of testing the deviation from normality for iron concentrations during the three months of monitoring are suggestively illustrated in Figures 4-6.

By Normal Probability Plot interpretation in June (Figure 4) the points follow a general trend, but exhibit a pronounced 'S' shaped curve, which indicates a distribution with heavy tails or bimodality.

The points at the extremes, especially at low values (approximately 0.00) and high values (above 0.05-0.06), visibly deviate from the reference line. The last point at approximately 0.15 is outside the confidence limit.

In July (Figure 5) the measured data has a general linear trend but shows a significant upward curve towards the right, especially at the higher percentiles. This shape indicates positive skewness (right-skewness). Some points in the upper tail (above 0.10), including the last point at approximately 0.15, are on the upper confidence limit.

The points in the lower tail (around 0.00) also deviate, indicating a higher-than-expected density. Although most of the data clusters around the mean, the presence of larger values in the tail causes the distribution to be non-normal.

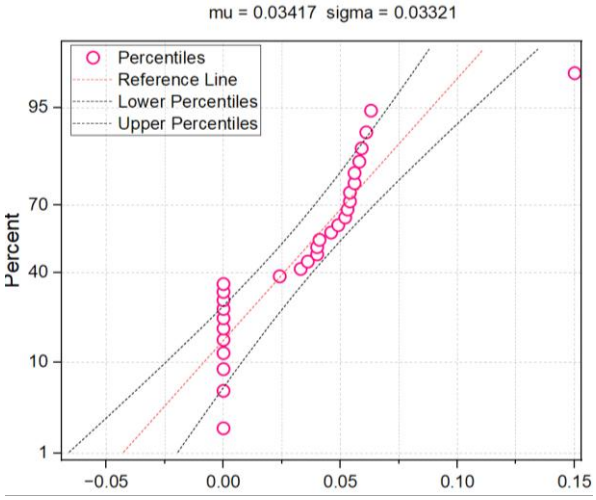

Figure 4. Normal Probability Plof of Fe -June

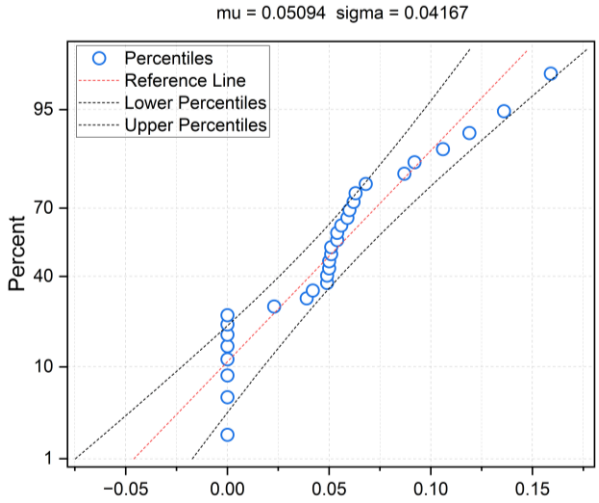

Figure 5. Normal Probability Plof of Fe -July

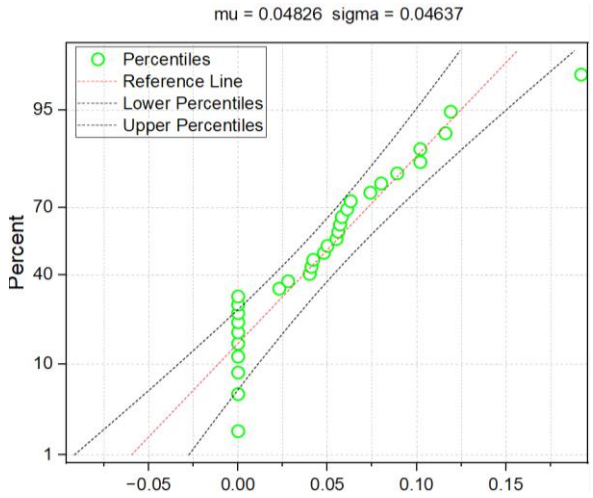

Figure 6. Normal Probability Plof of Fe -August

The observed data from August (Figure 6) shows a general linear trend but exhibits a steep upward and rightward curve, much more pronounced than in July. This indicates a strong positive skewness.

The points in the upper tail (above 0.10), especially the last point at approximately 0.15, are clearly outside the upper confidence limit. This suggests the presence of extreme values, larger than those expected in a normal distribution. Furthermore, the points in the lower tail (around 0.00) deviate from the line, indicating increased density. The sharp curvature and the outlier points in the Normal Probability Plot indicate strong skewness and a non-normal distribution due to this severe asymmetry.

CONCLUSIONS

The combined analysis of the Iron (Fe) distributions using Ridgeline Charts and Normal Probability Plots over the three months highlights an evolution from a bimodal structure towards a unimodal form with positive skewness.

- In June, the distribution is bimodal, with two distinct peaks, and the Normal Probability Plot for June confirms this through its 'S' shaped curve and deviations at the extremes.
- In July, the iron concentration shifts towards a distribution with a main peak at approximately 0.05-0.06, but it exhibits positive skewness, also seen in the upward curve of the Normal Probability Plot for July, where the values in the upper tail exceed the confidence limits.
- In August, this positive skewness is maintained, variability increases, and an extended right tail appears. The corresponding Normal Probability Plot for this month confirms this deviation from normality through its sharp curvature and values falling outside the reference limit in the upper tail.

Thus, over the three months studied, the iron levels indicate a growing deviation from a normal distribution. These data reflect the seasonal dynamics of iron.

REFERENCES

[1] ***, Guidelines for drinking-water quality, 4th Edition, Geneva: World Health Organization, 2022.
[2] GOEL P.K., Water pollution: Causes, effects and control, New Delhi: New Age International, 2006.
[3] HAIDUC I., Chimia mediului ambiant, Controlul calității apei, Editura Universității Babeș Bolyai, Cluj-Napoca, 1996.
[4] ŞTEFĂNESCU O.E., ŞTEFĂNESCU M., Chimie analitică instrumentală. Principii, aplicaţii, experimente, Vol. II, Editura Politehnica Timişoara, 2019.
[5] FARRUKH M.A., Atomic Absorbtion Spectroscopy, InTech Publication, 2011.
[6] ROMAN L., SĂNDULESCU R. (1999), Chimie analitică – Volumul III – Metode de separare și analiză instrumentală, Editura Didactică și Pedagogică București, 1999.
[7] ***, Perkin Elmer Corp., Analytical Methods for Atomic Absorption Spectrophotometry, 2018.
[8] BADEA G.E., Prezentarea şi prelucrarea datelor experimentale, euoradea.ro, 2025.
[9] ŞTEFĂNESCU M., ŞTEFĂNESCU O.E., Chimie analitică instrumentală. Principii, aplicaţii, experimente, Vol. I, Editura Politehnica Timişoara, 2016.

DETERMINATION OF IRON AND ASCORBIC ACID FROM NETTLE, SPINACH AND PARSLEY

Claudia Mona MORGOVAN[1], Anda Ioana Grațiela PETREHELE[1], Alexandrina FODOR[1] Mihaela IONCU[2], Maria CĂRĂBAN[3], Camelia Daniela IONAȘ[1]

[1] Department of Chemistry, Faculty of Informatics and Sciences, University of Oradea, 1 University Street, 410087, Oradea, Romania
[2] Master student, Structural and Applied Chemistry, Faculty of Informatics and Sciences, University of Oradea, 1 University Street, 410087, Oradea, Romania
[3] Chemistry teacher, International School of Oradea, 4C Ceyrat Street, Oradea, Romania

Abstract: *The aim of this paper is to quantify the content of iron and ascorbic acid (vitamin C) in three plant species with high nutritional value: Urtica dioica (nettle), Spinacia oleracea (spinach) and Petroselinum crispum (parsley). The study is part of the field of applied biochemistry and aims to investigate the potential of these plants as natural sources of essential micronutrients in the context of preventive nutrition and public health.*
The work is based on the hypothesis that the absorption of non-heme iron, present in plant sources, is significantly improved in the presence of ascorbic acid, which justifies the importance of simultaneous evaluation of the two compounds. In this regard, the analysis focuses on determining the concentration of iron and vitamin C in fresh plant material by validated laboratory methods.
Keywords: iron, ascorbic acid, nettle, spinach, parsley

INTRODUCTION

In the current context of increasing interest in a healthy and balanced diet, natural sources of essential micronutrients, such as iron and vitamin C, are attracting more and more attention from researchers and consumers alike. Iron is an essential mineral for the optimal functioning of the human body, being involved in fundamental processes such as oxygen transport, DNA synthesis and energy metabolism. Iron deficiencies can lead to iron deficiency anemia, a widespread condition globally, with a major impact on quality of life [1-5].

Vitamin C, also known as ascorbic acid, plays a crucial role in maintaining the health of the immune system, protecting cells against oxidative stress and, last but not least, facilitating the absorption of iron in the intestine. Thus, the simultaneous presence of iron and ascorbic acid in plant-based food sources can provide significant nutritional benefits [6-8].

Green plants such as nettle (Urtica dioica), spinach (Spinacia oleracea) and parsley (Petroselinum crispum) are known for their high content of bioactive substances, including iron and vitamin C. These plants are widely used in food and phytotherapy due to their nutritional and therapeutic value, and exploring their chemical composition can help promote their use in preventing and combating nutritional deficiencies [9-14].

The present paper aims to investigate the iron and ascorbic acid content of nettle, spinach and parsley, by applying specific methods of extraction and analytical determination. The main objectives include the comparative analysis of the three plant species from the perspective of the concentration of Fe and vitamin C and the identification of the most efficient methods of determination for these compounds.

EXPERIMENTAL PART

1. Objectives of the paper

The general objective of this work is to determine the content of iron and ascorbic acid (vitamin C) in three common plant species — Urtica dioica (nettle), Spinacia oleracea (spinach) and Petroselinum crispum (parsley) — using chemical analysis methods applicable in the laboratory. The paper aims to highlight the quantitative variations between these species, in order to support

nutritional recommendations based on empirical data.

The specific objectives pursued are the following:

- ✓ Determination of iron content in nettle, spinach and parsley leaves by chemical analysis techniques (e.g. 1,10-phenanthroline reagent spectrophotometry or classical volumetric methods).
- ✓ Determination of ascorbic acid concentration in the same plant samples using redox titrimetry methods (with 2,6-dichlorophenolindophenol – DCPIP) or other validated processes.
- ✓ Comparison of the values obtained for the three species, in order to determine the plant with the highest content in each of the two compounds.
- ✓ Analysis of the relationship between iron and vitamin C from a biochemical and nutritional point of view, given that ascorbic acid facilitates the intestinal absorption of non-heme iron.
- ✓ Formulation of applicative conclusions, regarding the potential of using these plants in functional nutrition and prevention of iron deficiency anemia.

2. Materials and methods

During the elaboration of the paper, an experimental approach was adopted in order to quantitatively determine the iron and ascorbic acid content of three plant species with high nutritional value. The study was carried out between March and April 2025, in laboratory mode, by applying classic methods of quantitative chemical analysis.

In the study, three plant species recognized for their rich content of essential nutrients, especially iron and vitamin C, were selected and analyzed. The samples were taken fresh, and then homogenized to allow the extraction of the active compounds. The three species analyzed were:

1. ***Urtica dioica*** (nettle) – a perennial herbaceous plant, rich in iron, chlorophyll and phenolic compounds, with traditional use in phytotherapy;
2. ***Spinacia oleracea*** (spinach**)** – a vegetable with intensely pigmented green leaves, frequently eaten raw or boiled, with a relevant contribution of non-heme iron;
3. ***Petroselinum crispum*** (parsley) – an aromatic plant frequently used in food, with a significant content of ascorbic acid and mineral elements.

The spinach (*Spinacia oleracea*) and parsley (*Petroselinum crispum*) used in the experiment were harvested by hand from a local garden in Porț, Bihor County. The harvest was carried out under ordinary agrotechnical conditions, from an individual household garden, without the use of chemical fertilizers or phytosanitary treatments, in order to obtain a plant material as representative as possible for domestic consumption.

Figure 1. Garden parsley (*Petroselinum crispum*), fresh harvest.

Figure 2. Garden spinach (*Spinacia oleracea*), fresh at the time of harvest

The nettle was harvested from the spontaneous flora, where it was found growing naturally.

The plant was selected at the stage of young development, with fresh, integral leaves, characterized by an intense green appearance, jagged edges and the presence of

specific stinging bristles. The image below captures in detail the morphological appearance of fresh nettle leaves, as they were harvested from the field:

Figure 3. Great nettle (Urtica dioica) – specimens harvested from the banks of the Criș River.

The image below illustrates the appearance of the plant material used in its fresh state for the extraction of vitamin C, as well as the homogenized form of the samples prepared for extraction and analysis:

Figure 4. Plant samples analyzed: from left to right – Spinacia oleracea (spinach), Petroselinum crispum (parsley), Urtica dioica (nettle). At the top is the fresh plant material, and at the bottom the processed form for extraction.

To determine the iron content, the plant material was used in the dry state, being represented by the leaves of Urtica dioica (nettle), Spinacia oleracea (spinach) and Petroselinum crispum (parsley). The samples were dried at 100 °C, then shredded to facilitate the extraction of the mineral compounds. The image below illustrates what they look like before and after homogenization:

2.1. Reagents

To determine the iron content of the plant samples, the ortho-phenantholline method was used, in which the bivalent iron (Fe^{2+}) forms an intensely orange complex. The reagents used in this method, prepared according to the procedure applied practically in the laboratory, are the following:

- 1 mL 1:1 hydrochloric acid solution – to create an acidic environment necessary for the reaction;
- 10 mL acetate buffer solution – prepared to stabilize pH around 4;
- 2 mL of ortho-phenanthroline solution – for the formation of the complex stained with bivalent iron;
- A few drops of NH_4OH solution – to adjust the optimal pH of the reaction;
- Iron standard solutions – with different concentrations (0.2 mg Fe, 0.4 mg Fe, 0.6 mg Fe, 1 mg Fe, 1.5 mg Fe), used to construct the spectrophotometric calibration curve;
- Sample solution – obtained by mineralizing 0.15 g of dry plant with concentrated HCl, followed by filling the volume to 50 mL.

The following reagents were used to titration ascorbic acid:

- 2% hydrochloric acid solution (HCl 2%) – to provide the acidic environment necessary for the reaction;
- Potassium iodide solution 1% (KI 1%) – component necessary for the generation of iodine;
- Potassium iodate solution 0.001 N (KIO_3) – oxidizing agent that produces excess iodine;
- Starch solution 1% – used as an indicator, which forms a blue colored complex in the presence of free iodine.

2.2. Apparatus:

- UV-Vis spectrophotometer (for determination of iron at $\lambda \approx 510$ nm),
- analytical balance,
- burettes, Berzelius glasses, rated balloons, test tubes, magnetic stirrer with heating,
- usual laboratory glassware, crucibles

2.3. Experimental Methods and Procedures

2.3.1. Determination of ascorbic acid (vitamin C) content

For the determination of vitamin C, an indirect titrimetric method was applied, based on the oxidation of ascorbic acid to dehydroascorbic acid with iodine generated in situ from a mixture of iodide and potassium iodate, in an acidic medium. The titration

endpoint is evidenced by the appearance of a persistent blue coloration due to the reaction of free iodine with starch, used as an indicator.

The experimental stages were as follows:

From 2 g of fresh leaves, vitamin C was extracted by homogenization in 20 mL of distilled water, followed by filtration. Each sample was then treated with the specific reagents and titrated with 0.001 N potassium iodate solution, according to the protocol.

In each test were added:

- 0.5 mL KI 1% solution,
- 0.5 mL HCl 2% solution,
- 2 mL of 1% starch solution.

The samples were immediately titrated with a solution of KIO_3 0.001 N, until the appearance of blue coloration

.

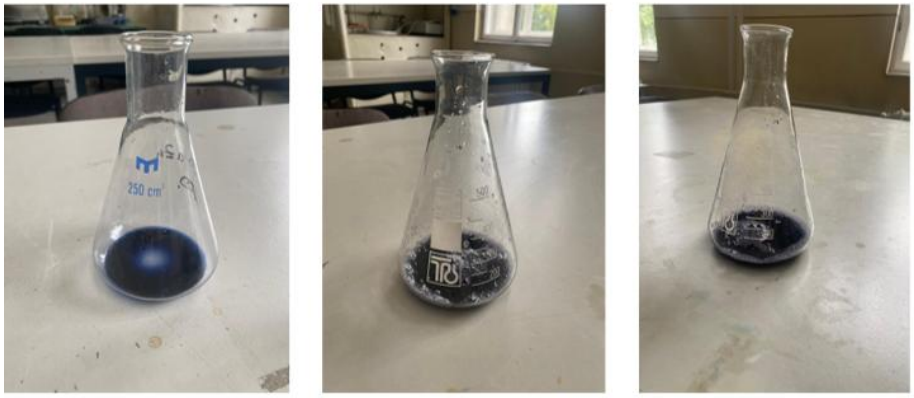

Figure 5. Visual steps of the titration reaction in the determination of vitamin C: from left to right – the solution reacts progressively until the appearance of the persistent blue coloration, specific to the end point of iodine titration, in the presence of starch as an indicator.

Calculation of vitamin C content

The determination of the ascorbic acid (vitamin C) content was carried out by volumetric titration, using a standard solution of potassium iodate 0.001 N. The oxidation reaction of ascorbic acid by iodate takes place in an acidic environment, in the presence of a starch-type indicator, which highlights the end point of the titration by the appearance of a persistent blue coloration.

2.3.2. Determination of iron content

To determine the iron content, a colorimetric method based on the reaction of bivalent iron (Fe^{2+}) with orthophenanthroline was applied, in the presence of a reducing agent, forming an intense orange colored complex. The intensity of the developed color is proportional to the concentration of iron in the sample and was measured spectrophotometrically at the wavelength of 510 nm.

In order to determine the iron content of the analyzed samples, it was necessary to draw a calibration curve. For this purpose, five standard solutions with known iron concentrations of 0.20 have been prepared; 0,40; 0,70; 1.00 and 1.50 mg Fe/dm^3. The solutions were prepared by adding precise volumes of the working standard solution: 1 mL for the concentration of 0.20 mg Fe/dm^3, 2 mL for 0.40 mg Fe/dm^3, and so on, up to 7.5 mL for 1.50 mg Fe/dm^3. The control solution was obtained using the same method with the addition of distilled water.

Then the same volumes of reagents were added to all samples: 1 mL of 10% hydroxymine solution (which reduces trivalent iron to bivalent iron), 10 mL of acetate buffer and 2 mL of orthophenanthroline. The pH was adjusted to approximately 4, using diluted ammonia solution, to ensure optimal reaction conditions. Each sample was then filled with distilled water to the final volume of 50 mL.

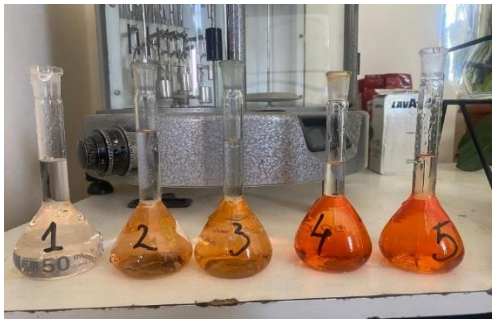

Figure 6. Standard solutions with increasing concentrations of Fe^{2+} (0–1.5 mg/

The solutions obtained this way were left to rest for 15 minutes and then the

absorption was measured at 510 nm, the values being used to build the calibration curve.

For the preparation of the plant material, the samples (spinach, parsley and nettle) were subjected to a dehydration process in the oven. Drying was carried out at a controlled temperature of over 100 °C for about an hour until a constant mass was reached. This step was essential for the complete removal of the water and to ensure the accuracy of subsequent iron content determinations, relative to the dry mass of the sample.

After the drying process was completed, 0.5 g of dry material was weighed from each plant sample. The samples thus prepared were subjected to a preliminary calcination step in crucibles, directly on an open flame (gas bulb), with the aim of completely removing the organic components and preparing the mineral residue for the determination of iron content.

After the calcination was completed, the resulting residue was treated with concentrated hydrochloric acid to solubilize the metal salts. The resulting solution was gravitationally filtered, and the filtrate obtained was supplemented with distilled water in a flask rated at the final volume of 50 mL. The sample thus prepared was subsequently used for comparative analysis with the iron standard solutions, in order to photometric determination of the concentration.

Figure 7..Mineralized samples completed at 50 mL, prepared for iron content analysis.

The samples were left to rest for 15 minutes for full color development, then the absorption was read at 510 nm relative to a control. The amount of iron was determined by interpolation on the calibration curve.

RESULTS AND DISCUSSIONS

The experimental results on the vitamin C content determined in the analyzed samples were summarized and presented in the table 1. For the determination of iron, each of the 5 samples in turn was inserted into the spectrophotometer after being calibrated according to the control and the following data were obtained from table 2.

Table 1. Vitamin C determined in samples

Sample	Vp (mL)	Vm (mL)	Viodate (mL)	Vit.C (mg)	Vit C mg/100 g
Spinach	2.7	0.4	2.3	0.2024	10.12
Parsley	3.5	0.4	3.1	0.2728	13.64
Nettle	1.1	0.4	0.7	0.0616	3.08

Table 2. Absorbances read for the standard solutions of iron

Nr.	Solution	Conc. (mg/L)	Absorbance	Wavelength (nm)
1	Standard	0	0,0301	510
2	Standard	0,2	0,0593	510
3	Standard	0,4	0,103	510
4	Standard	1	0,2271	510
5	Standard	1,5	0,3083	510

After the introduction of the standard samples into the spectrophotometer, both the above table, which contains the absorption values corresponding to the standard concentrations, and the

calibration curve, which illustrates the relationship between the measured absorption and the concentration of the analyzed substance, were generated.

After the calibration curve was done, the samples to be analyzed were inserted into the spectrophotometer. Following the measurements made, the absorption values for each sample were obtained, and based on them the corresponding concentrations were determined.

The results are presented in the following table 3.

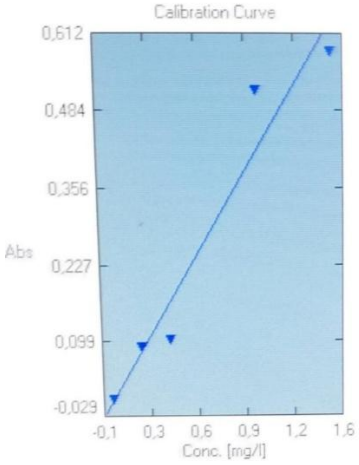

Figure 8..Calibration curve for iron

:

Table 3. Absorbances read for the plant solutions

Nr.	Plant	Conc. (mg/L)	Absorbance	Wavelength (nm)
1	spinach	0,0990	0,039	510
2	parsley	0,0970	0,038	510
3	nettle	0,1740	0,071	510

For a better interpretation of the data obtained, the absorption and concentration values corresponding to the analyzed samples were graphically represented. The following graph highlights the correlation between the measured absorption and the determined concentration, providing an overview of the distribution and uniformity of the results.

Following the measurements, the absorbance values were obtained, based on which the concentration was calculated. To determine the amount of iron (mg/L) in each plant sample, we use the calibration curve, i.e. the relationship between absorbance (Abs.) and standard concentration (Conc.). This relationship is usually linear and has the form of an equation of type:

$$\text{Abs} = a \cdot C + b$$

where:

- Abs = measured absorbance,
- C = unknown concentration,
- a = slope (regression coefficient),
- b = ordered at the origin (the intercept).

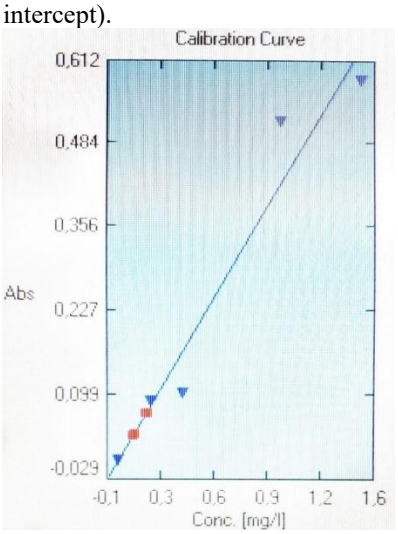

Figure 9..Calibration curve for iron and the absorbances read for the plant samples

The following table 4 shows the values obtained for the iron content of the analyzed plant species

.

Table 4. Content of iron in vegetal species analyzed

Nr.	Vegetal species	Analyzed mass (g)	Extract volume (mL)	Determined concentration (mg/L)	Total iron (mg)	Iron content (mg/kg)
1	*Urtica dioica* (Nettle)	0,5	50	0,1620	0,0081	16,2
2	*Petroselinum crispum* (Parsley)	0,5	50	0,0834	0,00417	8,34
3	*Spinacia oleracea* (Spinach)	0,5	50	0,0858	0,00429	8,58

CONCLUSIONS

The values obtained from the determination of the vitamin C (ascorbic acid) content for the three species analyzed were generally lower than those reported in the literature.

In the case of Spinacia oleracea (spinach), a value of 10.12 mg/100 g was recorded, while in the reference sources there are significantly higher ranges, ranging from 18.95 mg/100 g ('Snapper' variety) to 46.39 mg/100 g (freshly harvested spinach), but also lower values, such as 8.37 mg/100 g, depending on the source and method of determination [14].

For Urtica dioica (nettle), a concentration of 3.08 mg/100 g was determined compared to the ranges in the literature, which range from 8.17 to 112 mg/100 g, including a reference value of 36.4 ± 0.02 mg/100 g [15-17].

As for Petroselinum crispum (parsley), the value obtained was 13.64 mg/100 g, while the literature mentions a wide range, between 8 and 125 mg/100 g, depending on the source, variety and analysis conditions [15].

These differences can be justified by a number of factors. First of all, the vitamin C content varies depending on the stage of development of the plant**,** the environmental conditions (brightness, temperature, humidity), as well as the time of harvest. Young plants or harvested after a long period of exposure to the sun may have a lower ascorbic acid content.

Also, pedoclimatic conditions and the origin of the plants (home garden, spontaneous flora) can influence the vitamin C content, as nutrient-poor soils and lack of fertilization often lead to a reduced synthesis of bioactive compounds.

Another important aspect is the post-harvest handling and extraction process, vitamin C being a compound that is very sensitive to light, temperature and oxidation. Significant losses may occur during homogenization and exposure to air, which may reduce the measurable amount in the samples.

Last but not least, differences can also result from the analytical method used, as various determination techniques (such as titrimetry, spectrophotometry or HPLC) can provide different results depending on their sensitivity and accuracy.

The comparative analysis of the iron content in the dry plant samples (Table 6) highlights significant differences between the species analyzed. The highest concentration was identified in Urtica dioica (nettle), with a content of 16.2 mg/kg, followed by Spinacia oleracea (spinach**)** with 8.58 mg/kg and Petroselinum crispum (parsley) with 8.34 mg/kg. This hierarchy suggests a higher capacity for iron accumulation in nettle, compared to the other two species.

By comparing the results obtained with the data from the literature, it is observed that the experimental values are within the limits previously reported, with some variations explainable by differences in geographical origin, cultivation conditions, drying method and analytical protocol. For example, the determined value for nettle (16.2 mg/kg) is comparable to the lower limits reported by Konieczyński et al. (2007) [18] and Djurović et al. (2017) [19], but well below the maximum values reported by Bukva et al. (2019) [20], or Radman et al. (2015) [21], which can even exceed 2000 mg/kg

.

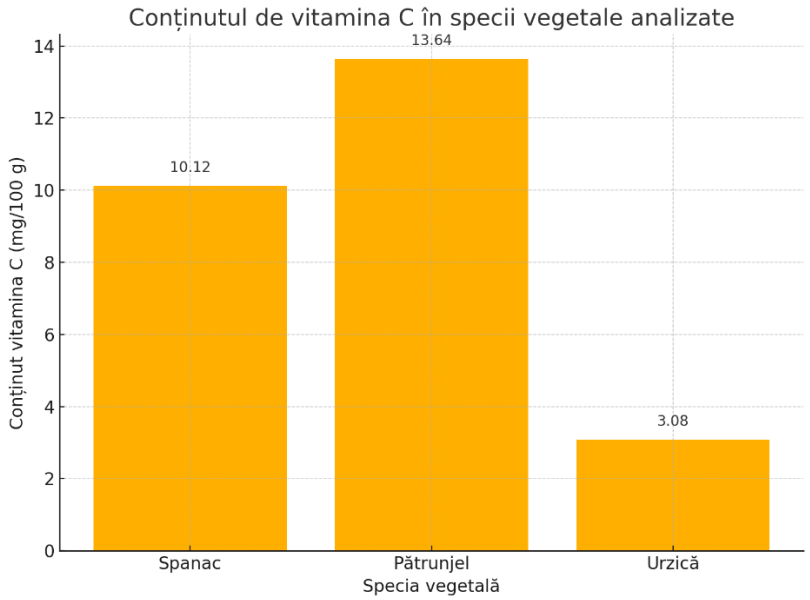

Figure 10. Content of vitamin C in vegetal species analyzed

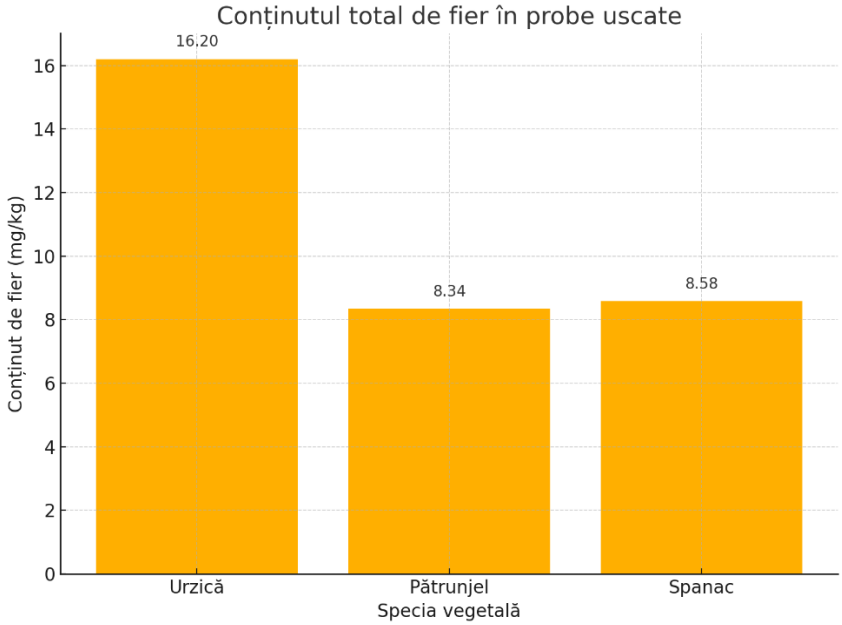

Figure 11. *Content of iron in vegetal species analyzed*

In the case of parsley, the determined value (8.34 mg/kg) is well aligned with the ranges mentioned by Valšíková et al. (2016) [22] and Sitarek-Andrzejczyk et al. (2018) [23], confirming the relevance of the method applied. For spinach, the concentration of 8.58 mg/kg slightly exceeds the reference value of 3 ± 0.02 mg/kg, which could reflect a difference in variety, soil, or sample preparation method.

Nettle has the highest iron content (16.2 mg/kg), while parsley excels in vitamin C content (13.64 mg/100g), followed by spinach (10.12 mg/100g). This complementarity suggests the benefits of varied consumption of these plants.

The synergy between vitamin C and iron is the determining factor for the real nutritional value of these plants. Although nettle has a higher iron content, parsley and spinach may provide superior iron

bioavailability due to their increased vitamin C content. The combined consumption of these plants in the diet can significantly contribute to iron intake and the prevention of mineral deficiencies, providing a balanced nutritional strategy. Combining nettle (rich in iron) with parsley or spinach (rich in vitamin C) maximizes iron absorption.

Urtica dioica, known as an ecological indicator of heavy metal pollution, showed in our study a moderate iron content (16.2 mg/kg dry), lower than the maximum values reported in the literature. This suggests that although the harvesting area has oil activity, local conditions and soil characteristics have limited the level of metal accumulations in the plant. The results confirm the potential of nettle as a bioindicator for environmental monitoring, but also highlight the importance of specific local assessments, as the concrete values can vary significantly depending on the particularities of the ecosystem.

The research makes contributions in the field of preventive nutrition and public health, demonstrating the nutritional value of these common and accessible plants. By highlighting the content of essential micronutrients and the synergy between them, the study supports the potential of using the analyzed plants in preventing iron deficiency anemia and improving the nutritional status of the population.

For the future, it is recommended to expand research by including more plant species and evaluating the influence of different processing methods on nutrient content and bioavailability. It would also be valuable to analyze the presence of other bioactive compounds that can interact with iron and vitamin C.

REFERENCES

[1] Burgess, John, și Martyn V. Twigg. „Iron: Inorganic & Coordination ChemistryBased in Part on the Article Iron: Inorganic & Coordination Chemistry by Pelham N. Hawker & Martyn V. Twigg Which Appeared in the Encyclopedia of Inorganic Chemistry, First Edition.” Encyclopedia of Inorganic Chemistry, ediție de R. Bruce King și colab., 1 ed., Wiley, 2005. DOI.org (Crossref), https://doi.org/10.1002/0470862106.ia108.

[2] Theil, Elizabeth C., și Dixie J. Goss. „Living with Iron (and Oxygen): Questions and Answers about Iron Homeostasis”. Chemical Reviews, vol. 109, nr. 10, octombrie 2009, pp. 4568–79. DOI.org (Crossref), https://doi.org/10.1021/cr900052g.

[3] Condrat, D**.** Contribuții la obținerea unor extracte din plante (phanerogame) cu efect antioxidant. Teză de doctorat, Universitatea „Politehnica” din Timișoara, Facultatea de Chimie Industrială și Ingineria Mediului, 2010. Conducător științific: Prof. dr. ing. Alfa Xenia Lupea.

[4] Winter, William E., și colab. „The Molecular Biology of Human Iron Metabolism”. Laboratory Medicine, vol. 45, nr. 2, mai 2014, pp. 92–102. DOI.org (Crossref), https://doi.org/10.1309/LMF28S2GIMXNWHMM.

[5] Santiago, Palacios. „Ferrous versus Ferric Oral Iron Formulations for the Treatment of Iron Deficiency: A Clinical Overview”. The Scientific World Journal, vol. 2012, 2012, pp. 1–5. DOI.org (Crossref), https://doi.org/10.1100/2012/846824.

[6] Ionica, E., Costache, M., Biochimie Generala: Vol III, Vitamine si Elemente Minerale, 300 p. Ars Docendi ed., Universitatea din Bucuresti, 2004. DOI.org, https://doi.org/10.13140/RG.2.1.1099.7849.

[7] Linster, Carole L., și Emile Van Schaftingen. „Vitamin C: Biosynthesis, Recycling and Degradation in Mammals”. The FEBS Journal, vol. 274, nr. 1, ianuarie 2007, pp. 1–22. DOI.org (Crossref), https://doi.org/10.1111/j.1742-4658.2006.05607.x.

[8] Duda Seiman D, Batalu A, Duda Seiman C, et al. Pharmacological Effects of Natural Compounds Extracted from Urtica dioica Evaluated by in Silico and Experimental Methods. Rev Chim 2018; 69: 2377–2381.

[9] Abubaker, Samih et al. “Nitrate accumulation in spinach (Spinacia oleracea L.) tissues under different fertilization regimes.” Journal of Food Agriculture & Environment 8 (2010): 778-780.

[10] Chauhan E S, Aishwarya J. INutraceuticals Potential of Petroselinum crispum: A Review. J Complement Med Alt Healthcare. 2018; 7(2): 555707. DOI: 10.19080/JCMAH.2018.07.555707.

[11] Aishwaya J. Nutraceuticals Potential of Petroselinum Crispum: A Review. JCMAH; 7. Epub ahead of print 22 August 2018. DOI: 10.19080/JCMAH.2018.07.555707.

[12] Pârvu C. Universul plantelor: mică enciclopedie. Ed. a 3-a, rev. și completată. București: Editura

[13] Tatyana Aleksandrovna Skalozubova, and Valentina Olegovna Reshetova. “Leaves of Common Nettle (Urtica Dioica L.) As a Source of Ascorbic Acid (Vitamin C),” 2013
[14] Paulauskienė A, Tarasevičienė Ž, Laukagalis V. Influence of Harvesting Time on the Chemical Composition of Wild Stinging Nettle (Urtica dioica L.). Plants 2021; 10:686. https://doi.org/10.3390/plants10040686.
[15] Abbas, Ghiath and Rami Mohammad Al-Taher Salem Hassan."Study on the Effect of Storage, Heat, and Iron Ions on the Stability of Vitamin C in Some Foods."2016
[16] Sandrika A, Munir MA, Aprilia V, Emelda E. Determination of vitamin c in spinach (amaranthus sp.) using titration method. J Pena Sains 2023; 10:73–9. https://doi.org/10.21107/jps.v10i2.19172.
[17] Nolasco, M.K., & Barrientos, E.M. (2013). Determinación de los fitoconstituyentes y nutrientes de las hojas de spinacia oleracea l. “espinaca”, provenientes de las localidades de Santa Rosa y Pedregal de la provincia de Trujillo, noviembre 2012.
[18] Konieczyński, P., Wesołowski, M., Rafalski P., et al. (2007). Total and extractable iron in selected herbs collected from natural areas in Northern Poland. Herba Polonica, 53(4), 28-33.
[19] Đurović, Saša, et al. "Chemical composition of stinging nettle leaves obtained by different analytical approaches." *Journal of Functional Foods* 32 (2017): 18-26.
[20] Bukva, Mersa, et al. "Iron content in fruits, vegetables, herbs and spices samples marketed in Sarajevo, Bosnia and Herzegovina." *Kemija u industriji: Časopis kemičara i kemijskih inženjera Hrvatske* 68.7-8 (2019): 281-287.
[21] S. Radman, I. Žutić, S. Fabek, J. Žlabur, B. Benko, N. Toth, and L. Čoga. “Influence of Nitrogen Fertilization on Chemical Composition of Cultivated Nettle,” 2015.
[22] Valšíková, M. ., Mezeyová, I. ., Rehuš, M. ., & Šlosár, M. . (2016). Changes of vitamin C content in celery and parsley herb after processing. *Potravinarstvo Slovak Journal of Food Sciences*, *10*(1), 637–642. https://doi.org/10.5219/687.
[23] Sitarek-Andrzejczyk, Monika & Przybył, Jarosław & GAJEWSKI, Marek. (2018). The effect of post-harvest treatment and storage conditions on vitamin C content in two leafy parsley cultivars. International scientific conference Rural development 2017. 10.15544/RD.2017.018.

COMPARATIVE ANALYSIS OF HYDRO- AND LIPOSOLUBLE VITAMINS UNDER ENVIRONMENTAL STRESS CONDITIONS

Ioana Maria BĂBĂLAI[1], Ramona Lia CORNEA (PĂDUREANU)[1], Andrei Daniel ȚICĂRAT[1], Camelia Daniela IONAŞ[2], Alina GROZE[2]

[1]Department of Chemistry, Faculty of Informatics and Sciences, University of Oradea, 1 University Street, 410087, Oradea, Romania, Chemistry students
[2]Department of Chemistry, Faculty of Informatics and Sciences, University of Oradea, 1 University Street, 410087, Oradea, Romania

Abstract: *Vitamins are essential micronutrients that play a critical role in maintaining metabolic balance and preventing deficiency-related disorders. Their biological effectiveness largely depends on molecular stability, which can be affected by environmental factors such as temperature, light, UV radiation, and pH.This study evaluates the influence of these parameters on nine representative vitamins, five water-soluble (B_1, B_2, B_6, B_{12}, C) and four fat-soluble (A, D_3, E, K_1) using UV–VIS spectrophotometry. Each vitamin solution was subjected to controlled conditions of heat (82 °C), light exposure (natural and UV), and pH variation (4–10).The results demonstrated that water-soluble vitamins exhibited higher sensitivity to external factors, particularly vitamin C and B_1, which degraded rapidly under elevated temperature and UV light. Riboflavin (B_2) was notably photolabile, while B_{12} showed the greatest stability among the hydrosoluble group. In contrast, fat-soluble vitamins were more resistant: vitamin A was the most thermolabile, vitamin K_1 degraded under UV light, and vitamin E remained remarkably stable under all tested conditions.Overall, a direct relationship was observed between solubility, molecular structure, and environmental resistance. Maintaining optimal storage conditions, low temperature, neutral pH, and protection from light, is crucial to preserve vitamin bioactivity during formulation and storage.*

Key words: vitamins, stability, photodegradation, temperature, pH, UV–VIS spectrophotometry

INTRODUCTION

Vitamins are essential organic micronutrients that play key roles in metabolic regulation, cellular protection, and enzymatic function. They are required in small amounts but are indispensable for maintaining physiological balance and preventing deficiency-related disorders. Based on solubility, vitamins are classified as water-soluble (B-complex and vitamin C) and fat-soluble (A, D, E, and K), each category exhibiting distinct chemical and stability characteristics [2, 5, 6].

However, vitamin molecules are often unstable when exposed to environmental stressors such as temperature, light, oxygen, and pH variations. The main degradation mechanisms involve oxidation, isomerization, hydrolysis, and photolysis, processes that result in significant loss of biological activity. For example, ascorbic acid undergoes rapid oxidation under heat and UV exposure, while riboflavin is known to be highly sensitive to light-induced degradation [3, 7-8].

Understanding these degradation pathways is essential for developing stable formulations in both the food and pharmaceutical industries, where vitamins are widely used as bioactive additives and therapeutic agents [4].

In this study, the stability of nine representative vitamins, five water-soluble (B_1, B_2, B_6, B_{12}, C) and four fat-soluble (A, D_3, E, K_1), was comparatively evaluated under controlled conditions of temperature, light, UV radiation, and pH, using UV–VIS spectrophotometry as a quantitative tool to assess degradation intensity [1].

RESULTS AND DISCUSSION

The obtained data demonstrate that the environmental stability of vitamins is strongly influenced by their solubility class, molecular structure, and exposure conditions. In general, water-soluble vitamins (B_1, B_2, B_6, B_{12}, C) exhibited higher sensitivity to external stress, while fat-soluble vitamins (A, D_3, E, K_1) showed greater resistance, although not immunity, to degradation caused by temperature, light, and pH variations.

The following subsections discuss in detail the main degradation patterns observed for each vitamin.

WATER-SOLUBLE VITAMINS

Vitamin B_1 (Thiamine)

The absorbance of vitamin B_1 decreased sharply in alkaline conditions, indicating strong base-catalyzed degradation. This behavior is associated with the cleavage of the thiazole–pyrimidine linkage in the thiamine molecule, which leads to inactive degradation products. Exposure to UV radiation caused a pronounced drop in absorbance, confirming its high photosensitivity. Elevated temperature (82 °C) further accelerated decomposition, consistent with the thermolability of thiamine reported in literature (Ahmad et al., 2018). These findings suggest that thiamine stability is particularly compromised under combined heat and light stress

.

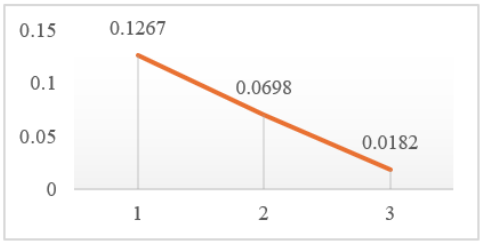

Figure 1. Effect of pH on the absorbance of vitamin B1

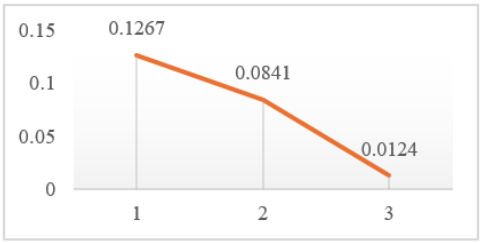

Figurure 2. Effect of light exposure on the absorbance of vitamin B1

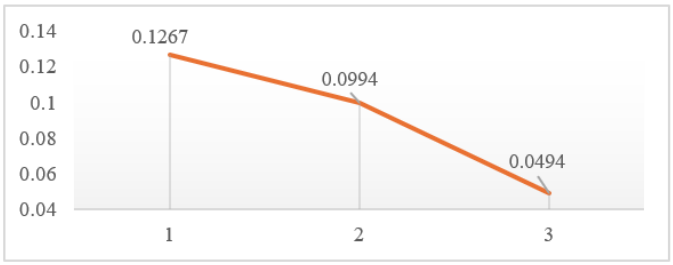

Figure 3. Effect of temperature on the absorbance of vitamin B1

Vitamin B_2 (Riboflavin)

Riboflavin showed distinct sensitivity to light exposure. Absorbance decreased from 2.79 under control conditions to 1.75 under sunlight and 1.84 under UV radiation, highlighting significant photodegradation. The phenomenon is attributed to photo-oxidative reactions involving the isoalloxazine ring, leading to the formation of lumichrome and lumiflavin derivatives.

Temperature increase from ambient to 82 °C reduced absorbance to 1.63, indicating partial thermal breakdown. The vitamin remained relatively stable in basic medium but degraded under acidic conditions due to protonation of the ribityl side chain.

Vitamin B_6 (Pyridoxine)

Vitamin B_6 displayed moderate sensitivity to light and temperature. The absorbance decreased from 1.31 (standard) to 0.97 under UV radiation and 1.10 at 82 °C. The reduction in acidic medium (pH 4) confirmed acid-catalyzed cleavage of the hydroxymethyl group, whereas basic medium offered slightly higher stability. Pyridoxine's degradation kinetics align with previous studies indicating its vulnerability to oxidative and photolytic reactions, particularly in aqueous formulations.

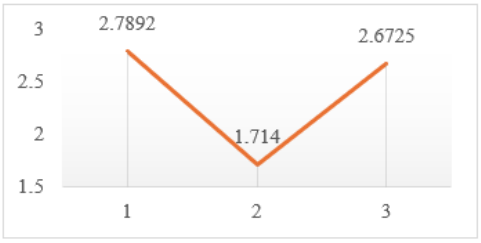

Figure 4. Effect of pH on the absorbance of vitamin B2

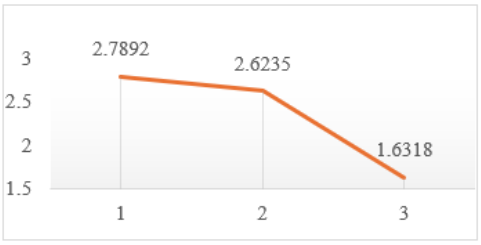

Figure 5. Effect of light exposure on the absorbance of vitamin B2

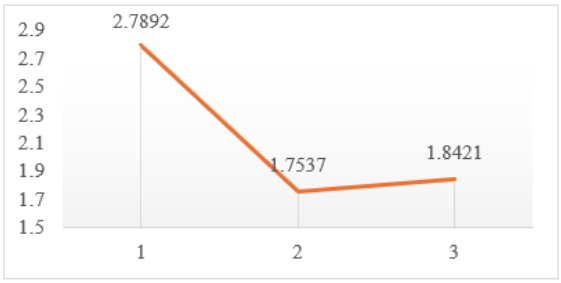

Figure 6. Effect of temperature on the absorbance of vitamin B2

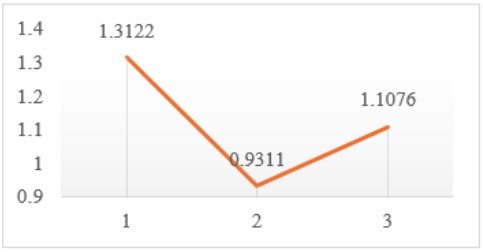

Figure 7. Effect of pH on the absorbance of vitamin B6

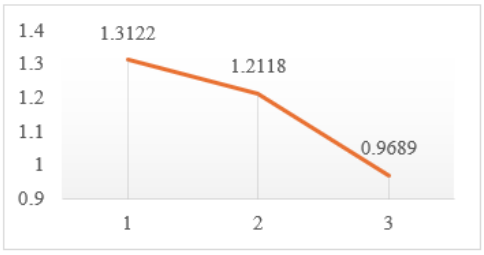

Figure 8. Effect of light exposure on the absorbance of vitamin B6

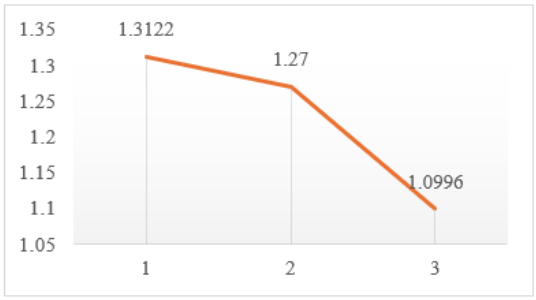

Figure 9. Effect of temperature on the absorbance of vitamin B6

Vitamin B_{12} (Cobalamin)

Among all B-complex vitamins, vitamin B_{12} proved the most stable. Its absorbance showed minimal variation with pH and only moderate decreases under sunlight and UV radiation. This relative resistance arises from its corrin ring structure and cobalt coordination complex, which provides strong electronic stability. Slight thermal degradation was observed at 82 °C (from 3.63 to 3.46), suggesting that the integrity of the cobalt–carbon bond remains largely preserved under mild heat exposure.

Vitamin C (Ascorbic Acid)

Vitamin C exhibited the highest environmental sensitivity. Its absorbance declined dramatically under UV radiation (from –0.0434 to –0.2666), confirming rapid photodegradation. The process occurs via oxidation of ascorbic acid into dehydroascorbic acid and subsequent hydrolysis into diketogulonic acid, leading to loss of antioxidant activity. Elevated temperature (82 °C) also caused a marked decrease in absorbance (–0.1652), highlighting its thermolabile nature. The data confirm that ascorbic acid degradation follows both oxidative and pH-dependent pathways, consistent with prior reports [8]

.

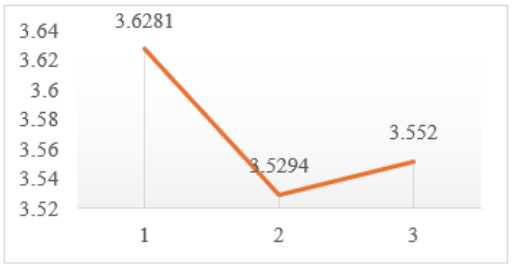

Figure 10. Effect of pH on the absorbance of vitamin B12

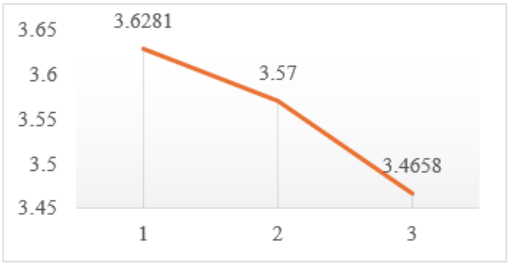

Figure 12. Effect of light exposure on the absorbance of vitamin B12

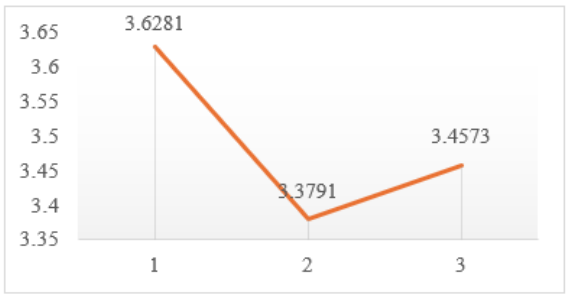

Figure 11. Effect of temperature on the absorbance of vitamin B12

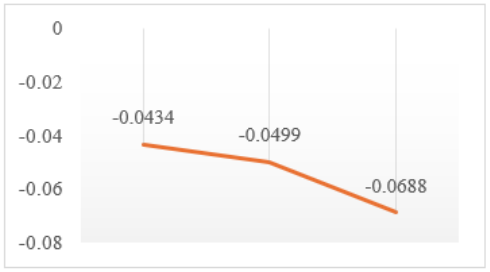

Figure 13. Effect of pH on the absorbance of vitamin C

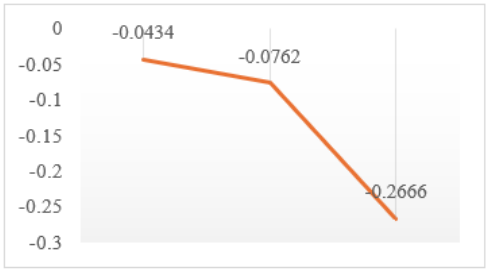

Figura 14. Effect of light exposure on the absorbance of vitamin C

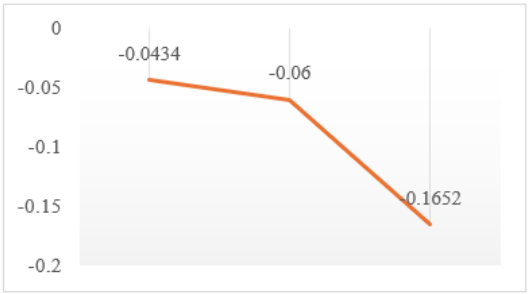

Figure 15. Effect of temperature on the absorbance of vitamin C

FAT-SOLUBLE VITAMINS

Vitamin A (Retinol)

Vitamin A showed pronounced instability under light and heat. Absorbance decreased significantly under UV radiation and at high temperature, suggesting photooxidation of the conjugated polyene chain. The degradation mechanism involves isomerization and cleavage of the double bonds, resulting in color fading and loss of bioactivity. Its stability was higher in acidic medium, but declined in alkaline pH, where oxidation is favored.

Vitamin D_3 (Cholecalciferol)

Cholecalciferol maintained good stability across different pH levels but exhibited sensitivity to UV radiation and elevated temperature. The absorbance decline observed under UV exposure indicates cleavage of the secosteroid ring system, a known pathway for photolytic degradation of vitamin D derivatives. Although partially reversible under certain storage conditions, the overall loss of absorbance at 82 °C suggests that high temperature accelerates oxidation and decreases vitamin potency.

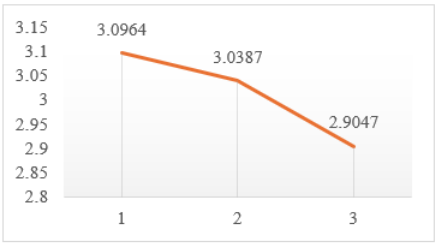

Figure 16. Effect of pH on the absorbance of vitamin A

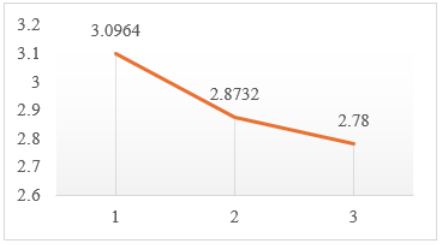

Figure 17. Effect of light exposure on the absorbance of vitamin A

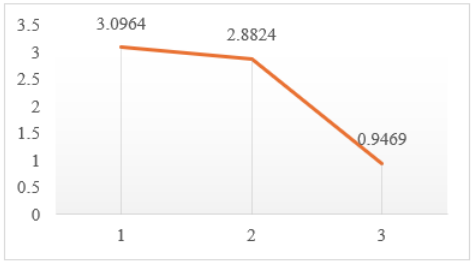

Figure 18. Effect of temperature on the absorbance of vitamin A

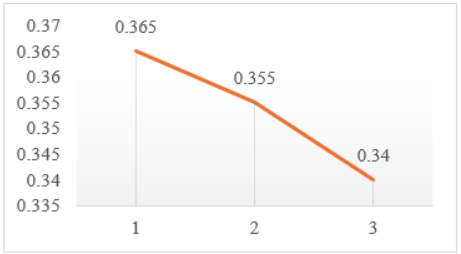

Figure 19. Effect of pH on the absorbance of vitamin D3

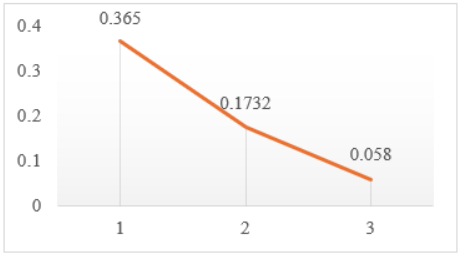

Figure 20. Effect of light exposure on the absorbance of vitamin D3

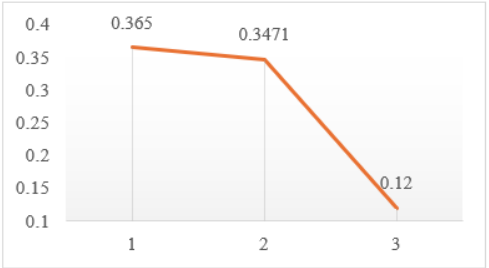

Figure 21. Effect of temperature on the absorbance of vitamin D3

Vitamin E (α-Tocopherol)

Vitamin E remained the most stable among the fat-soluble vitamins. Its absorbance showed only slight variations under all tested conditions, confirming strong antioxidant capacity. The stability is attributed to its phenolic hydroxyl group, which readily donates a hydrogen atom to neutralize reactive oxygen species, thereby preventing oxidative chain reactions. Interestingly, its presence can reduce the degradation rate of other lipophilic compounds, indicating a protective, synergistic effect.

Vitamin K_1 (Phylloquinone)

Phylloquinone displayed pronounced sensitivity to UV radiation, with a drastic reduction in absorbance. This behavior is associated with the breakdown of its quinone structure, resulting in photoreduction and loss of biological activity. It remained stable in neutral medium but degraded in both acidic and basic environments, suggesting that pH-induced redox reactions contribute to its instability. Temperature increase also accelerated decomposition, particularly in the presence of light.

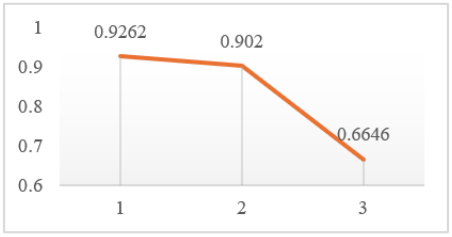

Figure 22. Effect of pH on the absorbance of vitamin E

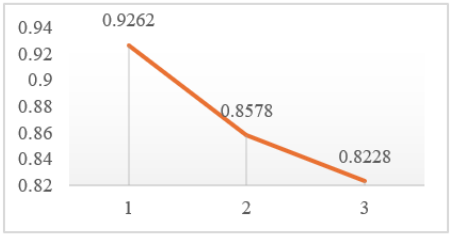

Figure 23. Effect of light exposure on the absorbance of vitamin E

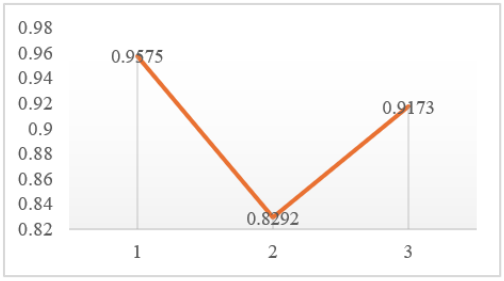

Figure 24. Effect of temperature on the absorbance of vitamin E

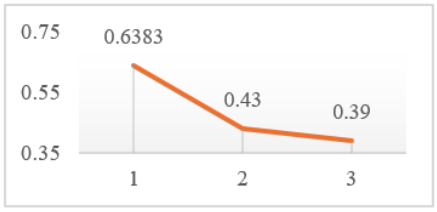

Figure 25. Effect of pH on the absorbance of vitamin K1

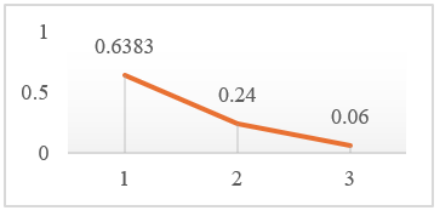

Figure 26. Effect of light exposure on the absorbance of vitamin K1

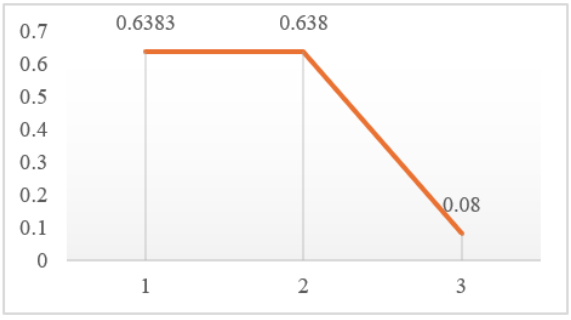

Figure 27. Effect of temperature on the absorbance of vitamin K1

Comparative Overview

Comparing all results, a clear trend emerges: **water-soluble vitamins** degrade faster under combined environmental stress due to their polar nature and high reactivity, while **fat-soluble vitamins** exhibit slower degradation rates but are still affected by oxidation and photo-induced reactions.

The hierarchy of stability can be summarized as follows:

Most stable → least stable: E > B_{12} > D_3 > K_1 > B_2 > B_6 > A > B_1 > C

This ranking demonstrates the interplay between molecular structure and environmental exposure. The results highlight the importance of **controlled processing, light-protective packaging, and pH optimization** to minimize degradation and preserve vitamin bioactivity in pharmaceutical and food formulations.

CONCLUSIONS

The comprehensive evaluation of nine vitamins under various environmental stress conditions has demonstrated that each compound exhibits a distinct degradation pattern depending on its solubility and molecular structure.

Overall, water-soluble vitamins (B_1, B_2, B_6, B_{12}, C) showed a higher sensitivity to temperature, light, and pH variations, whereas fat-soluble vitamins (A, D_3, E, K_1) were more resistant, yet still susceptible to oxidation and photo-induced degradation.

Among the water-soluble compounds, vitamin C displayed the greatest thermal and oxidative instability, with a sharp decrease in absorbance at elevated temperatures and under UV radiation, confirming its well-known sensitivity to environmental factors. Thiamine (B_1) and pyridoxine (B_6) were particularly affected in acidic environments, while riboflavin (B_2) showed significant photodegradation under both natural and UV light. Vitamin B_{12}, on the other hand, maintained relatively good stability across all tested conditions.

For the fat-soluble group, vitamin A proved highly sensitive to heat and light exposure, exhibiting a marked decline in stability at 82°C, whereas vitamin D_3 and vitamin K_1 were moderately affected by UV radiation and elevated temperature. In contrast, vitamin E stood out as the most stable compound, confirming its antioxidant role and its potential to enhance the stability of other vitamins in multicomponent systems.

These findings collectively highlight that the stability of vitamins is governed by both chemical nature and environmental exposure, and that maintaining proper storage conditions, low temperature, absence of direct light, and neutral pH, plays a critical role in preserving their biological activity.

From a practical perspective, the results emphasize the necessity of controlled formulation and packaging strategies in food and pharmaceutical industries, ensuring minimal degradation and optimal bioavailability of vitamins throughout product shelf life.

REFERENCES

[1] Ahmad, I., Abbas, S. H., Anwar, Z., Sheraz, M. A., Ahmed, S., Mobeen, M. F., Mustaan, N., & Gul, W. (2018). *Stability-indicating photochemical method for the assay of thiamine by spectrophotometry.* **Journal of Spectroscopy, 2018**, Article 3178518. https://doi.org/10.1155/2018/3178518

[2] Bender, D. A. (2003). *Nutritional biochemistry of the vitamins* (2nd ed.). Cambridge University Press, pp 2 https://drhazhan.com/Nutritional%20Biochemistry%20of%20the%20Vitamins.pdf

[3] Cheung, P. C. K., & Mehta, B. M. (Eds.). (2015). *Handbook of food chemistry*. Springer-Verlag GmbH, pp 10, https://doi.org/10.1007/978-3-642-36605-5

[4] Coelho, S. C., Estevinho, B. N., & Rocha, F. (2022). Recent advances in water-soluble vitamins delivery systems prepared by mechanical processes (electrospinning and spray-drying techniques) for food and nutraceuticals applications—a review. *Foods*, 11(9), 1271, pp 4. https://doi.org/10.3390/foods11091271

[5] Combs, G. F., Jr. (2012). *The vitamins: Fundamental aspects in nutrition and health* (4th ed.). Academic Press., pp 4. https://www.enacnetwork.com/files/books/vitamins_%26_minerals/The_Vitamins_Fourth_Edition.pdf

[6] Kareem, M. M., & Jabir, M. (2020). Chapter: Vitamins. În *Malnutrition* (pp. 1–19). IntechOpen. https://doi.org/10.5772/intechopen.92074
[7] Ottaway, P. B. (1993). Stability of vitamins in food. În P. B. Ottaway (Ed.), *The technology of vitamins in food* (pp. 90–113). Springer. https://doi.org/10.1007/978-1-4615-2131-0_5
[8] Yin, X., Chen, K., Cheng, H., Chen, X., Feng, S., Song, Y., & Liang, L. (2022). Chemical stability of ascorbic acid integrated into commercial products: A review on bioactivity and delivery technology. *Antioxidants*, 11(1), 153. https://doi.org/10.3390/antiox11010153

STATISTICAL ANALYSIS OF CALORIMETRIC EXPERIMENTAL RESULTS OBTAINED FROM THE COMBUSTION OF ETHYL ALCOHOL IN AN OPEN SYSTEM

Alexandru Nicolae BADEA[1], Gabriel Petru BADEA[2], Oana Delia STĂNĂȘEL[2], Sorin HODIȘAN[2], Alina GROZE[2]

[1]University of Oradea, Faculty of Informatics and Sciences, Master CSA I
[2]University of Oradea, Faculty of Informatics and Sciences, Master SDI I
[3] University of Oradea, Faculty of Informatics and Sciences, Department of Chemistry

Abstract
This paper presents the results obtained in the determination of the heats of combustion of some aliphatic alcohols by the open-system calorimetric method, their comparative analysis and the correlation of these results with the formula and molecular structure of the alcohols. Following the correlation of the calculations and statistical analysis, it was observed that the heats of combustion increase with the increase of the chain, i.e. the number of carbon atoms. Also, alcohols with a branched chain molecule:iso-propanol, iso-butanol had a slightly higher heat of combustion than the linear chain isomers: n-propanol, n-butanol.
Key words: aliphatic alcohol, combustion, thermodinamics, statistical

INTRODUCTION

Chemical thermodynamics is a branch of thermodynamics that studies the relationships between energy and heat in chemical processes. It analyzes how substances change their energy state during chemical reactions and physical interactions. The main concepts include enthalpy, entropy, and free energy, which are essential for understanding chemical equilibrium and the spontaneity of reactions. Chemical thermodynamics is therefore a science that deals with the energy changes that occur during chemical reactions[1-16].

An application through which the heat released by a combustion reaction can be determined, for example, is the calorimetric experiment, an important application in determining the heat of combustion of liquid fuels [14-16].

The combustion of fuels is an exothermic reaction, and the thermal effect of the reaction is called the heat of combustion (calorific value), Qc

$$\text{Combustibil(C, H,…)}_{(s,l,g)} + O_2(g) \rightarrow CO_2(g) + H_2O(g) + Qc$$

Liquid fossil fuels, fundamentally composed of diverse hydrocarbons, require precise calorimetric determination of their heats of combustion to correlate molecular structure with energetic output and to support accurate characterization, classification, and quality control in fuel analysis.

EXPERIMENTAL

Calorimetric experiments take place in solution and are performed at constant (atmospheric) pressure - figure 1, because they occur without appreciable changes in volume. There are also cases in which the effects of chemical reactions are determined at constant volume. This is the case of combustion reactions, which take place in a calorimetric bomb (figure 1), where the heat released by the combustion reaction is absorbed by the water and the components of the calorimetric bomb[5,6].

The amount of heat released in the chemical reaction can be calculated from the increase in the temperature of the water:

$$Q = m_{apa}\, c_{apa}\, (T_f - T_i) \qquad (7)$$

where m_{apa}-is the mass of water, c_{apa}-the specific heat of water and Ti,f the initial and final heat of water, respectively.

The calculation is even more precise as it takes into account other heat exchanges,

such as if working in an open system (without an adiabatic shell): heat storage in the component parts of the installation, water evaporation, radiation losses (figure 1). In the case of the experiment presented below, a simplified hypothesis was taken into account and these components were neglected for objective reasons[6].

Figure 1. Bomb calorimetry (open system).

This paper presents the results obtained in the determination by the open system calorimetry method of the heats of combustion of ethyl, n-propyl, isopropyl and isobutyl alcohols (figure 2) as well as their comparative analysis and the correlation of these results with the formula and molecular structure of the alcohols. For each alcohol, the experiment was repeated 5 times.

Figure 2. Studied alcohol.

The initial and final temperatures of the water in the calorimeter vessel, the initial and final masses of the still were measured to determine the amount of alcohol burned and the volume of water that evaporated. The stages of the experiment are presented in Figure 3.

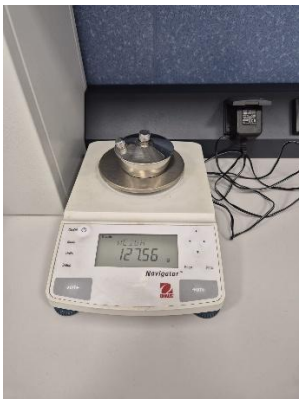

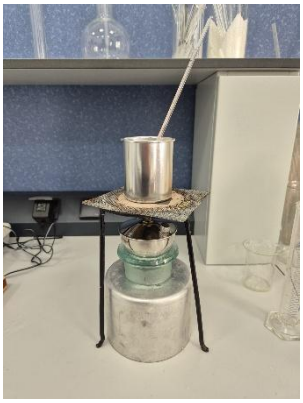

Figure 3. Stages of calorimetric experiment.

RESULTS AND DISCUSSIONS

Calorimetric results

Following the experimental calorimetric results obtained from the combustion of the studied alcohols and their reporting to 1 kg of liquid fuel, the values in table 1 were obtained.

In the case of the heats of combustion from thermodynamic data, several assessments can be made related to their values and the composition and structure of the studied alcohols.

Table 1. Heats of combustion, Qc, experimentally determined by the calorimetric method.

Alcohol	1	2	3	4	5
ethanol	1254	1362	1294	1342	1447
n-propanol	2479	1932	2118	1965	1942
isopropanol	1285	1843	1841	1502	1737
isobutanol	1693	1539	1515	1,726	2551

Theoretical results

For each alcohol, the thermochemical combustion equation is written with the stoichiometric coefficients, then using thermodynamic data tables, the reaction enthalpy variation is calculated, which is equal and opposite in sign to the heat of reaction. The reaction enthalpy variation is calculated for 1 mol of alcohol, and the heat of reaction is related to 1 kg (1000 g) of liquid fuel.

The thermodynamic calculations for the 4 combustion reactions of ethyl, n-propyl, isopropyl, n-butyl and isobutyl alcohols are presented below

Similarly, the heats of combustion were determined from thermodynamic data for the other alcohols studied.

Table 2 presents the values calculated from thermodynamic data of the heats of combustion of the studied alcohols.

A first observation would be the increase in the heats of combustion with the increase of the chain, i.e. the number of carbon atoms.

This follows from the fact that with the increase in the number of carbon atoms in the molecule, the number of moles of CO2 resulting from the combustion reaction increases, and therefore the value of the associated enthalpy, respectively the heat (figure 4).

- C_2H_5OH (l) +3 O_2 (g) → 2 CO_2 (g) + 3 H_2O(g) + Qc

Qc= $-\Delta H^o_{298}$

$$\Delta H^o_{298} = \sum_j n_P H^o_P - \sum_i n_R H^o_R$$

	CO_2(g)	H_2O(g)	O_2(g)	CH_3CH_2OH(l)
ΔH^o	-393,5	-241,8	0	-277,69

ΔH^o_{298}= (n_{CO2} H^o_{CO2} + n_{H2O} H^o_{H2O}) - (n_{C2H5OH} H^o_{C2H5OH}+ n_{O2} H^o_{O2})

= (2 H^o_{CO2}+ 3 H^o_{H2O}) - (1 H^o_{C2H5OH}+ 3 H^o_{O2}) <0

=2(-393,5)+3(-241,8)-(-277.69)-3*0=-1234,75 kJ/mol=-295,39 kcal/mol

1mol CH_3CH_2OH(46g) ..... 295,39 kcal

1000g ..... Qc

Qc=(295.39*1000)/46= 6421,52 kcal

Table 2. Heats of combustion of the studied alcohols calculated from thermodynamic data.

Alcohol	Formula	Qc, termod, kcal
ethanol	C_2H_5OH	6421,52
n-propanol	n-C_3H_7OH	7259,56
isopropanol	Iso- C_3H_7OH	7295,45
isobutanol	Iso-C_4H_9OH	7938,38
n-butanol	n-C_4H_9OH	7985,90

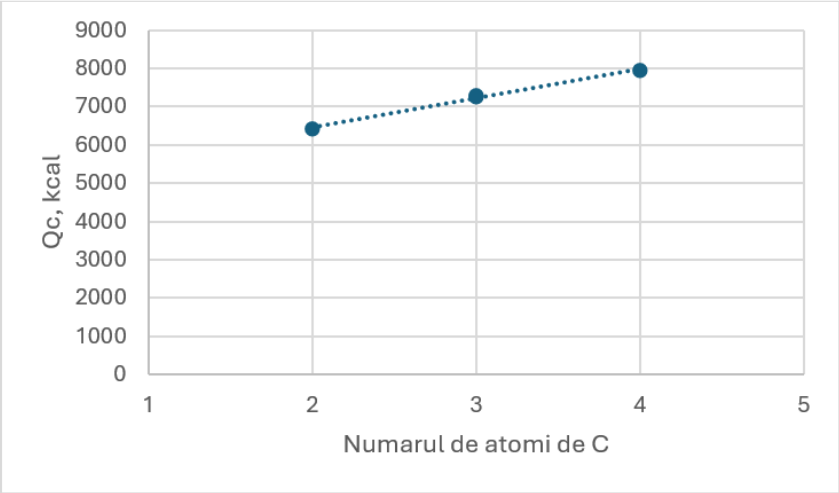

Figure 4. Increase in heat of combustion with increasing carbocation chain.

The second observation is related to the structure of alcohol molecules. In general, organic substances with side chains tend to have a different heat of combustion than those with linear chains, because branching affects the stability of the molecule and how it interacts with oxygen during combustion.

Figure 5 shows the molecular structures of the alcohols studied, the red marked atom being the oxygen atom from hydroxyl function.

.

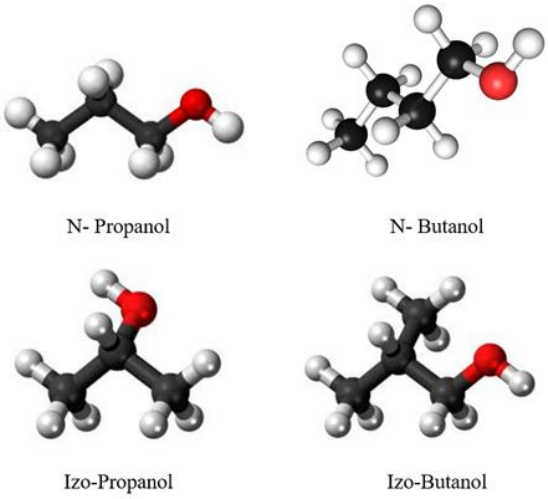

Figure 5. Molecular structures of the studied alcohols.

Kinetic data from the scientific literature state that straight-chain compounds (hydrocarbons) as engine fuels burn faster, which can damage the engine, so slower-burning branched-chain compounds are preferred.

However, from a thermodynamic point of view, the differences are quite small. This study is limited by the fact that only 2 pairs of isomers were analyzed and a general estimate cannot be made. The calculation resulted in the branched-chain molecule having a slightly higher heat of combustion than the linear-chain molecule (Figure 6).

From the analysis of the experimental data and theoretical calculations regarding the heats of combustion of the studied alcohols, the following analyses can be made.

The heats of combustion determined experimentally are in all cases lower than those determined from thermodynamic data, because the experiments were performed in an open system and the radiation losses were very high. Figure 7 presents the comparative experimental and theoretical values of Qc for ethyl alcohol. This pattern is repeated for the other 4 alcohols.

The average of the experimentally determined heats of combustion is lower than the theoretically determined heat, in all the analyzed cases and is presented comparatively in all the analyzed cases, as can be seen from table 3 and figure 8.

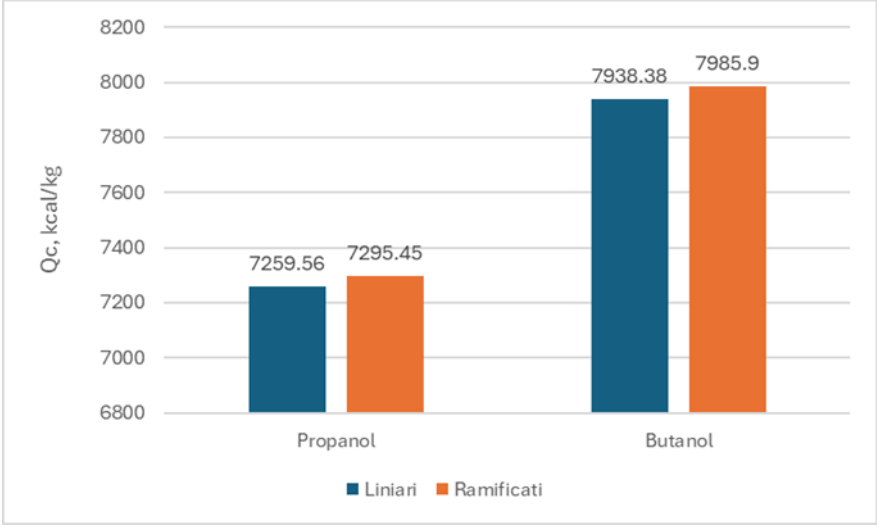

Figure 6. Comparison between the heats of combustion of propyl and butyl alcohols with linear and branched chains.

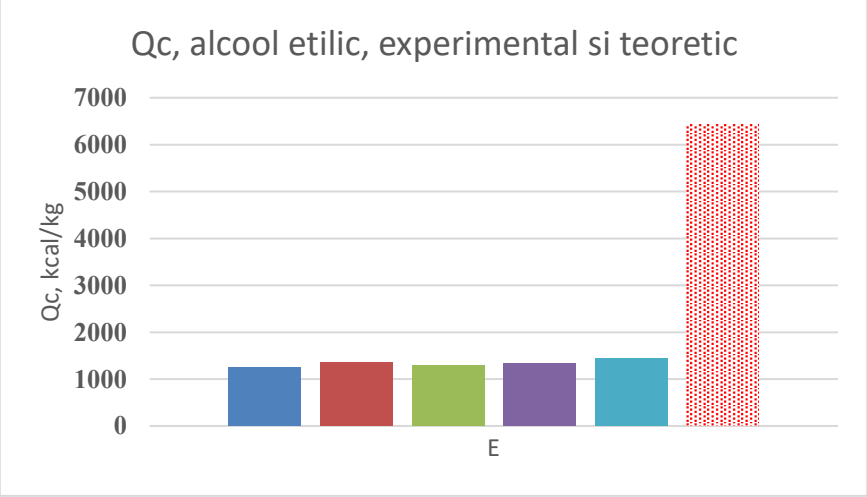

Figure 7. Comparison between experimental and theoretical values of the heat of combustion of ethyl alcohol.

Table 3. Comparative analysis of the experimental average and theoretical (from thermodynamic data) heats of combustion, related to the experiments.

Alcohol	**Q_c, average, kcal**	**Q_{termod} kcal**
ethanol	1339,80	6421,52
n-propanol	2087,20	7259,56
isopropanol	1641,60	7295,45
isobutanol	1804,80	7938,38

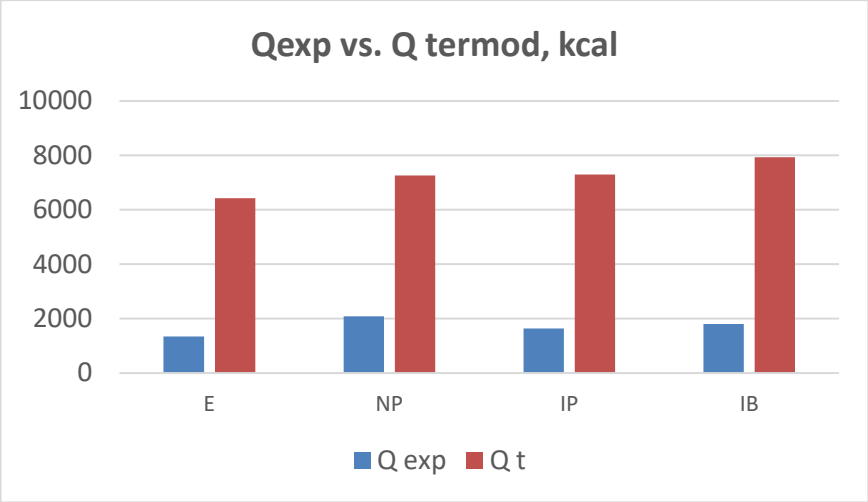

Figure 8. Average values of experimental heats of combustion vs heat of combustion from thermodynamic data for the 4 alcohols studied.

CONCLUSIONS

In this work, the heats of combustion of ethyl, n-propyl, iso-propyl, n-butyl, iso-butyl alcohols were determined by the methods: experimental calorimetric. The following conclusions can be drawn from the results obtained:

- A number of 5 determinations were made by the calorimetric method for each alcohol studied and the heats of combustion, also called lower calorific powers, were determined.
- Alcohols with a branched chain molecule (iso-propanol, iso-butanol) had a slightly higher heat of combustion than the linear chain isomers (n-propanol, n- butanol).
- An increase in the heats of combustion was observed with the increase in the chain, i.e. the number of carbon atoms.

REFERENCES

1. Stănășel O.– Termodinamică chimică – curs pentru uzul studenților, Platforma e-Learning UO 2023.
2. Stănășel, O. – Lucrări practice de chimie–fizică, structură şi termodinamică, Ed. Universităţii din Oradea, 2007.
3. Stănășel O. – Lucrări de laborator de termodinamică chimică, Platforma e-Learning UO 2023.
4. Stănășel O.- Termodinamică chimică, Notițe de curs, 2024.
5. Badea G.E., Note de curs- Bazele fizico-chimice ale tehnologiei chimice-(format electronic) pe platforma de e-learning a universitatii (www.e.uoradea.ro)
6. Badea G.E., Lucrari de laborator- Bazele fizico-chimice ale tehnologiei chimice-(format electronic) pe platforma de e-learning a universitatii (www.e.uoradea.ro)
7. .Rădulescu G.A, Petre I., Combustibili, uleiuri şi exploatarea autovehiculelor, Ed.Tehnică, București, 1986.
8. https://en.wikipedia.org/wiki/Ethanol
9. https://ro.wikipedia.org/wiki/1-propanol

10. https://ro.wikipedia.org/wiki/Izopropanol
11. https://ro.wikipedia.org/wiki/Izobutanol
12. https://www.sciencephoto.com/media/723319/view/n-butanol-molecule
13. https://ro.wikipedia.org/wiki/Alcool
14. Dhairiyasamy, R., Varshney, D., Singh, S. *et al.* Impact of biodiesel concentration and temperature on fuel properties: a comprehensive analysis of diesel and biodiesel mixtures. *Int J Energ Water Res* **9**, 2219–2237 (2025). https://doi.org/10.1007/s42108-025-00384-6
15. Rising, R., Kittrell, H.D. & Albu, J.B. Proposed shorter duration protocols for measuring resting energy expenditure utilizing whole-room indirect calorimetry. *Int J Obes* **49**, 731–736 (2025). https://doi.org/10.1038/s41366-024-01667-4
16. Zhou, G., Bao, K., Xiao, H. *et al.* Measurement of Energy Expenditure by Indirect Calorimetry with a Whole-Room Calorimeter. *Phenomics* **4**, 203–212 (2024). https://doi.org/10.1007/s43657-023-00127-9

(12pt)

INSTRUCTIONS FOR AUTHORS (TIMES 14 PT BOLD, CAPITAL LETTERS, CENTRED)

(10pt)

First name SURNAME[1], First name SURNAME[2] (12 pt bold)

[1]Affiliations and addresses (10 pt)Affiliations and addresses (10 pt)

(10pt)

(10pt)

Abstract: *Abstract of 50-120 words (11 pt italic). It contains concise information about: objectives of the work, the results obtained, conclusions*

Key words: List 2-6 keywords. (l1 pt, italic)*.*

(10pt)

(10pt)

INTRODUCTION (l2PT. CAPITAL, BOLD)

The paper has to be written in English. Each paper should be concise including text, figures and tables. Authors are kindly requested to submit a paper a hard copy or in electronic format in Microsoft Word file form. Acceptable versions are MS-Word 2003- Office 365. The suggested structure of the main text: Introduction; Methods, techniques, materials, Study area; Results and Discussions; Conclusions; References. (10pt)

(10pt)

INFORMATION (12 PT CAPITAL, BOLD)

Page layout (10 pt, bold)

- Use A4 format (210 x 297 mm),
- Margins: Top – 2.5 cm, Bottom - 3cm, Left - 4 cm and Right - 3 cm
- Paragraphs: alinment - justified, line spacing – 1,
- Font style: Times New Roman.
- Text: l0pt.: regular, text in tables: 10 pt, 1 line space and centred, 2 columns,
- equations: Equation editor, 11 pt, centred,
- c*aption of tables and figures: 11 pt, italic*

(10pt)

All tables and figures follow the References or could be inserted within the text. Tables, together with figures should be placed in their order of appearance in the text. Tables should be numbered consecutively. Table captions containing the number of the tables, followed by the caption, and should be placed above the table. Tables should be clearly captioned and all symbols should be properly explained in either the table or its caption.

Figures (min. 300 dpi) can be in colour, but must also be clear enough for black and white reproduction. They should be centred and numbered consecutively and so referred to in the text. Each must be clearly captioned (after the Figure number) below the figure.

Equations will be centred and numbered consecutively (right aligned).

All references would be cited within the text as superscripts after the punctuation's marks.[1]

All papers cited should be listed under the **REFERENCES** (1 column), in alphabetical order according to the author's last name. The list of references should follow the format given below:

(Journal Article)

[1] Abbott, M. B., Petersen, M. M., and Skovgaard, O. (1978). On the numerical modelling of short waves in shallow water, Jnl Hydraulic Res; Vol 16 (3), pp. 23-44.

(Report)

[2] Carter, B., and Connell, C. (1980). Moa Point Wastewater Treatment Plant and Outfall Study, Report for the Wellington City Council, Wellington, pp. 31.

(Book)

[3] Grady, C.P.L., and Lim, H.(1980). Biological Wastewater Treatment Theory and Application, Marcel Dekker, New York, pp. 375.